AD-A117 436 SCIENCE APPLICATIONS INC MCLEAN VA F/G 19/4
NUCLEAR AIR BLAST EFFECTS.(U)
JUN 82 M FRY
UNCLASSIFIED SAI-83-836-WA N00014-81-C-2267
NL

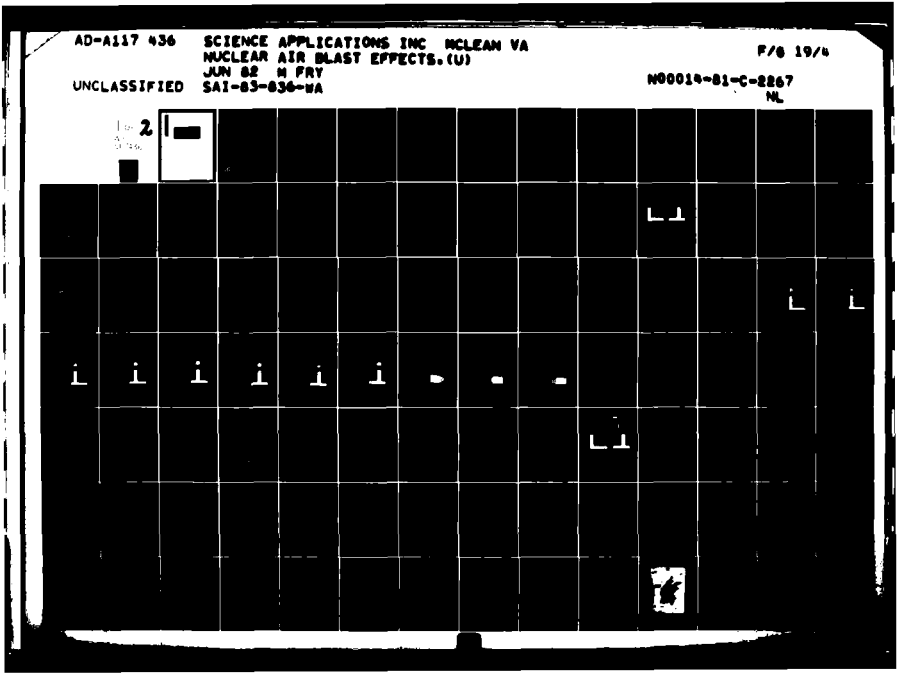

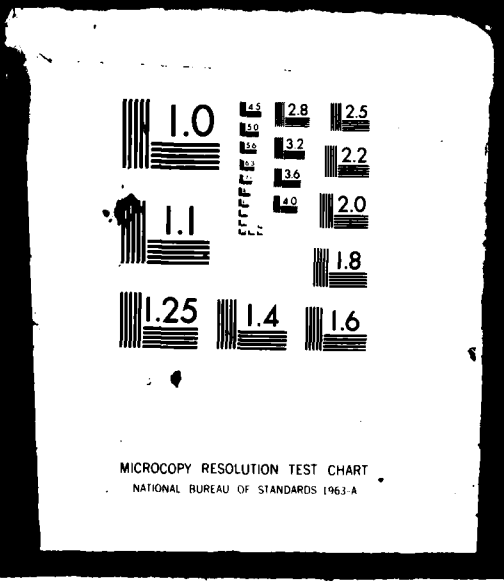

SECURITY CLASSIFICATION OF THIS PAGE (When Data Entered)

REPORT DOCUMENTATION PAGE	READ INSTRUCTIONS BEFORE COMPLETING FORM

NUCLEAR AIR BLAST EFFECTS
FINAL REPORT

SAI-83-836-WA

Prepared by
Mark Fry

ATLANTA • ANN ARBOR • BOSTON • CHICAGO • CLEVELAND • DENVER • HUNTSVILLE • LA JOLLA
LITTLE ROCK • LOS ANGELES • SAN FRANCISCO • SANTA BARBARA • TUCSON • WASHINGTON

NUCLEAR AIR BLAST EFFECTS

FINAL REPORT

SAI-83-836-WA

Submitted to:

Laboratory for Computational Physics
Naval Research Laboratory
Washington, D.C. 20375

Prepared under:

Contract # N00014-81-C-2267

Prepared by:

Mark Fry

SCIENCE APPLICATIONS, INCORPORATED

1710 Goodridge Drive, McLean, Virginia 22102

SECURITY CLASSIFICATION OF THIS PAGE (When Data Entered)

REPORT DOCUMENTATION PAGE		READ INSTRUCTIONS BEFORE COMPLETING FORM
1. REPORT NUMBER	2. GOVT ACCESSION NO.	3. RECIPIENT'S CATALOG NUMBER
4. TITLE (and Subtitle) NUCLEAR AIR BLAST EFFECTS		5. TYPE OF REPORT & PERIOD COVERED Final Report 5/1/81 - 4/30/82 6. PERFORMING ORG. REPORT NUMBER
7. AUTHOR(s) Mark Fry		8. CONTRACT OR GRANT NUMBER(s) N00014-81-C-2267
9. PERFORMING ORGANIZATION NAME AND ADDRESS Science Applications, Inc. 1710 Goodridge Drive McLean, VA 22102		10. PROGRAM ELEMENT, PROJECT, TASK AREA & WORK UNIT NUMBERS
11. CONTROLLING OFFICE NAME AND ADDRESS Naval Research Laboratory 4555 Overlook Avenue, S.W. Washington, D.C. 20375		12. REPORT DATE June 1982 13. NUMBER OF PAGES
14. MONITORING AGENCY NAME & ADDRESS(if different from Controlling Office)		15. SECURITY CLASS. (of this report) UNCLASSIFIED 15a. DECLASSIFICATION/DOWNGRADING SCHEDULE

16. DISTRIBUTION STATEMENT (of this Report)

17. DISTRIBUTION STATEMENT (of the abstract entered in Block 20, if different from Report)

18. SUPPLEMENTARY NOTES

19. KEY WORDS (Continue on reverse side if necessary and identify by block number)

Airblast, shock waves, nuclear and conventional munitions, numerical algorithms, flux-corrected transport

20. ABSTRACT (Continue on reverse side if necessary and identify by block number)

The accomplishments achieved over the contract period are documented. Computational results for nuclear and conventional airblast are presented. Improvements in the numerical algorithms are discussed. Theoretical computation of shock waves is compared with available data.

DD FORM 1 JAN 73 1473 EDITION OF 1 NOV 65 IS OBSOLETE
S/N 0102-LF-014-6601

SECURITY CLASSIFICATION OF THIS PAGE (When Data Entered)

TABLE OF CONTENTS

SECTION I

GENERAL DISCUSSION

The SAI program in Nuclear Airblast Effects under contract number N00014-81-C-2267 has addressed the improvement of the numerical algorithms and the simulation of high-explosive and nuclear detonations. Significant improvement in the basic numerical algorithm, Flux Corrected Transport, FCT, has been achieved. In addition a nuclear height of burst, HOB, calculation and several high explosive detonation calculations were completed.

The nuclear airblast program began with a two-dimensional calculation of a 1-kiloton nuclear explosion detonated at 104 feet above the ground surface (Appendix A) Fortran Computer Code, FAST2D, which embodied the FCT algorithm JPBFCT (a derivative of ETBFCT (Boris, 1976) was used to predict the unsteady flow field. The calculation predicted the transition from regular to Mach reflection at a ground range approximately equal to the HOB. Comparisons to shock tube wedge experiments showed similarity in the flow fields (Appendix B). When compared to the best available data agreement was found to be within 20% for the high-over-pressure (regular reflection) region and within 10% in the double peaked (Mach) region.

Further HOB investigations lead to simulation of high explosive calculations. HE Blast wave phenomena include

reactive and two-phase flows associated with the motion of the chemical explosion products. Additionally, the existence of two shocks, contact discontinuity, and a rarefaction region make the HE simulation more difficult numerically and physically. (Appendix C) The FCT scheme in general represents an accurate and flexible class of methods for solving such nonsteady compressible flow problems. However, in models which treat all the physical effects required for blast wave simulation, truncation errors inherent in the underlying finite-difference scheme are exacerbated by nonlinear coupling between the fluid equations and by the greater complexity of the phenomena being simulated. The type of errors are the "terraces" which develop in the rarefaction regions. Elimination of these errors became necessary to accurately simulate the high explosive flow field. The solution was to improve the short wavelength phase and amplitude properties of the underlying algorithm.

Tests carried out on scalar advection of simple density profiles by a uniform flow field show that terracing does not require either diverging velocities or discontinuities in the profile, but appears typically (for $v > 0$) where the first and second derivatives of density have the same sign. In order to improve the properties of the basic difference scheme, we developed a new algorithm for integrating generalized continuity equations over a timestep δt. Consider the following three-point transport scheme:

$$\tilde{\rho}_j = \rho_j^o - \eta(\rho_{j+1}^o - \rho_{j-1}^o) + \kappa(\rho_{j+1}^c - 2\rho_j^c + \rho_{j-1}^c);$$

$$\bar{\rho}_j = \tilde{\rho}_j - \theta(\rho_{j+1}^o - \rho_{j-1}^o) + \lambda(\rho_{j+1}^o - 2\rho_j^o + \rho_{j-1}^o);$$

$$\rho_j^n = \bar{\rho}_j - \mu(\phi_{j+1/2} - \phi_{j-1/2}),$$

where

$$\phi_{j+1/2} = \tilde{\rho}_{j+1} - \tilde{\rho}_j.$$

The arrays $\{\rho_j^o\}$ and $\{\rho_j^n\}$ are the old and new densities, $\tilde{\rho}_j$ and $\tilde{\tilde{\rho}}_j$ are temporary intermediate densities, and η, θ, κ, Λ, and μ are velocity-dependent coefficients. Here κ and λ are diffusion coefficients, and μ is the antidiffusion coefficient. In the actual algorithm, $\phi_{j+1/2}^c$ is corrected (hence the name FCT) to a value $\phi_{j+1/2}^c$ chosen so no extrema in ρ_j^n can be enhanced or new ones introduced in ρ_j^n. Previous FCT algorithms had $\theta = 0$; the widely used ETBFCT and related algorithms (Boris, 1976) have in addition $\kappa = 0$. If we define ρ_j to be sinusoidal with wave number k on mesh with uniform spacing δx, so that $\rho_j^o = \exp(ij\beta)$ where $\beta = k\delta x$, then the new density array satisfies

$$\rho_j^n/\rho_j^o \equiv A = 1 - 2i(\eta+\theta)\sin\beta + 2(\kappa+\lambda)(\cos\beta - 1)$$
$$- 2\mu(\cos\beta - 1)[1 - 2i\eta\sin\beta + 2\kappa(\cos\beta - 1)].$$

From A we can determine the amplification $\alpha = A$ and relative phase error $R = (1/\varepsilon\beta)\tan^{-1}(-\mathrm{Im}A/\mathrm{Re}A)-1$, where $\varepsilon = v\delta t/\delta x$ is the Courant number. Expanding in powers of β we find

$$\alpha = 1 + \alpha_2\beta^2 + \alpha_4\beta^4 + \alpha_6\beta^6 + \ldots \quad ;$$

$$R = R_0 + R_2\beta^2 + R_4\beta^4 + R_6\beta^6 + \ldots \quad .$$

First-order accuracy entails making R_0 vanish, which requires that $\eta + \theta = \varepsilon/2$. Second-order accuracy ($\alpha_2 = 0$) implies that $\mu = \kappa + \lambda - \varepsilon^2/2$. Analogously, the "reduced-phase-error" property $R_2 = 0$ (Boris and Book, 1976) determines $\mu = (1-\varepsilon^2)/6$, thus leaving two free parameters. One of these can be used to make R_4 vanish also. The resulting phase error $R(\beta)$ is small not only as $\beta \to 0$, but also for larger values of β, corresponding to the short wavelengths responsible for terraces. The remaining parameter η can be chosen to relax the Courant number restriction needed to ensure positivity from $\varepsilon < 1/2$ to $\varepsilon < 1$. When coded, these changes necessitate a small increase in the operation count of ETBFCT along with a small increase in overhead to precalculate the two new arrays of velocity-dependent transport coefficients.

The technique described here improved the high explosive simulation considerably. The decrease in phase error reduced terracing dramatically (but did not completely eliminate it everywhere). Smoothing the velocity used in the advection

coefficients and the pressure used in the driving terms used in the advection coefficients and the pressure used in the driving terms completely eliminated the problem.

Next, a two-dimensional (2D) numerical calculation was performed to simulate one of Carpenter's (1975) height-of-burst experiments which used spherical 8-lb. charges of PBX 9404. The previous fine-zone 1D calculation was used to initialize the problem. It was mapped onto the 2D grid just prior to the onset of reflection. The solution was then advanced in time, with pressure being calculated from a real-air equation of state and a JWL equation of state for the combustion products. The front of the blast wave was captured in a finely gridded region which moved outward horizontally. Special care was taken to ensure that the grid moved smoothly. The resulting solution, particularly the curve of peak over-pressure vs. range, was in excellent agreement with Carpenter's experimental data. We believe that this calculation represents the most accurate simulation of the double-Mach-stem region that occurs when a spherical blast wave reflects from a planar surface which has thus far been carried out.

REFERENCES

Boris, J., "Flux-Corrected Transport Modules for Generalized Continuity Equations," NRL Memo Report 3327 (1976).

Carpenter, H.J., Proc. Fourth International Symp. on Military Applications of Blast Simulation (1974).

APPENDIX A

Transition to Double Mach Stem for Nuclear Explosion at 104 Ft Height of Burst

NRL Memorandum Report 4630

Transition to Double Mach Stem for Nuclear Explosion at 104 Ft Height of Burst

M. FRY

Science Applications, Inc.
McLean, VA 22102

J. M. PICONE, J. P. BORIS, AND D. L. BOOK

Laboratory for Computational Physics

November 17, 1981

This work was supported by the Defense Nuclear Agency under Subtask Y99QAXSG, work unit 00001, and work unit title "Flux-Corrected Transport."

NAVAL RESEARCH LABORATORY
Washington, D.C.

SECURITY CLASSIFICATION OF THIS PAGE (When Data Entered)

REPORT DOCUMENTATION PAGE	READ INSTRUCTIONS BEFORE COMPLETING FORM
1 REPORT NUMBER: NRL Memorandum Report 4630	2 GOVT ACCESSION NO. / 3 RECIPIENT'S CATALOG NUMBER
4 TITLE (and Subtitle): TRANSITION TO DOUBLE MACH STEM FOR NUCLEAR EXPLOSION AT 104 FT HEIGHT OF BURST	5 TYPE OF REPORT & PERIOD COVERED: Interim report on a continuing NRL problem. / 6 PERFORMING ORG REPORT NUMBER
7 AUTHOR(s): M. Fry*, J. M. Picone, J. P. Boris, and D. L. Book	8 CONTRACT OR GRANT NUMBER(s)
9 PERFORMING ORGANIZATION NAME AND ADDRESS: Naval Research Laboratory, Washington, DC 20375	10 PROGRAM ELEMENT, PROJECT, TASK AREA & WORK UNIT NUMBERS: 44-0578-0-1
11 CONTROLLING OFFICE NAME AND ADDRESS: Defense Nuclear Agency, Washington, DC 20305	12 REPORT DATE: November 17, 1981 / 13 NUMBER OF PAGES: 71
14 MONITORING AGENCY NAME & ADDRESS(if different from Controlling Office)	15 SECURITY CLASS. (of this report): UNCLASSIFIED / 15a DECLASSIFICATION/DOWNGRADING SCHEDULE

16 DISTRIBUTION STATEMENT (of this Report)

Approved for public release; distribution unlimited.

17 DISTRIBUTION STATEMENT (of the abstract entered in Block 20, if different from Report)

18 SUPPLEMENTARY NOTES

*Present address: Science Applications, Inc., McLean, VA 22102

This work was supported by the Defense Nuclear Agency under Subtask Y99QAXSG, work unit 00001, and work unit title, "Flux-Corrected Transport."

19 KEY WORDS (Continue on reverse side if necessary and identify by block number)

Double Mach stem
Height-of-burst (HOB)
Flux-corrected transport (FCT)
High-over-pressure

20 ABSTRACT (Continue on reverse side if necessary and identify by block number)

A nuclear height-of-burst (HOB) calculation has been performed using a two-dimensional flux-corrected transport (FCT) code. The calculation predicts the transition from regular to Mach reflection at ground ranges approximately equal to the HOB. The characteristics of the resulting waveforms are basically the same as those found in shock tube experiments when planar shocks reflect from wedges, and appear highly regular. In the double-Mach reflection region the first Mach stem is observed to toe out markedly compared with the planar case. In the high-over-pressure (regular reflection) region initialization errors and inadequate resolution caused pressure peaks to appear too low by about 20%. In the Mach reflection region the peak pressures are in good agreement with experimental data.

DD FORM 1 JAN 73 1473 EDITION OF 1 NOV 65 IS OBSOLETE
S/N 0102-014-6601

SECURITY CLASSIFICATION OF THIS PAGE (When Data Entered)

CONTENTS

TRANSITION TO DOUBLE MACH STEM FOR NUCLEAR EXPLOSION AT 104 FT HEIGHT OF BURST

I. INTRODUCTION

In a nuclear height-of-burst (HOB) detonation the spherical blast wave reflects from the ground, initially producing a regular reflection region. When the shock reaches a ground range approximately equal to the HOB an abrupt transition to Mach reflection occurs. This transition is responsible for an airblast environment more severe than the surface burst nuclear case. Qualitatively, it can be thought of as a partial flow stagnation in the Mach region that leads to the production of two static pressure peaks.

A 1 Kiloton (1 KT) atmospheric nuclear explosion at a HOB of 104 feet has been simulated using the two dimensional FAST2D code (Ref .1). Figure 1 illustrates the shock structure. The calculation predicts the transition of the shock from regular reflection to double Mach reflection. Because the spherical waves are expanding and thus decreasing in Mach number as well as angle of incidence with the ground, they create a dynamic Mach stem formation. In comparision to planar shocks on wedges one finds them to be qualitatively alike. The appearance of double peaks in the pressure and density profiles (versus time and distance) is interpreted as the point of transition. Other interesting phenomena such as the rollup of the contact surface generating a vortex ring and the associated phenomenon of toeing out of the first Mach stem can be observed.

The ability of the calculation to accurately predict the gasdynamic effects both temporally and spatially is due in part to the shock capturing and adaptive rezone features of the FAST2D code. A minimal number of very fine zones was placed around the shock front and these zones then moved with the first Mach stem to prevent shock smearing and distortion. This calculation is the first attempt to model the nuclear HOB case through the use of a Flux-Corrected Transport (FCT) algorithm (Ref. 2).

Manuscript submitted August 24, 1981.

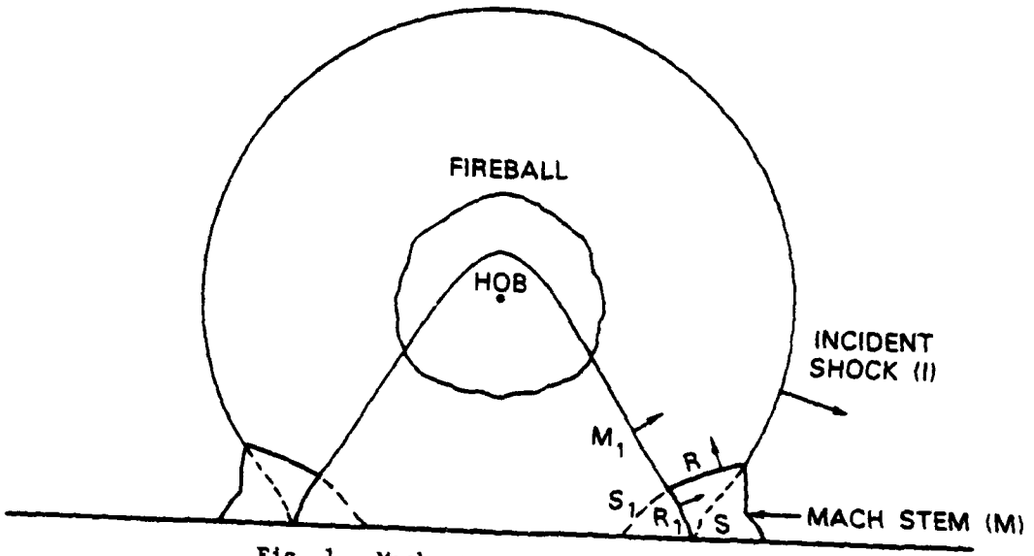

Fig. 1 - Mach stem structure from HOB

The results of this calculation agree well with the pressure-distance curve generated by the high explosive (HE) data of Carpenter (Ref. 3) and the analysis of Kuhl (Ref. 4). The peak overpressure of the first shock at the time of transition is about 4300 psi. Our simulation was run to 11.6 ms (total time with t_o = 3.76 ms), which corresponds to pressure peaks of about 2000 psi. In the regular reflection region the peak values tend to be about 20% low due to the clipping of the FCT algorithm and inaccuracies in the initialization of the flow. Reducing the minimum zone size from 5 cm to 1 cm in a one-dimensional test calculation eliminated this discrepancy, however. In the two-peak regions the agreement between the experimental data and the values presented here is very good. The resolution of the calculation is adequate for studying qualitatively the characteristics of the flow field. For future work we recommend that the transition region be explored with improved resolution.

II. DESIGN OF PROBLEM

The problem of a 1-KT nuclear detonation at 104 ft (31.7m) HOB was chosen since it can be scaled conveniently to various HE tests. The use of the 1KT standard is also expendient; one could, however, have used realistic initial conditions, such as the Los Alamos Scientific Laboratory RADFLO or Air Force Weapons Laboratory (AFWL) SPUTTER calculations. A simple constant ambient atmosphere was used with a density of 1.22×10^{-3} g/cm^3 and pressure 1.01×10^6 dyne/cm^2. To relate the energy and mass densities to the pressure, a real-air equation of state (EOS) was used. This "table-lookup" EOS is derived from Gilmore's data (Ref. 5.) and has been vectorized for the TI Advanced Scientific Computer at NRL (Ref. 6). Figure 2 illustrates the effective gamma versus specific energy per unit mass for different values of the density. The internal energy density used in the call to the EOS is found by subtracting kinetic energy from the total energy; this can be negative due to phase errors in the fluid variables. When this occurs, the value of the pressure is reset to zero.

The transition from regular reflection to double Mach reflection is known to occur at a ground range approximately equal to the HOB. Therefore, the size of the mesh should be roughly twice the HOB in both directions. The upper boundary should be far enough away from the blast front to be noninterfering. We set the boundaries at 5.5×10^3 cm for the radial direction and 1.035×10^4 cm for the axial direction. The fine grid in the radial direction contained 140 out of 200 total zones, each 5 cm in length. The largest zones initially filled the right section of the grid and were 80 cm in length. A smoothing involving 40 zones was performed between the region to guarantee that the zone sizes varied slowly. In the vertical direction the fine grid contained 75 out of 150 total zones, each 5cm in length. Beyond that region the zones increased geometrically by a factor of 1.112.

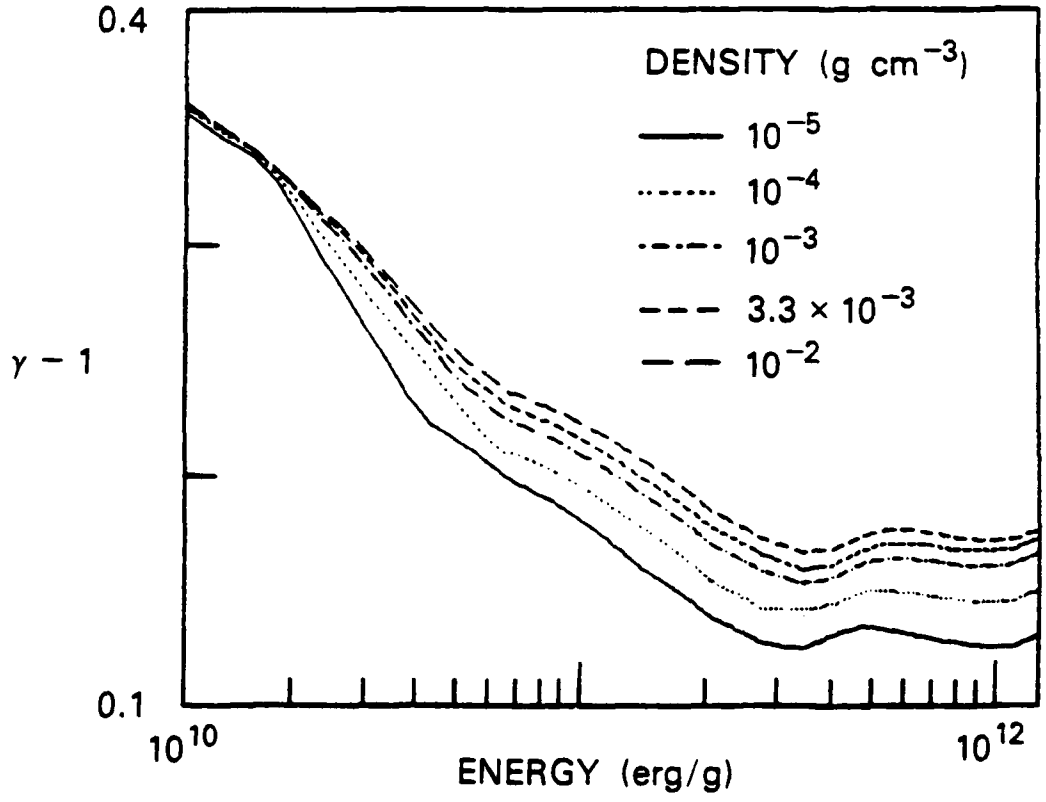

Fig. 2 - Gamma -1 vs. specific energy for Air EOS

Placement of the fine grid at the origin (ground zero - the point at which first reflection occurs) was determined to be optimum for capturing peak pressures in the airblast wave front. Thus, as the expanding wave moved along the ground surface, the fine grid was always locked to it, and each point along the incident blast front encountered the same spatial gridding as it approached the ground. By treating each point of the incident front in the same manner, we insured that the calculation was internally consistent and that the computed transition point was accurate to within the limits of the resolution. Finally, we point out that, as a section of the incident blast wave propagated within the fine grid, the wave steepened. The size of the fine grid was sufficient to insure that the incident wave had reached the maximum steepeness prior to intersecting the ground.

The initialization provides a strong shock with Mach number $M_I = 12$. This speed and the need for restart capability led to the choice of 200 timesteps as an interval for the spatial display ("snapshots"). The dump interval that resulted was $\sim \Delta t = 0.3$ milliseconds. These dumps were stored on magnetic tape and postprocessed.

Additional diagnostics were implemented in the calculation. Stations were created to gain information from fixed spatial positions within the calculational grid. These 25 physical variable sensors were placed along the ground and stored values of the energy and mass densities and velocity for every timestep. From this information one can construct static and dynamic pressure curves.

III. COMPUTATIONAL DETAILS

The evolution of the nuclear HOB flow field was modeled numerically with the FCT code FAST2D (Ref. 7). FCT yields accurate and well-resolved descriptions of shock wave propagation without the necessity of a priori knowledge of the essential gasdynamic discontinuities in the problem. Additionally, the code has a general adaptive regridding capability which permits fine zones to be concentrated in the region of greatest physical interest while the

remainder of the system is covered with coarse zones. Figure 3 depicts the grid setup initially and at transition to the double Mach stem structure. The rezone algorithm is programmed to track the Mach stem with the fine grid.

The transport algorithm used a low-phase-error phoenical FCT algorithm in a model called JPBFCT, an advanced version of the ETBFCT algorithm described in Ref 1. The linear part of this algorithm is fourth-order accurate spatially in advection problems with a given constant velocity and has a (nonlinear) flux-corrected antidiffusion needed to model shocks correctly. Finally, the transport subroutine is written in sliding-rezone form, which means that the mesh at the beginning and the end of the timestep need not be the same. Since the algorithm is one-dimensional, timestep splitting is employed to solve the 2-D problem.

The fluid transport routine JPBFCT is fully vectorized and requires about 2 μs per meshpoint-cycle. This time would have been still less if a vectorized fully two-dimensional routine had been used, since the 1-D loops are too short to permit full advantage to be taken of the vector capabilities of the NRL ASC. The table lookup in the EOS was also fully vectorized, so that pressure calculations required about 20% of the time needed for the hydrodynamics. These two items took up nearly all of the running time in the blast calculation itself. The cost of initialization was negligible, but the diagnositics cost up to 30% as much as the hydrodynamics, depending on how many of the various possible quantities were actually plotted. This latter number would be greatly reduced if the plot routines were fully vectorized.

A version of the AFWL 1 KT standard (Ref 8) was used to initialize the energy, density and velocity (flow field) at 3.76 milliseconds. The corresponding shock radius was 103.9 ft (31.69 m) peak overpressure of 1645 psi (1.134×10^4 K Pa). Because some areas of the grid were very coarse, interpolation onto the grid was performed. After the 1 KT flow was laid down inside a radius of 104 feet (31.7 m) the fine-zoned grid was activated to follow the peak pressure as it moved along

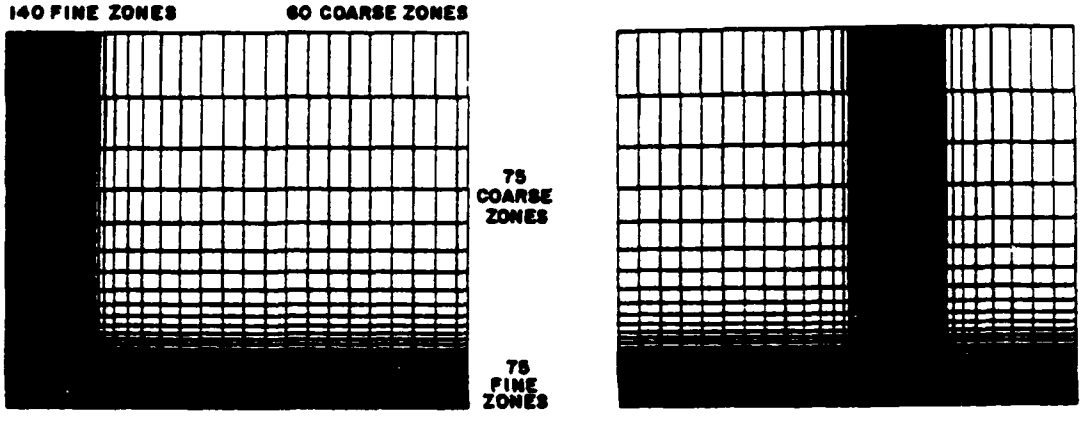

Fig. 3 - Adaptive gridding. The grid at initialization and at transition point (lines are drawn for every other zone, lines in fine-zone region are indistinguishable).

the ground surface, modelled as a perfectly reflecting boundary. This region comprised 140 zones, and a switch was set to keep 40 of these zones ahead of the reflection point. Permeable boundary conditions were used on the top and right edges of the mesh; i.e., density, pressure and velocity were set equal to ambient preshock conditions. Reflecting conditions were applied to the left and bottom.

The timestep was recalculated at every cycle according to the Courant condition

$$dt = 0.5 \min_{i,j} \frac{(\Delta x_i, \Delta y_j)}{(c+|V|)_{ij}} , \qquad (1)$$

where c is the speed of sound and $|V|$ is the modulus of the flow speed. This could have been relaxed somewhat by allowing violation of the local Courant limit at points ("hot spots") far from the region of chief physical interest. The total elapsed time in the 2-D calculation, 7.6 ms, required 5600 cycles.

Three types of diagnostics were employed, all in the form of plots made by post processing a dump tape. The first type of diagnostic consisted of CRT contour plots of density and static pressure, and arrows indicating the magnitude and direction of the velocity field, obtained at the dump intervals (every 200 cycles). The second type was pressure-range curves at z=0, obtained by finding the pressure peak(s) along the ground at each dump interval and hand-plotting them on the same graph. The third type consisted of pressure histories at a series of 24 stations, obtained by saving the energy and mass densities and the velocities at every cycle.

IV. RESULTS AND PHENOMENOLOGY

This calculation has been done to understand the violent effects of 1 KT of energy being released in the atmosphere at a HOB of 104 ft (31.7m). A strong spherical shock is created in the surrounding air, and reflects from the ground.

The outward-traveling airblast is then composed of two parts: one reflected upward approximately normal to the ground, and the original spherical blast. The peak pressure is coincident with the intersection of the two waves. This intersection continues to move outward until the angle of the spherical shock with respect to the ground reaches a critical value and the transition to a double Mach stem occurs. As shown by Ben-Dor and Glass (Ref. 9), this angle depends upon the incident strength of the shock (Fig. 4). Shocks with Mach numbers greater than 10 are not shown. Initially, the Mach number for the HOB simulation is well above 10. The Mach number at transition is approximately 11 and the angle is less than 50°. From Fig. 4 the corresponding region is double Mach reflection.

Figure 1 has been labeled with the notation of Ben-Dor and Glass (Ref. 9). It should be noted that what is generally regarded as the second Mach stem is in fact the second reflected wave, which is part of the second Mach structure. To be consistent, one must label the second Mach stem as M_1 at the indicated location. The definition used is the state of the fluid one obtains by passing through one shock wave (M_1) or two shock waves (R and R_1). The first reflected wave R becomes the incident wave for the second Mach structure. Density contours are shown in Fig. 5 for an planar shock on wedge with a Mach number of 7 and an angle of 50°. The complimentary figure illustrates the proper labeling of the multiple waves. Comparison of Fig. 5 and the HOB simulation (Fig. 6) shows that corresponding waves can be identified. Differences between the planar shock on wedge and the HOB can be explained in terms of the unsteady nature of the HOB case (a spherically expanding wave that continuously decreases in Mach number and angle.) Although the term irregular Mach reflection has been used to describe the complex shock structure that evolves from HOB events, we believe it to be very regular and explainable as a double Mach reflection that evolves as a function of time.

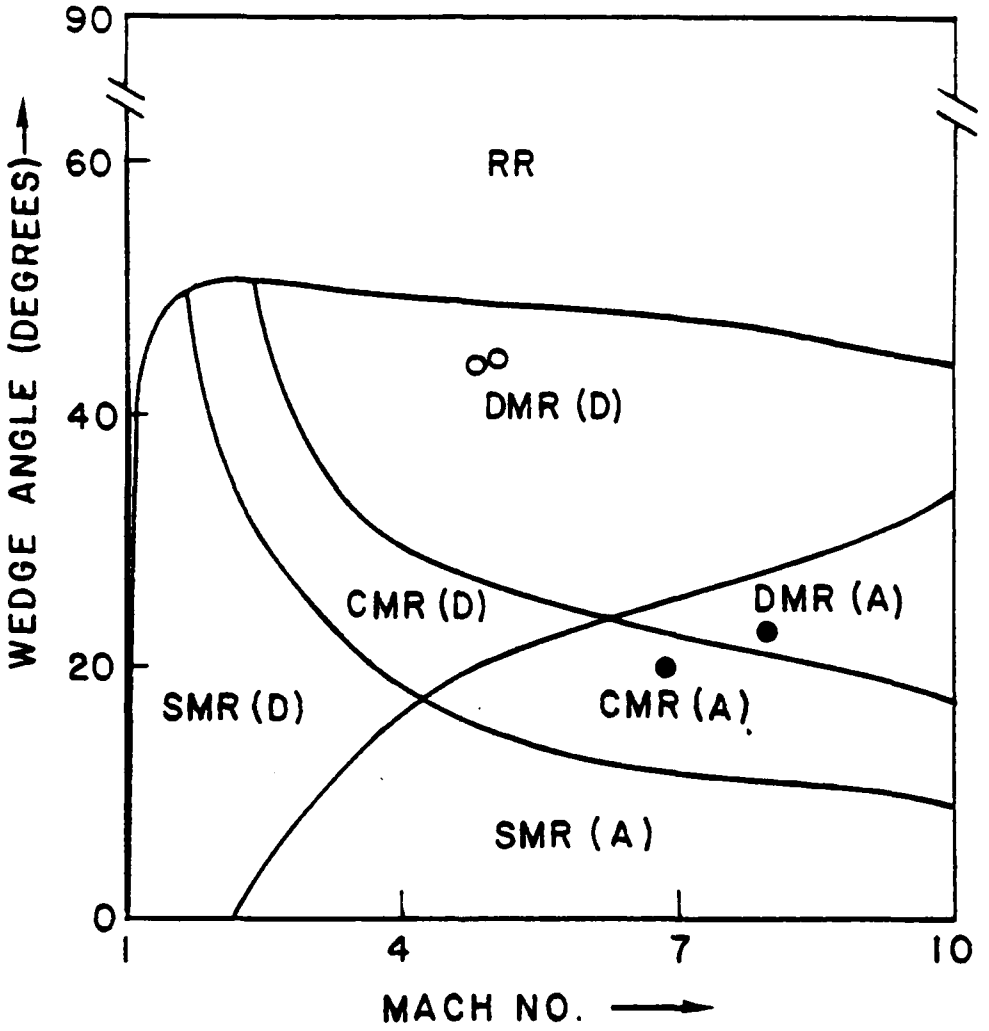

Fig. 4 - Types of shock reflection: RR, CMR, SMR, and DMR denote regular reflection and single, complex and double mach reflection, respectively. The D and A refer to attached and detached shocks.

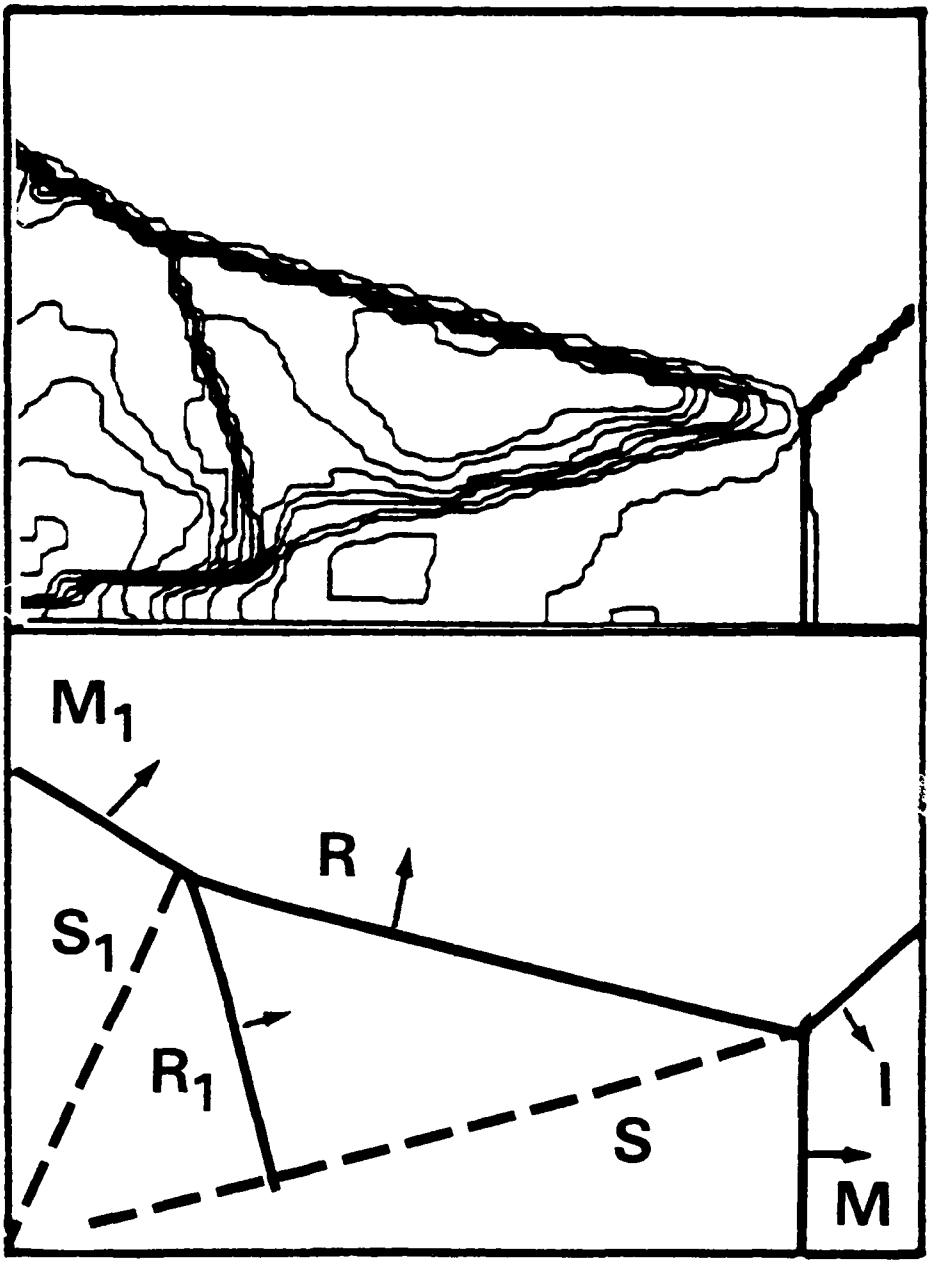

Fig. 5 - Planar shock (Mach 7) on 50° wedge with wave identification

The HOB numerical simulation begins just before the shock first reflects from the ground. As a summary of how the flow field then develops, we present snap-shots at the important stages. (A more complete display is presented in Appendix A). Figure 6a indicates the pressure and density contours and velocity vectors at t = 3.18 ms. In Fig. 6b the reflected shock is shown moving upward, the outward flow begins to stagnate at the ground (transition). Fig. 6c, at t = 5.99 ms, shows an enlargement of the shock front, and the development of the Mach stem, slip surface and second Mach stem. The angle of the shock with respect to the ground is increasing with time, so that the effective wedge angle is decreasing. From the work of Ben-Dor and Glass one expects a transition to double Mach stem to occur at approximately 45°. The angle in Fig. 6b is about 45° and the shock front has entered the transition phase. Figure 6d shows the fully developed shock structure at 7.79 ms. Toeing out of the first Mach stem can be also seen in the contours of Fig. 6d and occurs as the fluid rolls forward where the slip line would otherwise intersect the ground. The velocity field in Fig. 6d also shows this detail.

Note the reflected shock properties (that part of the structure that contains the second Mach stem M_1). The reflected shock propagates rapidly through the high temperature fireball, due to the high local sound speed. The shape of this reflected wave is a primary difference between the HOB case and the planar wave on wedge case. The other major difference, of course, is the spherically expanding blast wave which decreases in strength approximately as r^{-2}.

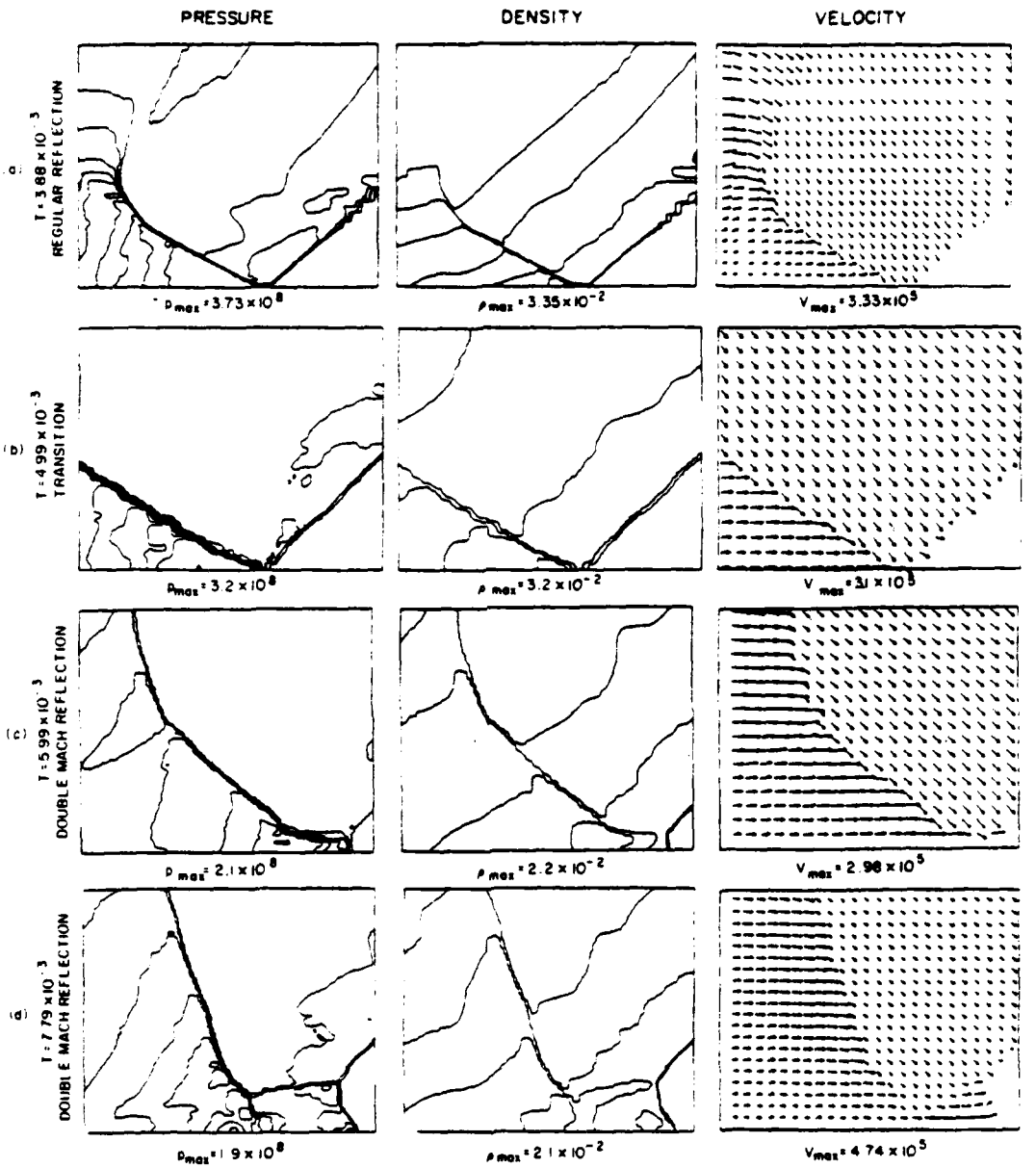

Fig. 6 - Pressure, density, and velocity fields for HOB calculation (a) in regular reflection state; (b) at transition to Mach reflection; (c) shortly afterward, when second peak has become larger than first; and (d) fully developed (note toe at base of first Mach stem). Units in cgs.

An effective way to quantitatively evaluate the calculation and observe in detail the transition to a Mach stem regime can be seen by examining the station data. The station sensors were placed in the bottom row of the calculation 100 to 200 cm apart. In Table I the maximum pressure recorded for each station along with the location can be found.

Besides giving a reliable value for the peak pressure to be used for constructing the pressure-distance curve, these data allow one to see effects fixed in space but varying in time. Figure 7 is a superposition of the pressure profiles from stations 15 to 24 (the transition region). Noteworthy is the profile from station 17, which is the first station to record a second peak on the back side. At station 19, 200 cm further away from ground zero, the second peak is almost equal to the first. The visible transition (as seen in Fig. 6b, occurs at a ground range between 3100 cm and 3300 cm (stations 19-21) revealing a dominant second peak and a "first peak" (i.e., first seen by the sensor) that is about half the magnitude of the second. The second peak does not exhibit a sharp almost discontinuous rise and then a rapid but slower decrease along the back side. Instead, it has the appearance of a density compression. This behavior has dramatic consequences for military planners because the pressure-distance curve is modified and the dynamic pressure is enhanced.

The analogous profiles for dynamic pressure are presented in Fig. 8. Again data from stations 15 to 24 is utilized. The development of the second peak and its correlation with the Mach stem formation can be observed. There is, in addition, a noticeable increase in the first peak values (station 15 to the maximum at station 18). After the structure becomes visibly resolved (station 20 and beyond) the second peak resembles a rounded profile suggesting the formation of a stagnation region behind the first peak (Mach stem).

Table 1

Station No.	Location (cm)	Time (sec)	Pres (dynes/cm^2)
1	2.0000E 02	2.25E-04	8.11E 08
2	4.0000E 02	2.80E-04	7.92E 08
3	8.0000E 02	5.28E-04	7.17E 08
4	1.0000E 03	7.23E-04	6.73E 08
5	1.2000E 03	9.54E-04	6.24E 08
6	1.4000E 03	1.23E-03	5.65E 08
7	1.6000E 03	1.54E-03	5.21E 08
8	1.8000E 03	1.91E-03	4.70E 08
9	2.0000E 03	2.34E-03	4.54E 08
10	2.2000E 03	2.81E-03	4.14E 08
11	2.3000E 03	3.07E-03	4.03E 08
12	2.4000E 03	3.35E-03	3.92E 08
13	2.5000E 03	3.62E-03	3.82E 08
14	2.6000E 03	3.88E-03	3.73E 08
15	2.7000E 03	4.19E-03	3.37E 08
16	2.8000E 03	4.48E-03	3.33E 08
17	2.9000E 03	4.79E-03	3.05E 08
18	3.0000E 03	5.11E-03	3.01E 08
19	3.1000E 03	5.41E-03	2.33E 08
20	3.2000E 03	6.06E-03	1.96E 08
21	3.3000E 03	6.49E-03	1.79E 08
22	3.4000E 03	6.82E-03	1.87E 08
23	3.5000E 03	7.28E-03	1.85E 08
24	3.6000E 03	7 .73E-03	1.69E 08

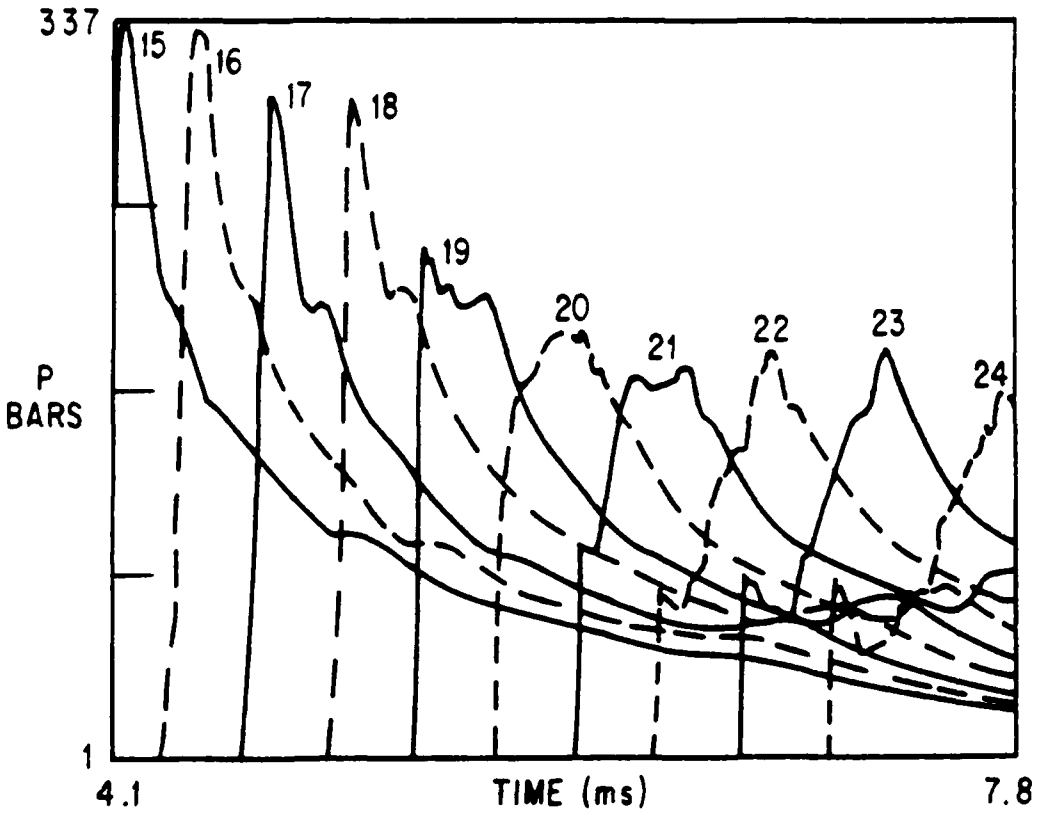

Fig. 7 - Station pressure data (nos. 15-24)

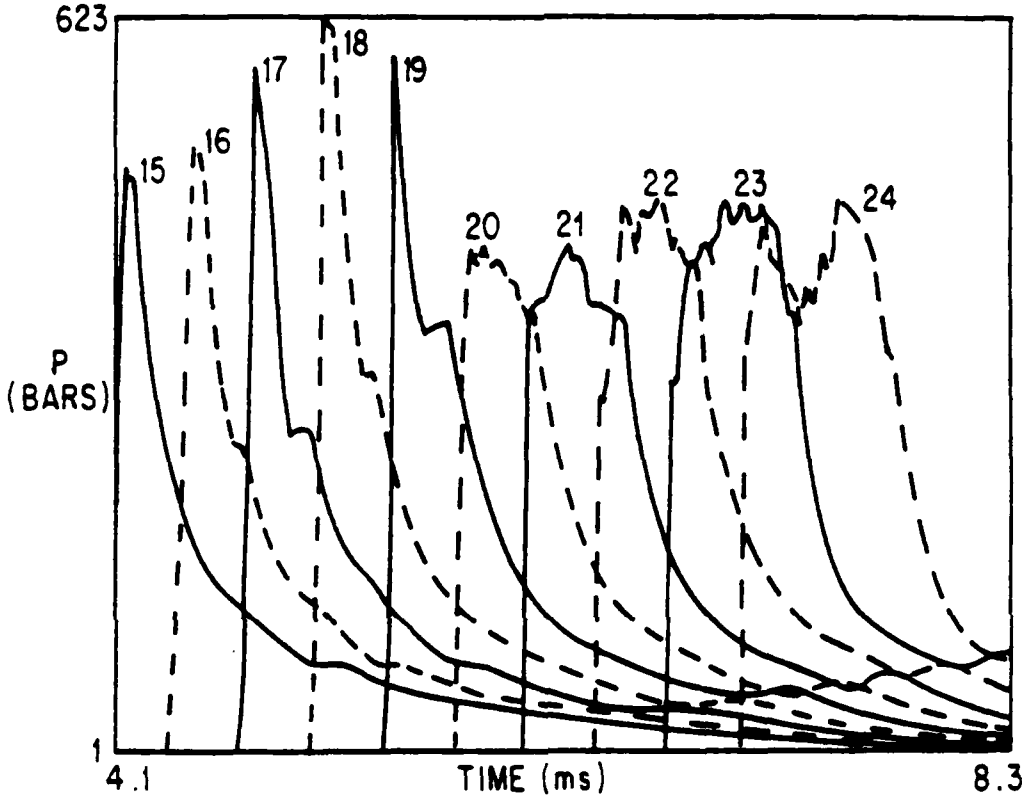

Fig. 8 - Station dynamic pressure data (nos. 15-24)

Finally we consider the pressure-distance relation for the HOB case. In Fig. 9 we compare the results of the numerical simulation with the data of Carpenter and with empirical analysis. Carpenter's data are based upon careful HOB experiments with 8 lb PBX9404 spheres. The empirical analysis was based on a 1 KT nuclear free air curve and HOB construction factors. The calculated values in the regular reflection regime are 20% low, which may be attributed to a combination of FCT clipping, the resolution of the grid, and inaccuracies in the initialization of the flow field. During and after Mach reflection, the peaks remain low until the Mach stem structure has grown large enough to be resolved on the mesh. By the time it occupies a region of 15 cells high and 35 cells wide, the peak pressures are in good agreement with the HE data and the empirical analysis.

Other attempts to model the transition region have been made. Needham and Booen (Ref. 10) present results of a 1100 lb pentolite sphere at 15 feet HOB. The general phenomena of the flow field can be seen from their simulation. When a pressure distance curve is constructed from this calculation, one finds that in the regular reflection region their results are 15% to 30% high relative to theory. After transition to double Mach reflection the first peaks are 20% low while the second peaks are 40% low (Ref. 4).

V. SUMMARY

The airblast from a 1KT nuclear event at 104 ft HOB has been numerically simulated with the FAST2D computer code. The results give insight to the formation and subsequent evolution of the Mach stem, the triple point, and the contact discontinuity. The transition from regular reflection to double Mach reflection is predicted. We suggest that the first signal for

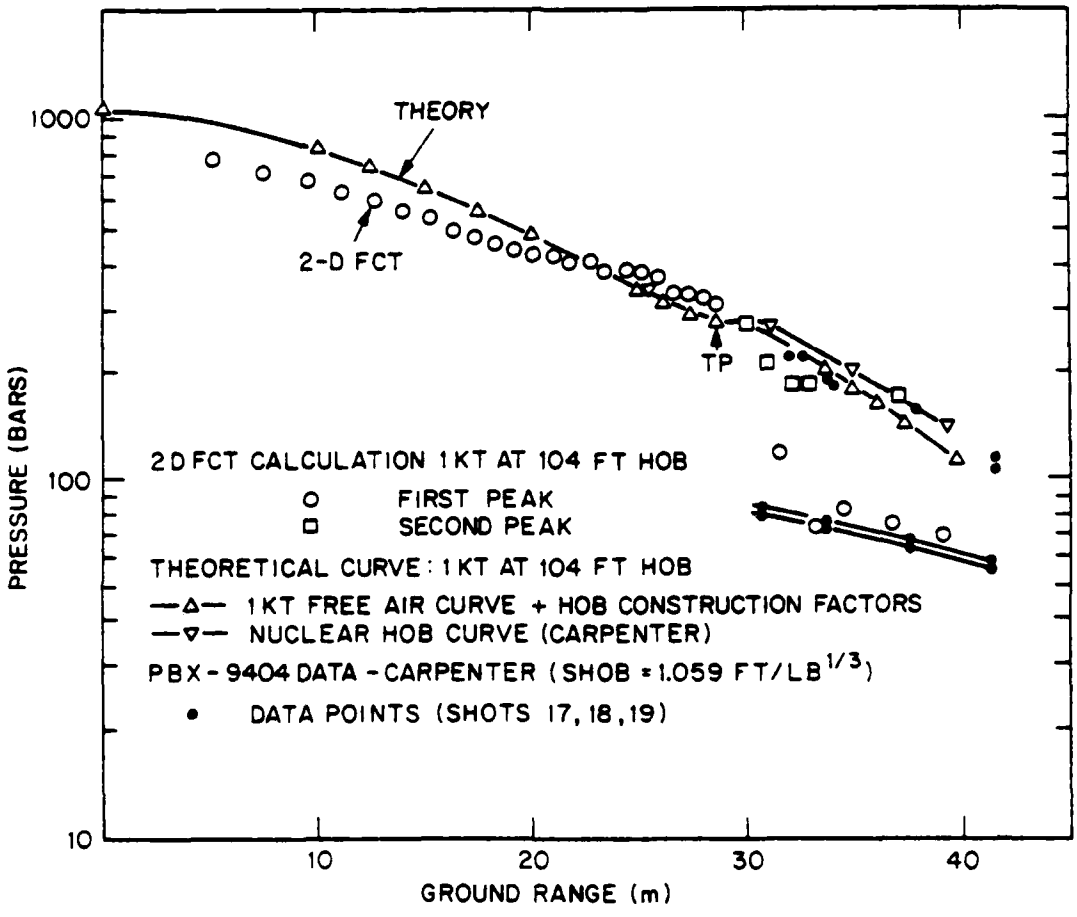

Fig. 9 - Pressure-range curves for first and second (after transition - denoted by TP - to double Mach reflection) peaks

transition is the appearance of a second peak behind the shock front due to stagnation in the flow. Comparison with the pressure-distance curves of Carpenter and Kuhl indicates agreement within 20%. Both first and second peaks are predicted with similar accuracy.

ACKNOWLEDGEMENT

We are grateful to Dr. Allen Kuhl of R&D Associates for his valuable advice and technical guidance.

This work was supported by the Defense Nulcear Agency under Subtask Y99QAXSG, work unit 00001, work unit title, "Flux-Corrected Transport."

References

1. Boris, J.P., Flux-Convected Transport Algorithms for Solving Generalized Continuity Equations, NRL Report #3237 (1976)

2. Boris, J.P., Book, D., "Flux-Corrected Transport I: SHASTA, a Fluid Transport Algorithm that Works", J. Comp. Phys., 11, 38 (1973).

3. Carpenter, H.J., Height-of-Burst Blast at High Overpressure, 4tn International Symposium on Military Applications of Blast Simulation (1974).

4. Kuhl, A. (Private Communication,1981).

5. Gilmore, F.R., "Equilibrium Composition and Thermodynamic Properties of Air to 24,000°K", RM-1543 (Aug 1955).

6. Young, T.R. (Private Communication,1981).

7. Book, D., Boris, J., Kuhl, A., Oran, E., Picone, M., and Zalesak, S. Simulation of Complex Shock Reflections from Wedges in Inert and Reactive Gaseous Mixtures, Proceedings of Seventh International Conference on Numerical Methods in Fluid Dynamics, Springer-Verlag, Stanford, 1980.

8. Needham, et al.,AFWL 1 KT Nuclear Airblast Standard, AFWL TR-73-55, Air Force Weapons Laboratory (April 1975).

9. Ben-Dor., Glass I.I., Domains and Boundaries on Non-Stationary Oblique Shock-Wave Reflections, I. Diatomic Gas, J. Fluid Mechanics, Vol. 92, Pt. 3, pp. 459-496 (1979).

10. Booen, M.W., and Needham, C.E., Two Dimensional Hull Code Simulation of Complex and Double Mach Reflections, Technical Note No. NTE-TN-81-001, Air Force Weapons Laboratory, New Mexico, January 1981.

APPENDIX A. DETAILED TIME HISTORY OF CALCULATION

The following figures comprise a temporal history of the numerical simulation. Each page contains pressure contours, velocity vectors, density contours, and the corresponding grid for a particular time. The series begins at $t_o = 0$ ($t_I = 3.76$ ms) and continues to $t_F = 8.28$ ms.

1 kt AT 104 ft HOB

TIME = 0.0 msec

CYCLE = 0

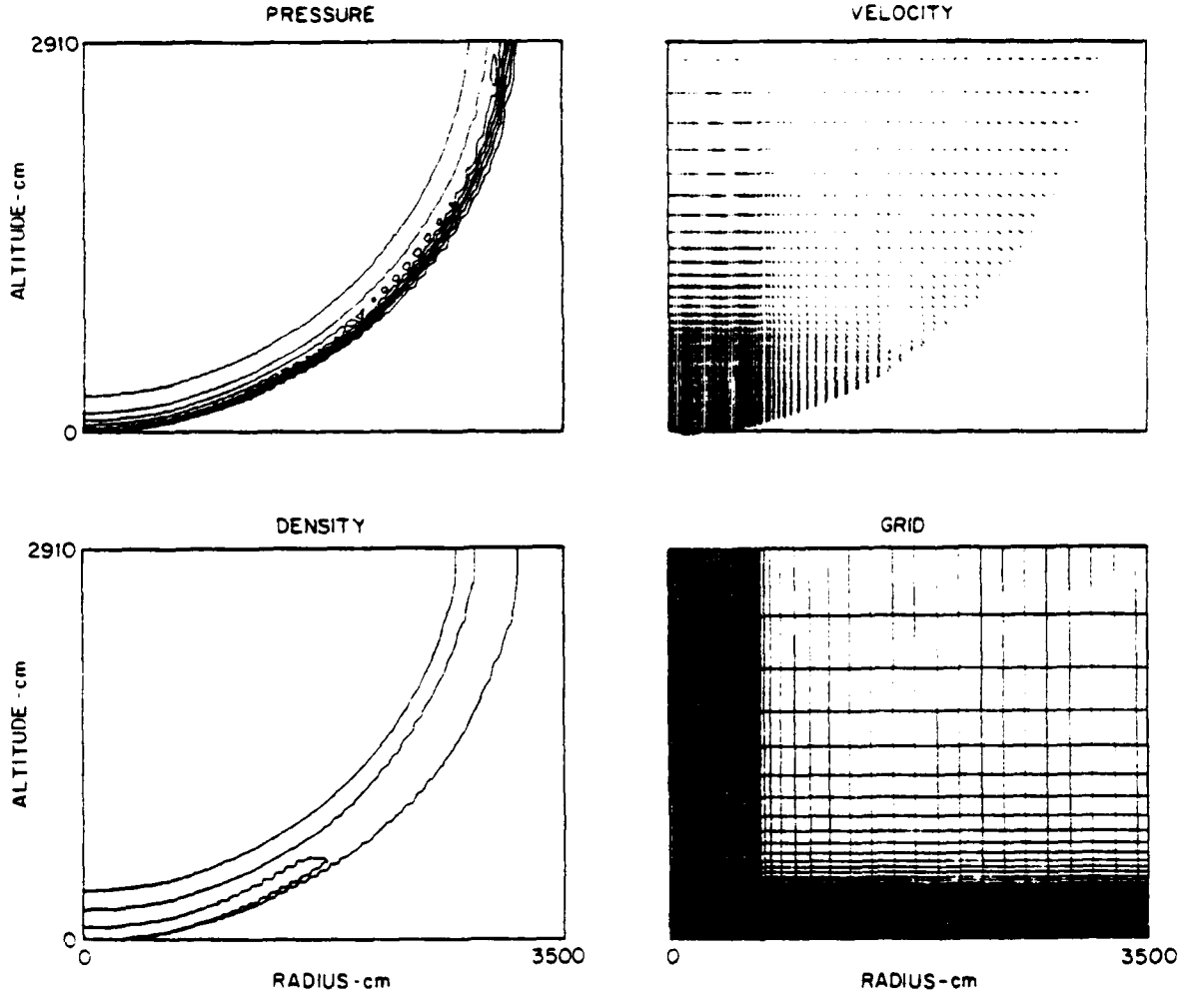

1 kt AT 104 ft HOB

TIME = 0.34 msec

CYCLE = 400

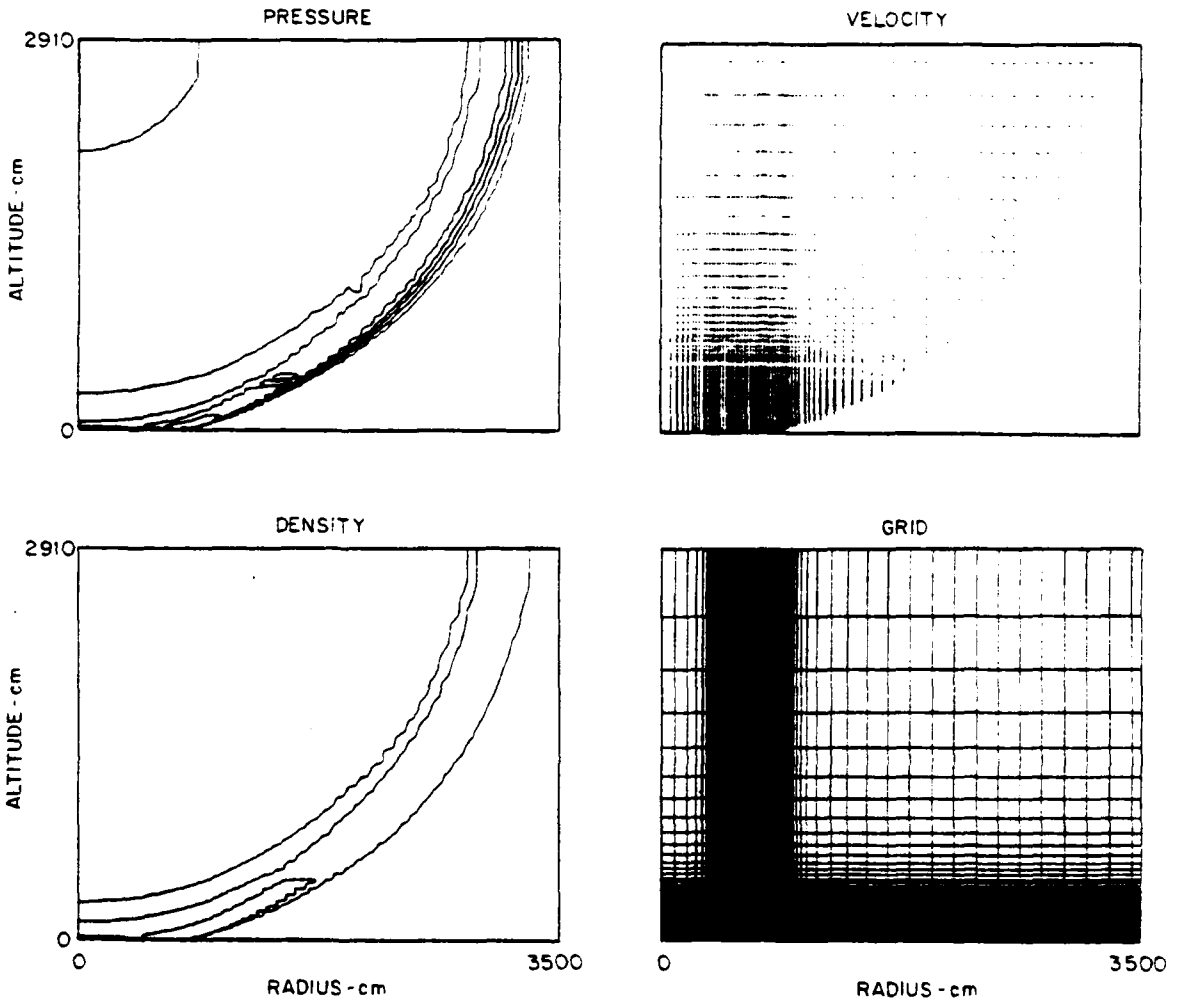

1 kt AT 104 ft HOB

TIME = 0.91 msec

CYCLE = 800

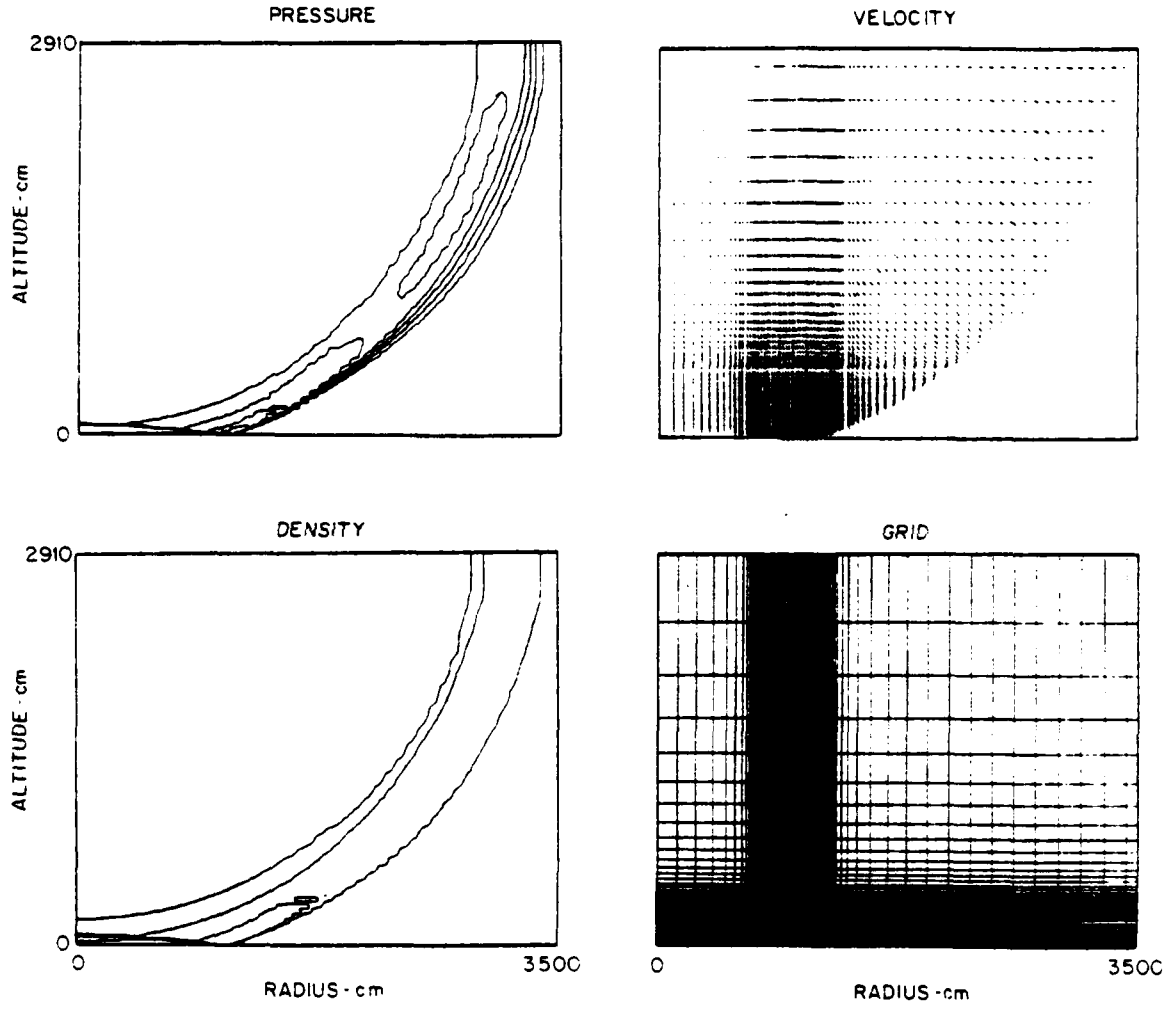

1 kt AT 104 ft HOB

TIME = 1.05 msec

CYCLE = 1200

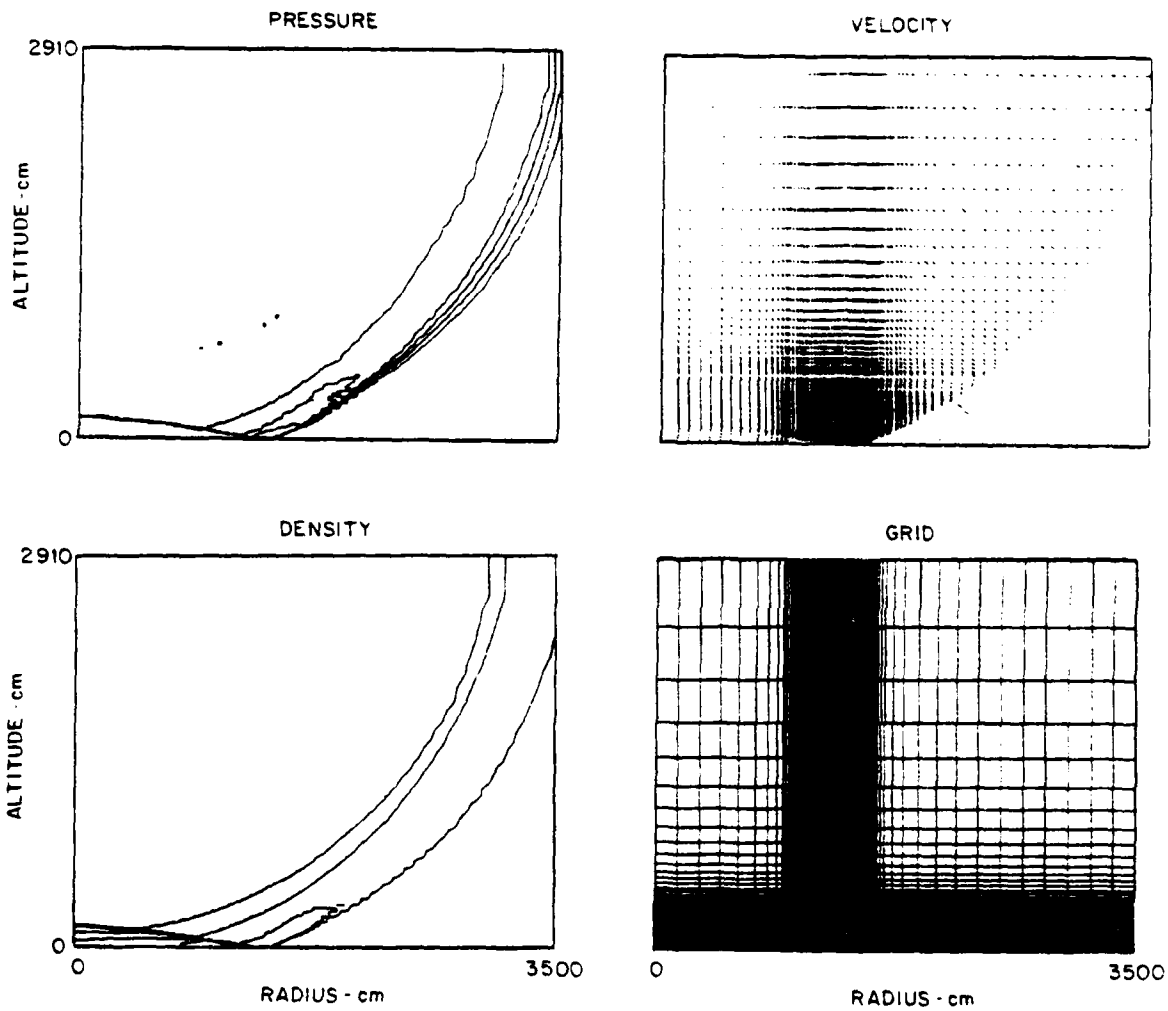

1 kt AT 104 ft HOB

TIME = 1.42 msec

CYCLE = 1600

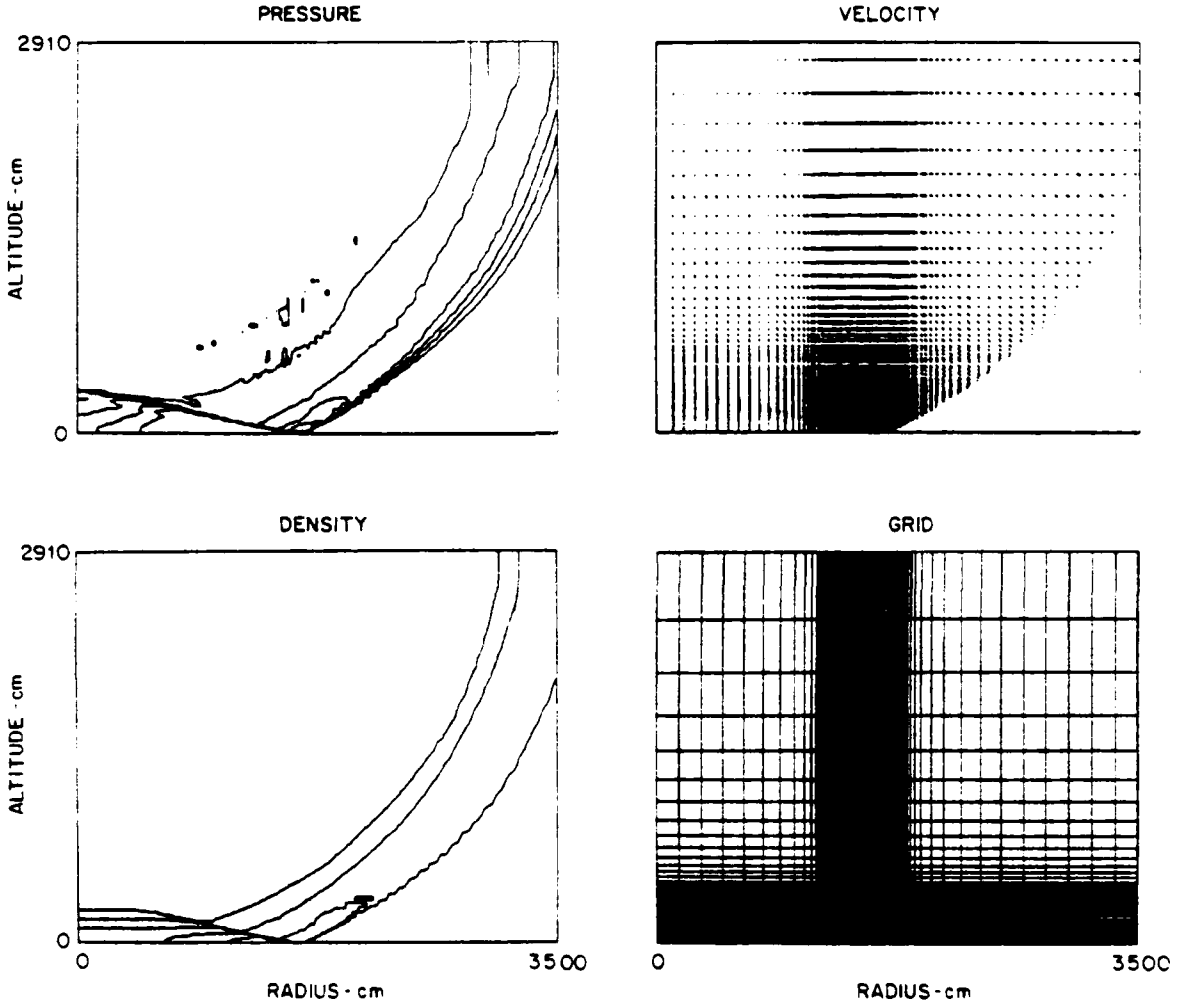

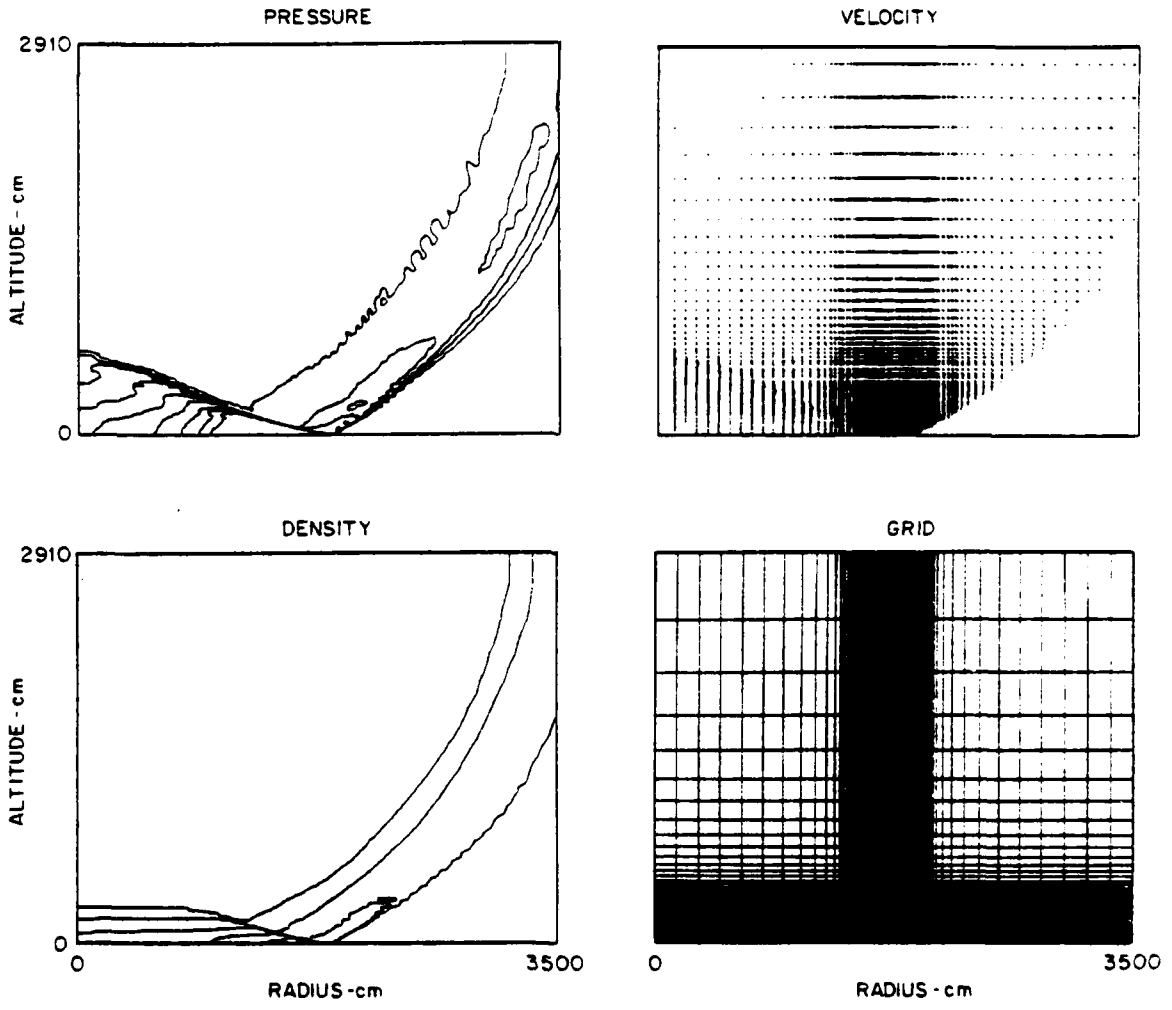
1 kt AT 104 ft HOB
TIME = 1.80 msec
CYCLE = 2000
PRESSURE
VELOCITY
DENSITY
GRID
2910
0
ALTITUDE - cm
0
3500
RADIUS - cm

1 kt AT 104 ft HOB

TIME = 2.20 msec

CYCLE = 2400

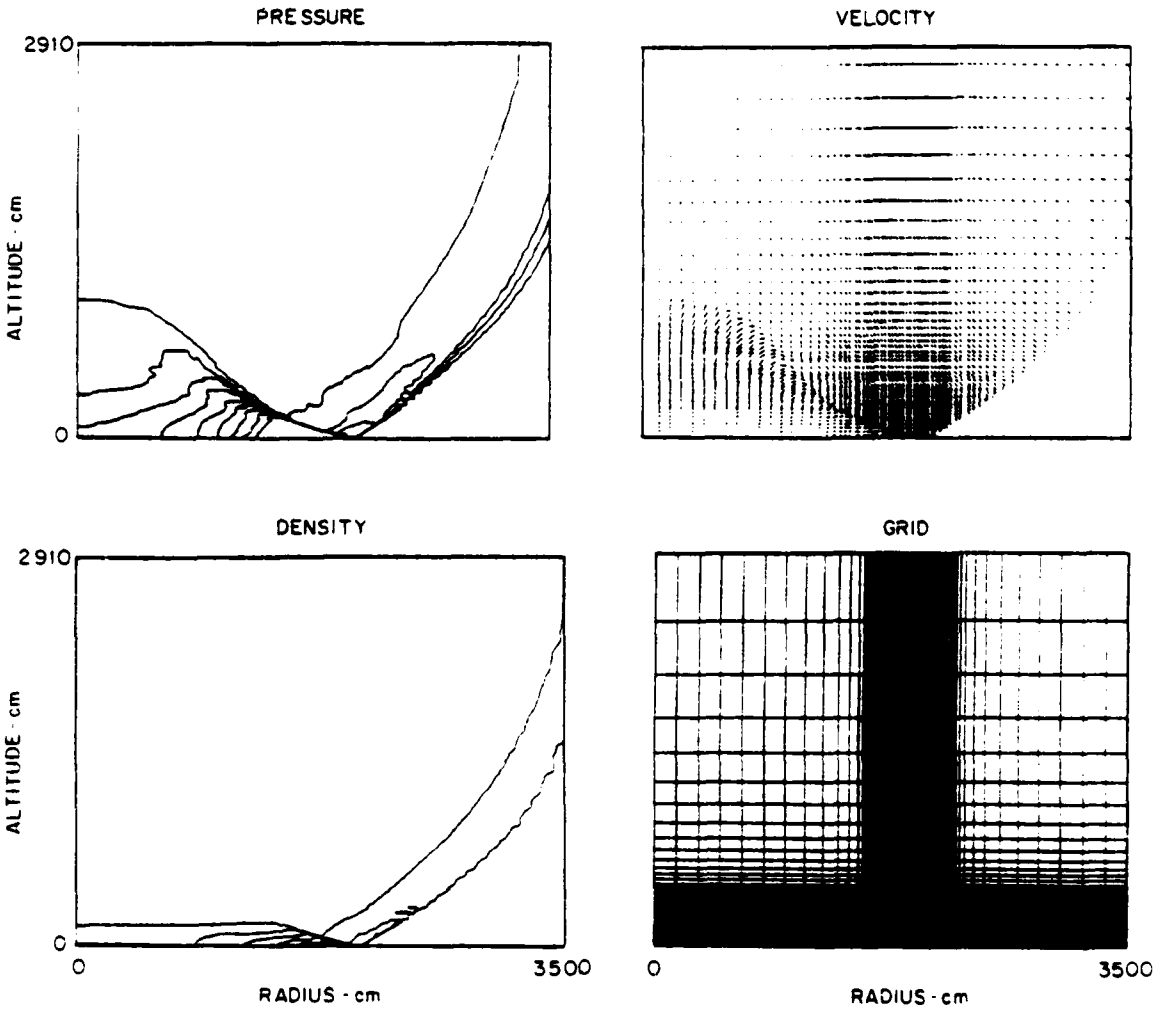

1 kt AT 104 ft HOB
TIME = 2.8 msec
CYCLE = 3000

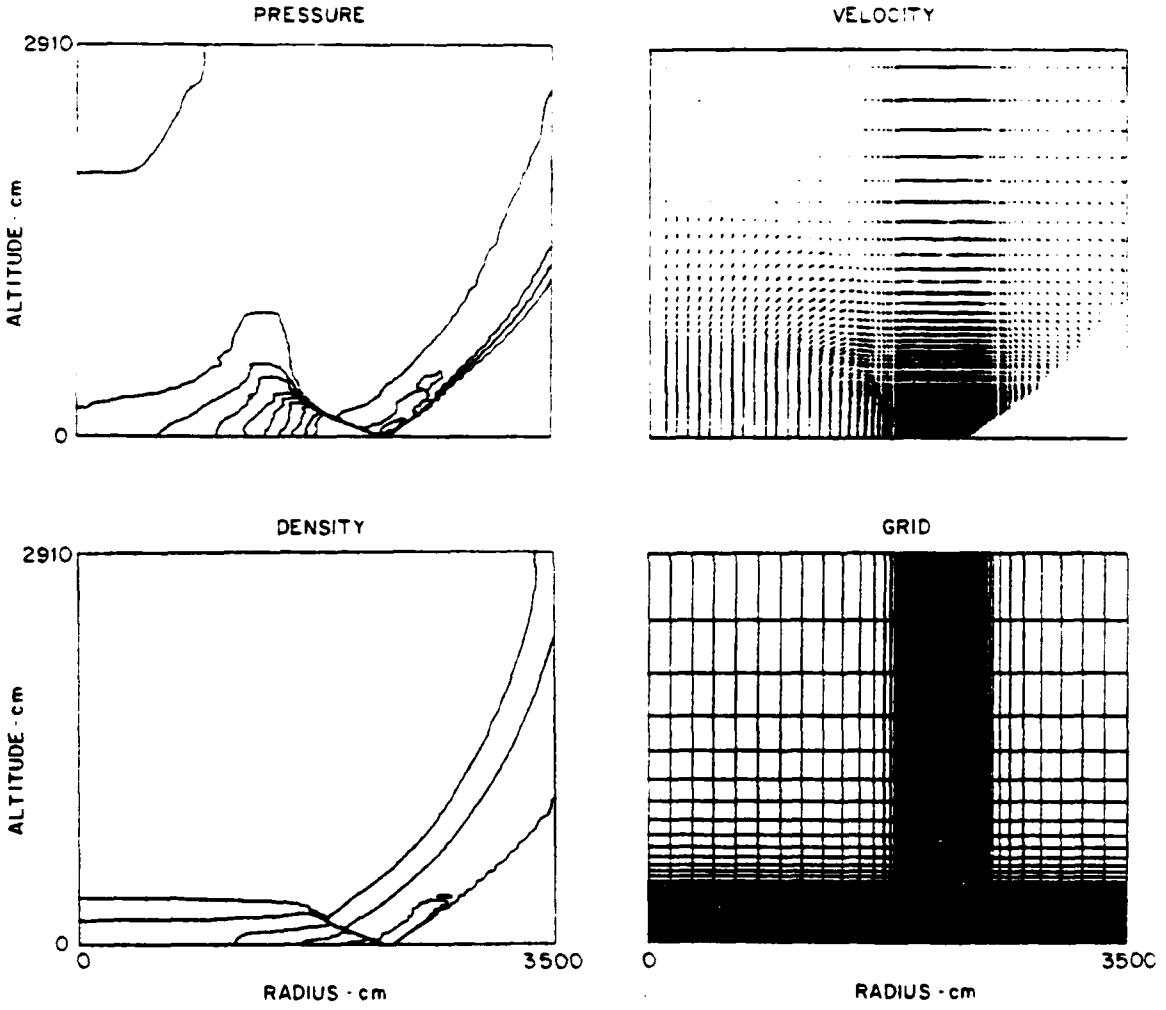

1 kt AT 104 ft HOB

TIME = 3.24 msec

CYCLE = 3400

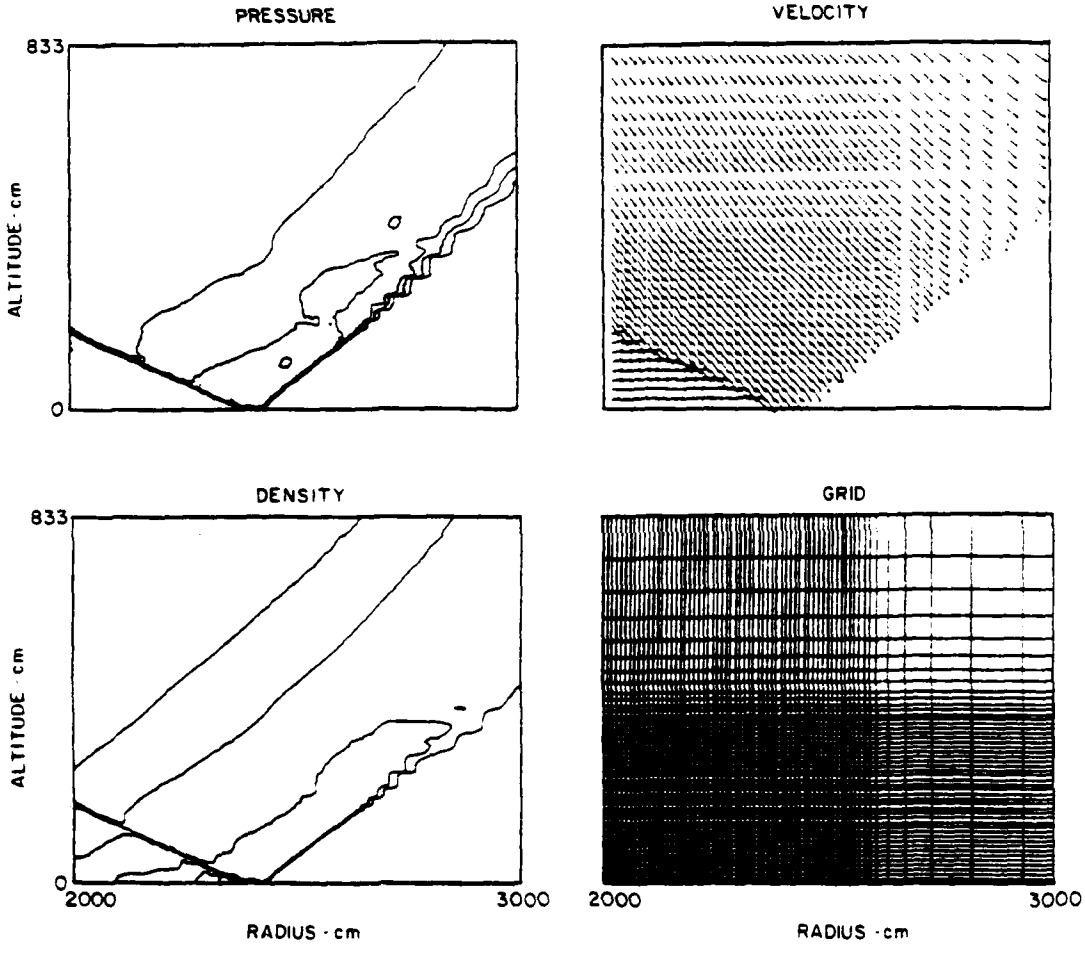

1 kt AT 104 ft HOB

TIME = 4.10 msec

CYCLE = 4200

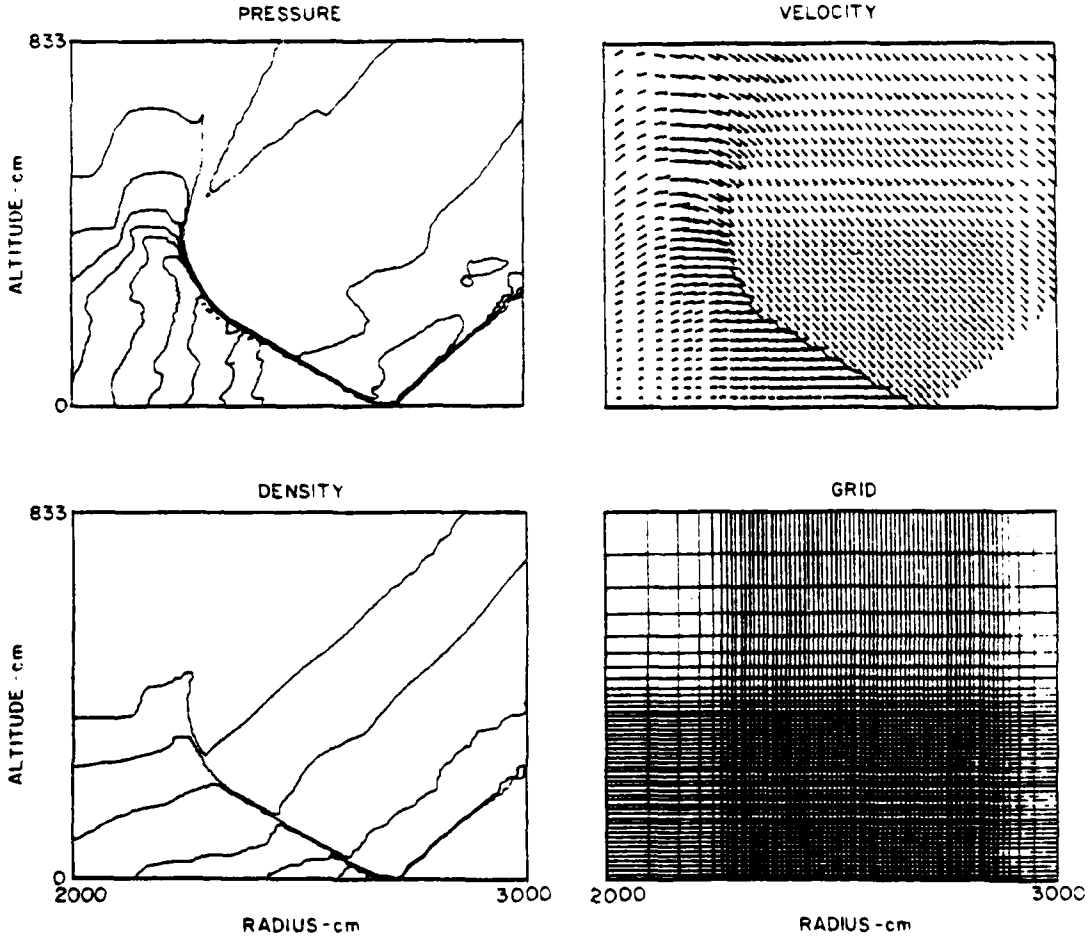

1 kt AT 104 ft HOB

TIME = 4.54 msec

CYCLE = 4600

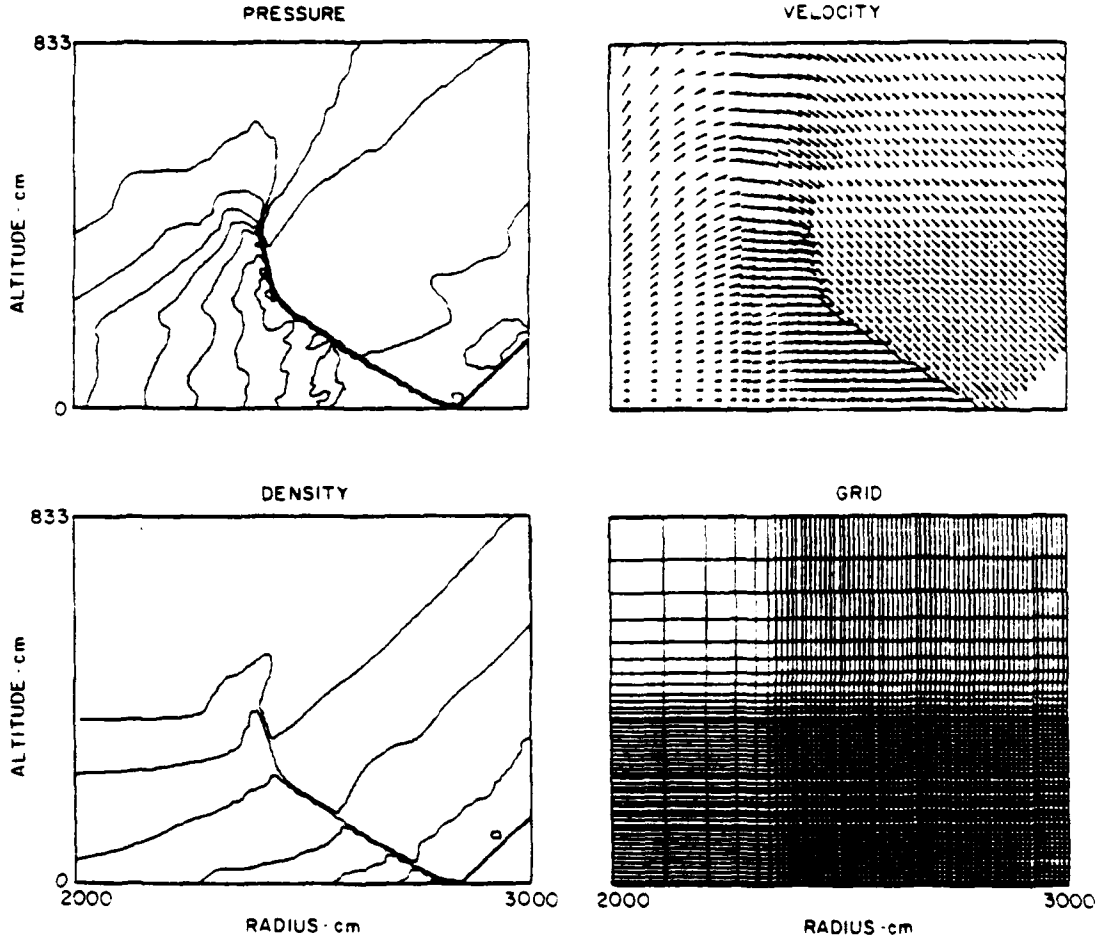

'KT AT 104 ft HOB

TIME = 4.99 msec

CYCLE = 5000

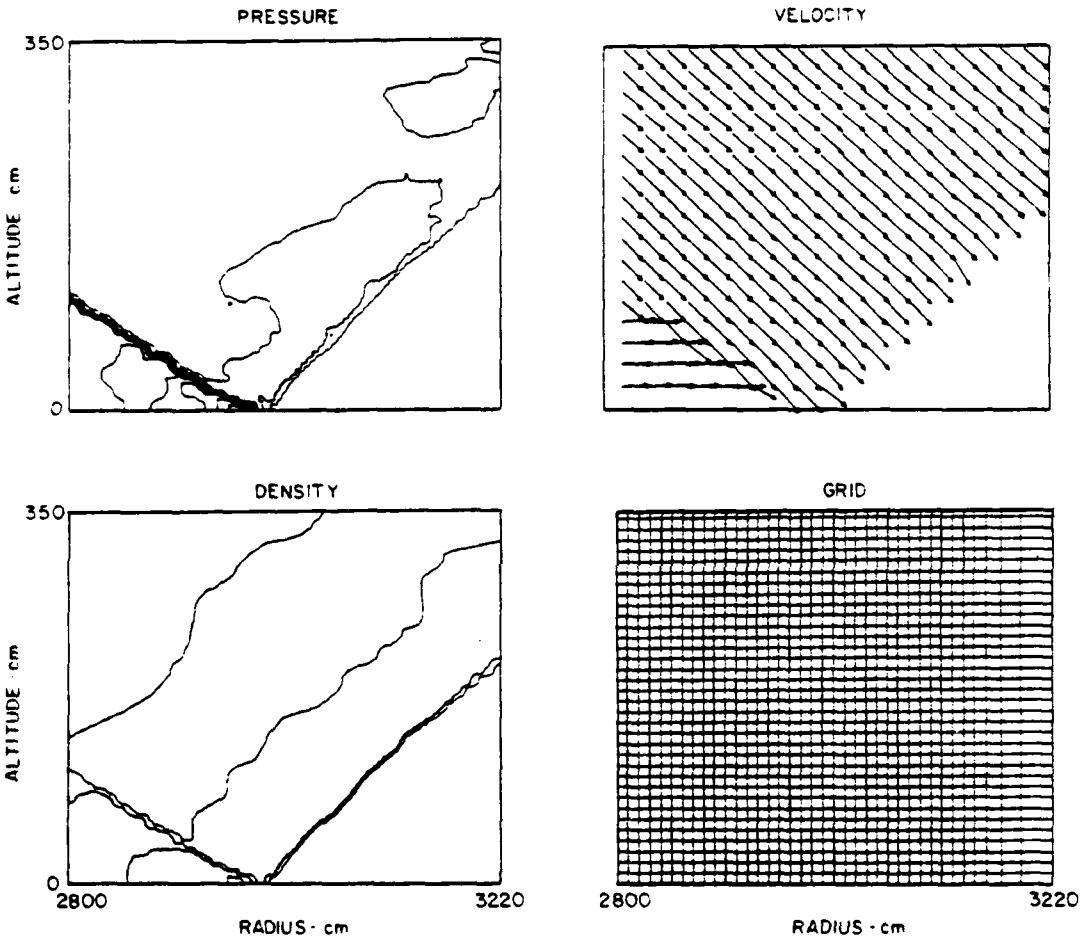

1 kt AT 104 ft HOB

TIME = 5.47 msec

CYCLE = 5400

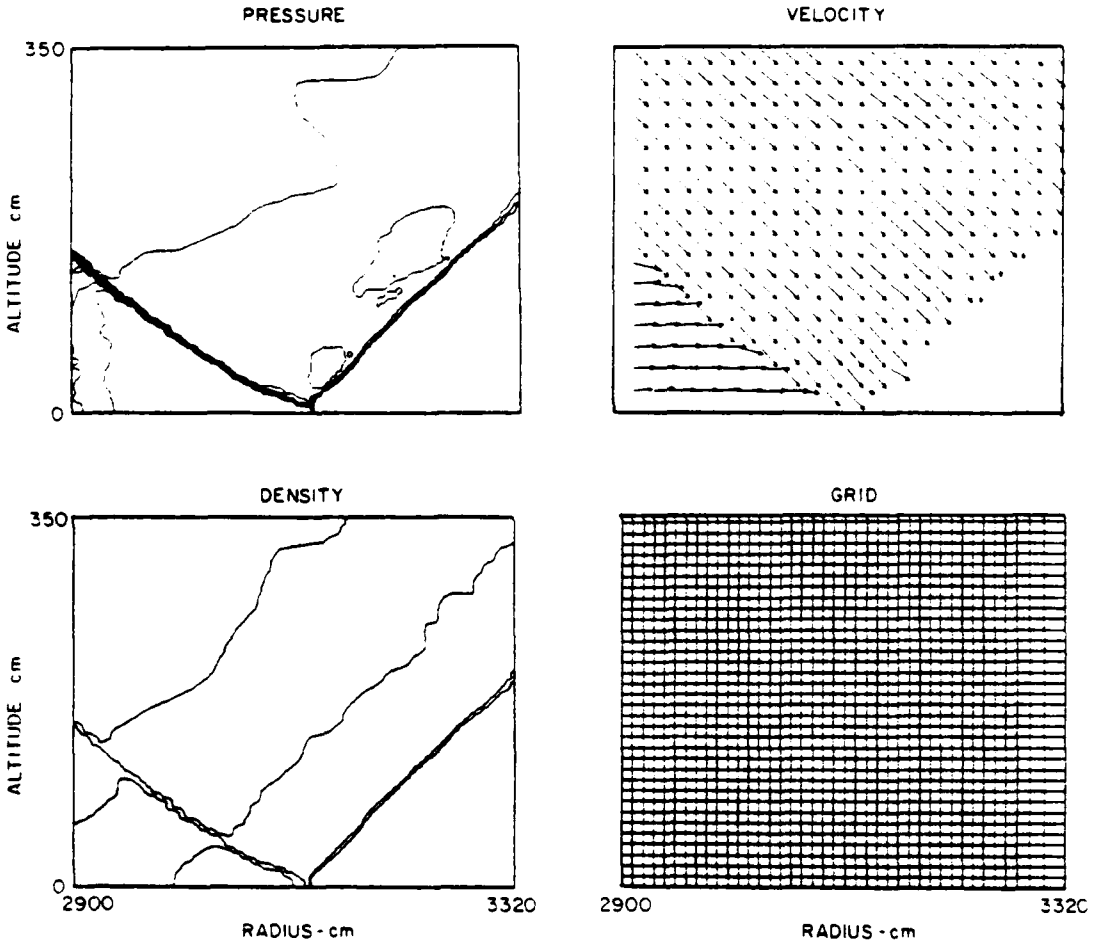

1 K' AT 104 ft HOB

TIME = 5.99 msec

CYCLE = 5800

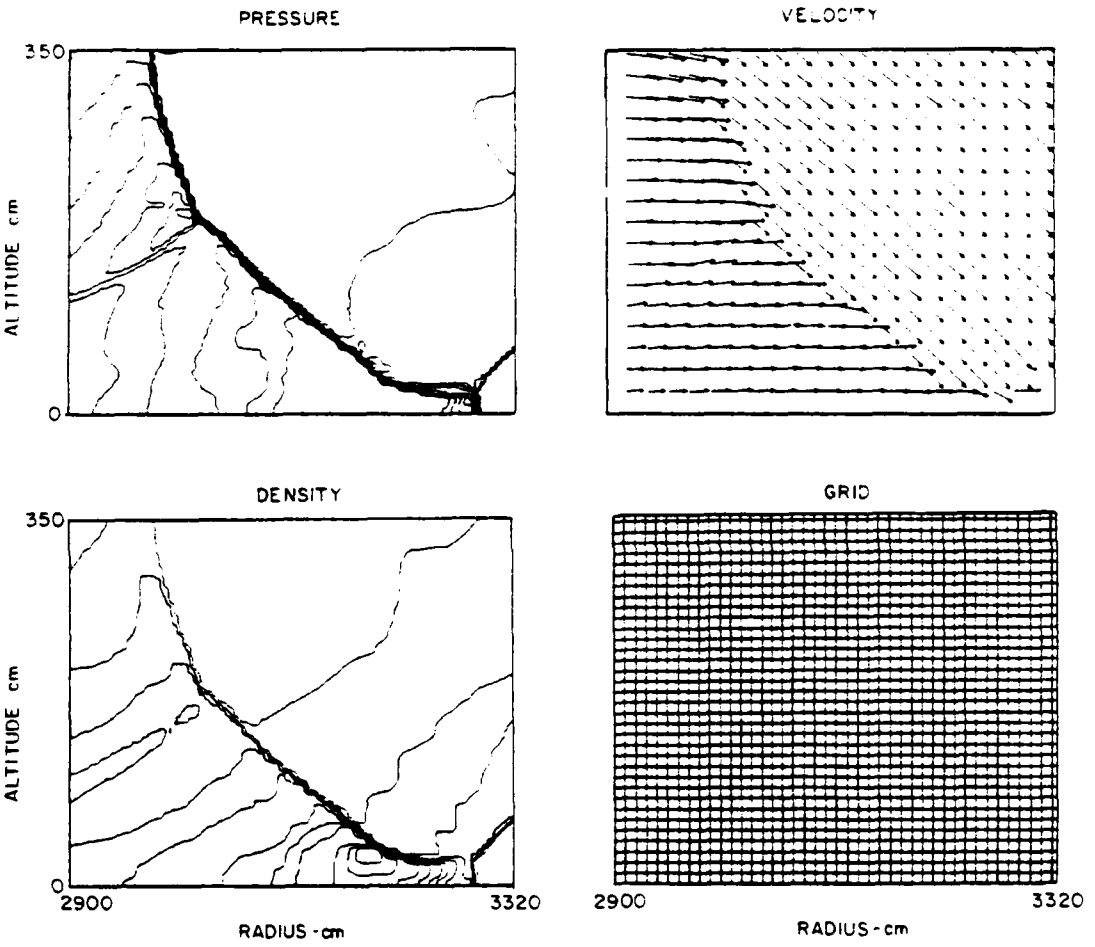

1 kt AT 104 ft HOB

TIME = 6.26 msec

CYCLE = 6000

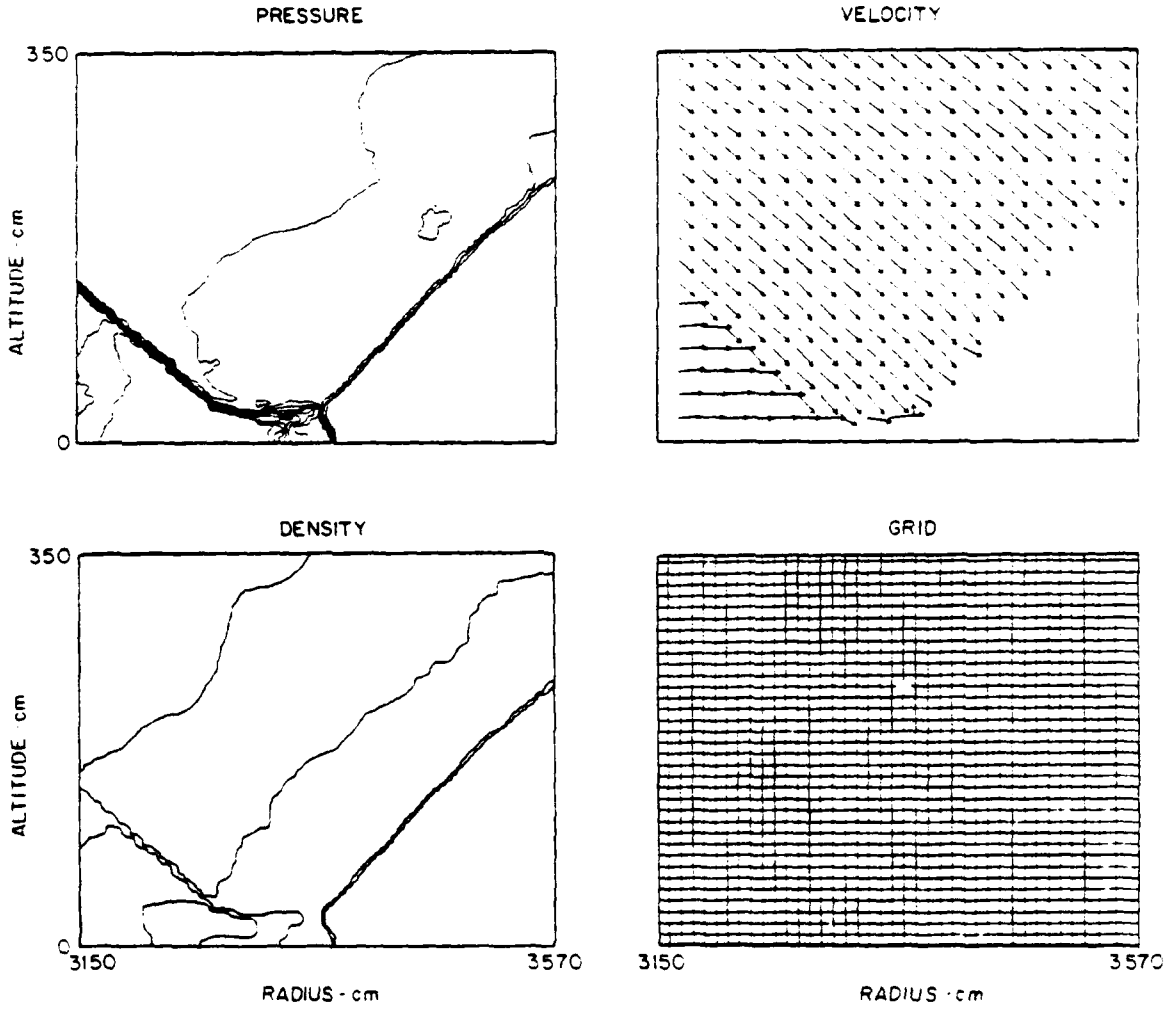

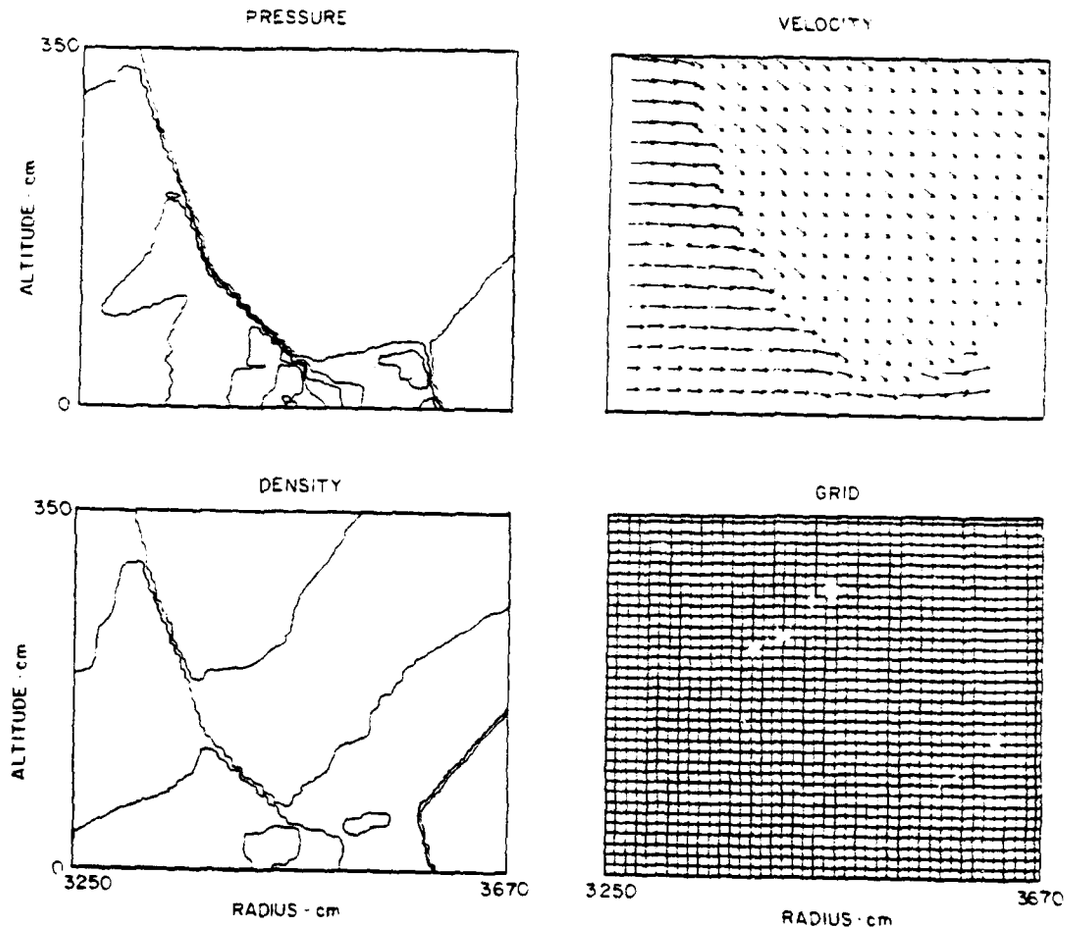
1 kt AT 104 ft HOB
TIME = 7.05 msec
CYCLE = 6600
PRESSURE
VELOCITY
DENSITY
GRID
350
0
ALTITUDE - cm
3250
3670
RADIUS - cm

1 kt AT 104 ft HOB

TIME = 7.39 msec

CYCLE = 6800

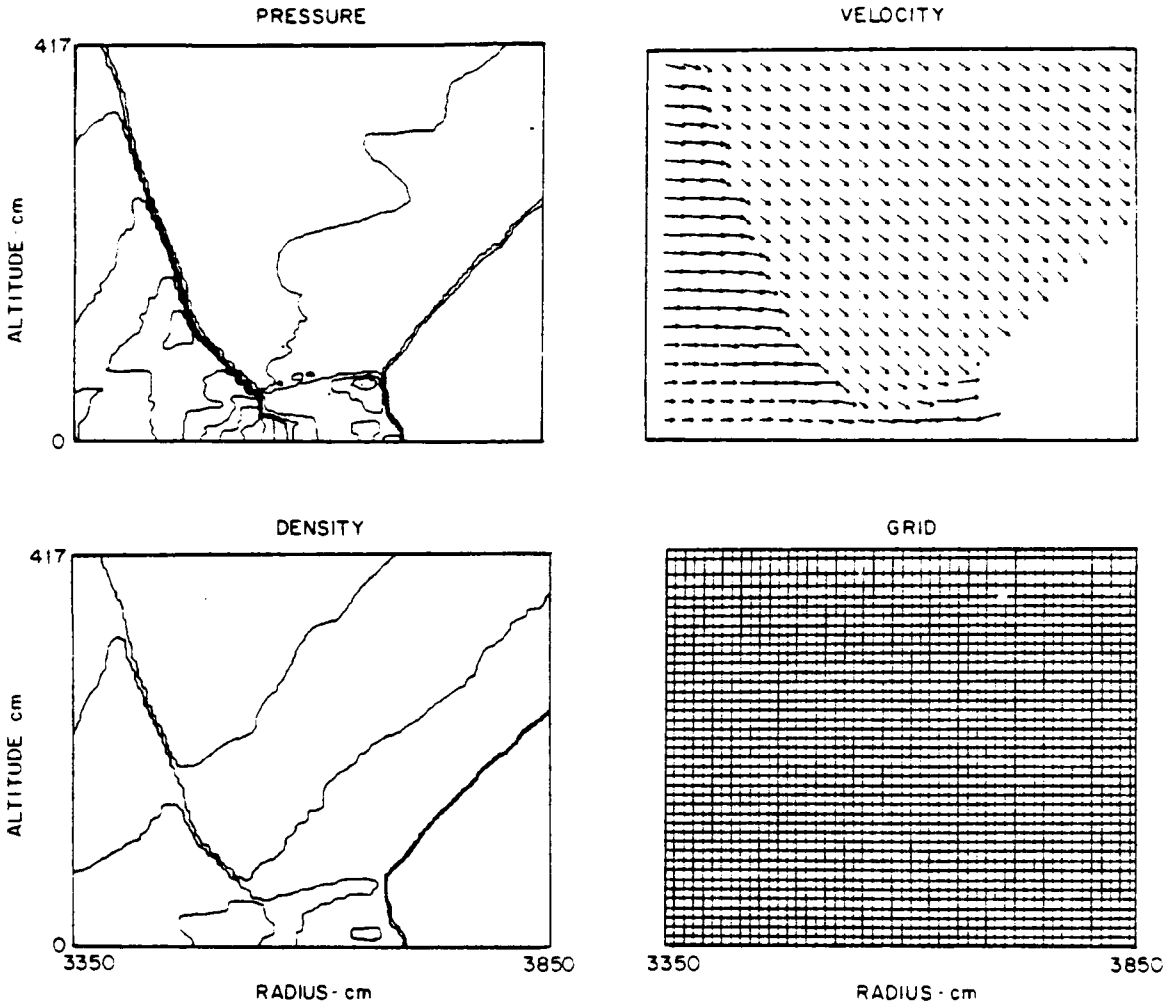

1 kt AT 104 ft HOB
TIME = 8.28 msec
CYCLE = 7200

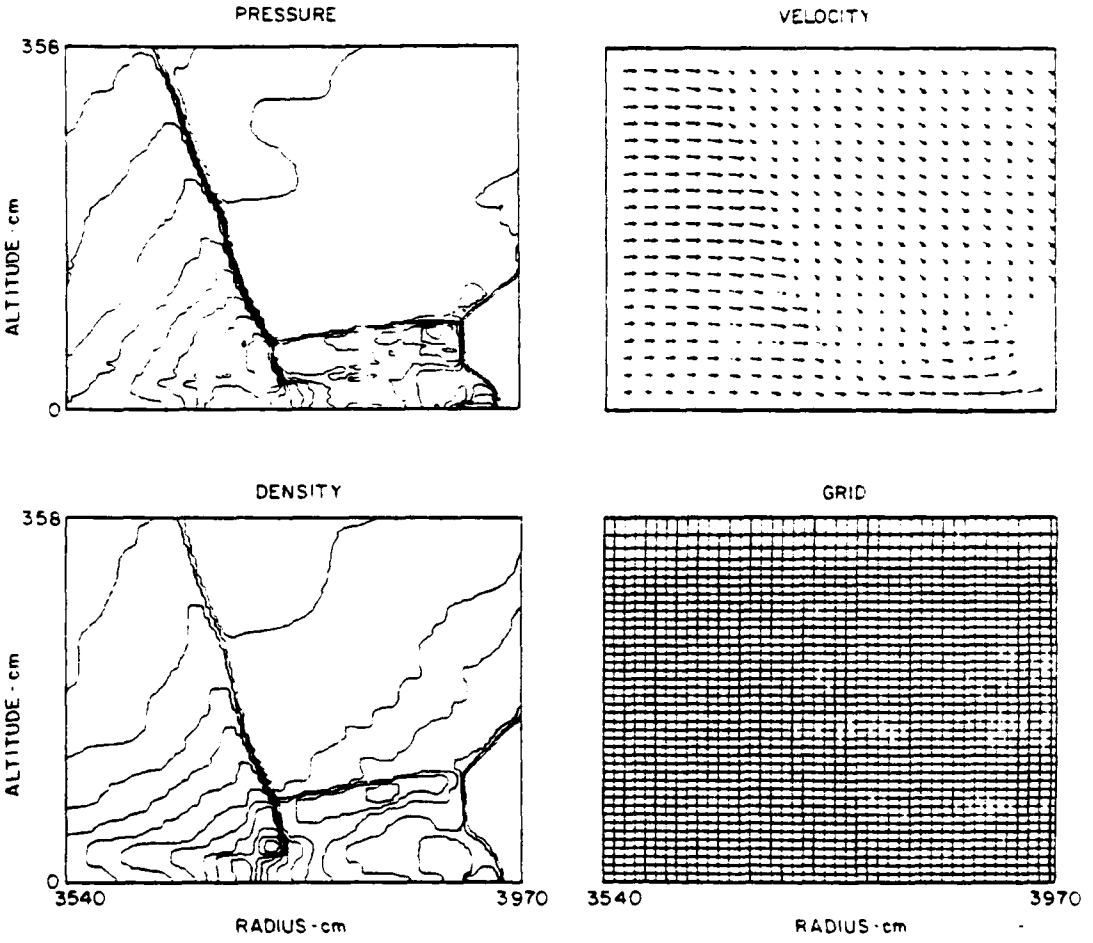

APPENDIX B

Shock Capturing Using Flux-Corrected Transport Algorithms with Adaptive Gridding

NRL Memorandum Report 4629

Shock Capturing Using Flux-Corrected Transport Algorithms with Adaptive Gridding

M. FRY AND J. TITTSWORTH

Science Applications, Inc.
McLean, VA 22102

A. KUHL

R & D Associates
Marina del Rey, CA 90291

D. BOOK, J. BORIS, AND M. PICONE

Laboratory for Computational Physics

October 14, 1981

This work was supported by the Defense Nuclear Agency under Subtask Y99QAXSG, work unit 00001, and work unit title "Flux-Corrected Transport."

NAVAL RESEARCH LABORATORY
Washington, D.C.

SECURITY CLASSIFICATION OF THIS PAGE (When Data Entered)

REPORT DOCUMENTATION PAGE	READ INSTRUCTIONS BEFORE COMPLETING FORM
1 REPORT NUMBER: NRL Memorandum Report 4629	2 GOVT ACCESSION NO. / 3 RECIPIENT'S CATALOG NUMBER
4 TITLE (and Subtitle): SHOCK CAPTURING USING FLUX-CORRECTED TRANSPORT ALGORITHMS WITH ADAPTIVE GRIDDING	5 TYPE OF REPORT & PERIOD COVERED: Interim report on a continuing NRL problem. / 6 PERFORMING ORG. REPORT NUMBER
7 AUTHOR(s): M. Fry*, J. Tittsworth*, A. Kuhl**, D. Book, J. Boris, and M. Picone	8 CONTRACT OR GRANT NUMBER(s)
9 PERFORMING ORGANIZATION NAME AND ADDRESS: Naval Research Laboratory, Washington, DC 20375	10 PROGRAM ELEMENT, PROJECT, TASK AREA & WORK UNIT NUMBERS: 44-0578-0-1
11 CONTROLLING OFFICE NAME AND ADDRESS: Defense Nuclear Agency, Washington, DC 20305	12 REPORT DATE: October 14, 1981 / 13 NUMBER OF PAGES: 38
14 MONITORING AGENCY NAME & ADDRESS(if different from Controlling Office)	15 SECURITY CLASS. (of this report): UNCLASSIFIED / 15a DECLASSIFICATION/DOWNGRADING SCHEDULE

16 DISTRIBUTION STATEMENT (of this Report)

Approved for public release; distribution unlimited.

17 DISTRIBUTION STATEMENT (of the abstract entered in Block 20, if different from Report)

18 SUPPLEMENTARY NOTES

*Present address: Science Applications, Inc., McLean, VA 22102
**Present address: R & D Associates, Marina del Rey, CA 90291
This work was supported by the Defense Nuclear Agency under Subtask Y99QAXSG, work unit 00001, and work unit title "Flux-Corrected Transport."

19 KEY WORDS (Continue on reverse side if necessary and identify by block number)

Flux-corrected transport (FCT)
Mach reflection
Shock-on-wedge
Height-of-burst (HOB)

20 ABSTRACT (Continue on reverse side if necessary and identify by block number)

A numerical technique has been developed for capturing complex, nonsteady shock structures in multidimensions. The technique relies on moving the computational mesh with the shock wave so that the features of principal interest appear approximately stationary. The method has been implemented using coordinate-split Flux-Corrected Transport (FCT) algorithms which allow the mesh to evolve arbitrarily with respect to the fluid in each coordinate. The grid may thus be optimized in response to the needs of a

(Continues)

DD FORM 1 JAN 73 1473 EDITION OF 1 NOV 65 IS OBSOLETE
S/N 0102-014-6601

SECURITY CLASSIFICATION OF THIS PAGE (When Data Entered)

20. ABSTRACT (Continued)

given problem. Synchronizing the grid and fluid motions permits significant reduction of numerical transients and eliminates numerical diffusion. Shocks develop naturally, with no fitting. The method is illustrated by calculating complex, two-dimensional Mach reflection phenomena associated with airblasts and shock diffraction on wedges. The numerical results are in good agreement with available experimental data.

CONTENTS

SHOCK CAPTURING USING FLUX-CORRECTED TRANSPORT ALGORITHMS WITH ADAPTIVE GRIDDING

M. Fry and J. Tittsworth
Science Applications, Inc.
McLean, Virginia, 22102, USA

A. Kuhl
R and D Associates
Marina del Rey, California, 90291, USA

D. Book, J. Boris and M. Picone
Laboratory for Computational Physics
U. S. Naval Research Laboratory
Washington, D.C., 20375, USA

A numerical technique has been developed for capturing complex, nonsteady shock structures in multidimensions. The technique relies on moving the computational mesh with the shock wave so that the features of principal interest appear approximately stationary. The method has been implemented using coordinate-split Flux-Corrected Transport (FCT) algorithms which allow the mesh to evolve arbitrarily with respect to the fluid in each coordinate. The grid may thus be optimized in response to the needs of a given problem. Synchronizing the grid and fluid motions permits significant reduction of numerical transients and eliminates numerical diffusion. Shocks develop naturally, with no fitting. The method is illustrated by calculating complex, two-dimensional Mach reflection phenomena associated with airblasts and shock diffraction on wedges. The numerical results are in good agreement with available experimental data.

INTRODUCTION

Numerical solution of transient multidimensional gas dynamics problems is always nontrivial. When, in addition, the problem involves reflecting supersonic flows, large variations in length scales in both space and time, or phenomena for which neither analytic solutions nor detailed experimental observations are at hand, the state of the computational art is challenged. Such a problem arises in calculating the oblique reflection of shocks from solid surfaces in planar geometries (e.g. shock tube experiments) or axisymmetric geometries (e.g. airblasts). The complications arise mainly from the presence of Mach reflections which occur when a shock front impinges on a reflecting surface at angles of incidence sufficiently far from normal. The formation of a Mach stem and, consequently, of a slip surface intersecting the triple point (the confluence of the incident, Mach, and reflected waves) results from the requirement that the flow behind the reflected shock be parallel to the reflecting surface, which cannot be achieved through regular reflection.

Attempts to calculate the properties of the flow in Mach reflections date back at least to von Neumann[1] and the research which grew out of the wartime explosive studies[2-4]. For the simplest problem, that of a planar shock

Manuscript submitted August 24, 1981.

reflecting from a plane surface, Jones, Martin, and Thornhill[5] noted that it is possible to reduce the number of independent variables to two by transforming to the similarity variables x/t, y/t, a device that was also used by Kutler, et al[6]. Ben-Dor[7] developed a theory which used shock polars to explain some of the features of this problem, and solved the system of algebraic equations obtained by combining the jump conditions across the various discontinuities (Courant and Friedrichs)[8] to describe the flow in the neighborhood of the triple point. To date, no satisfactory treatment of the complete flow field has been published, although some features (like the shape of various waveforms) are quite easy to model.

In connection with studies of both chemical and nuclear explosions there have been many attempts to model a spherical blast wave reflecting from the ground, the so-called height-of-burst (HOB) problem. The hydrodynamic phenomena in the two cases are identical, although nonideal effects (primarily explosive afterburn in the first instance and radiation preheating in the second) are different. Previous attempts to model two-dimensional complex shock reflection have suffered from restriction to describing part of the system, the use of a special assumption like that of self-similarity, or less than satisfactory agreement with experimental data.[9]

The calculations discussed here represent a step forward in overcoming these difficulties. They differ from previous numerical work in incorporating two important computational developments: Flux-Corrected Transport (FCT)[10] and an adaptive regridding procedure, called "sliding rezone",[11] which optimizes the mesh point distribution and hence the resolution of surfaces of discontinuity.

FCT is a finite-difference technique for solving the fluid equations in problems where sharp discontinuities arise (e.g. shocks, slip surfaces and contact surfaces). It modifies the linear properties of a second- (or higher) order algorithm by adding a diffusion term during convective transport, and then subtracting it out "almost everywhere" in the antidiffusion phase of each time step. The residual diffusion is just large enough to prevent dispersive ripples from arising at the discontinuity, thus ensuring that all conserved quantities remain positive. FCT captures shocks accurately over a wide range of parameters. No information about the number or nature of the surfaces of discontinuity need be provided prior to initiating the calculation.

The FCT routine used in the present calculations, called JPBFCT (an advanced version of ETBFCT)[12], consists of a flexible, general transport module which solves 1-D fluid equations in Cartesian, cylindrical, or spherical geometry. It provides a finite difference approximation to the conservation laws of the general form:

$$\frac{\partial}{\partial t}\int_{\partial V(t)} \Phi dV = -\int_{\partial A(t)} \Phi\,(\underline{u}-\underline{u}_g)\cdot d\underline{A} + \int_{\partial A(t)} \tau dA \qquad (1)$$

where Φ represents the mass, momentum, energy or mass species in cell $\partial V(t)$, $\underline{u}$ and $\underline{u}_g$ represent the fluid and grid velocities, respectively, and τ represents the pressure/work terms. This formulation allows the grid to slide with respect to the fluid without introducing any additional numerical diffusion. Thus, knowing where the features of greatest interest are located, one can concentrate fine zones where they will resolve these features most effectively as the system evolves (Fig. 1).

In the next section we describe the computational techniques used to solve the wedge problem and present the results of four simulations carried out to reproduce experimental results of Ben-Dor and Glass.[13] In Section III we present a parallel discussion for a HOB calculation. Finally, in Section IV we summarize our conclusions.

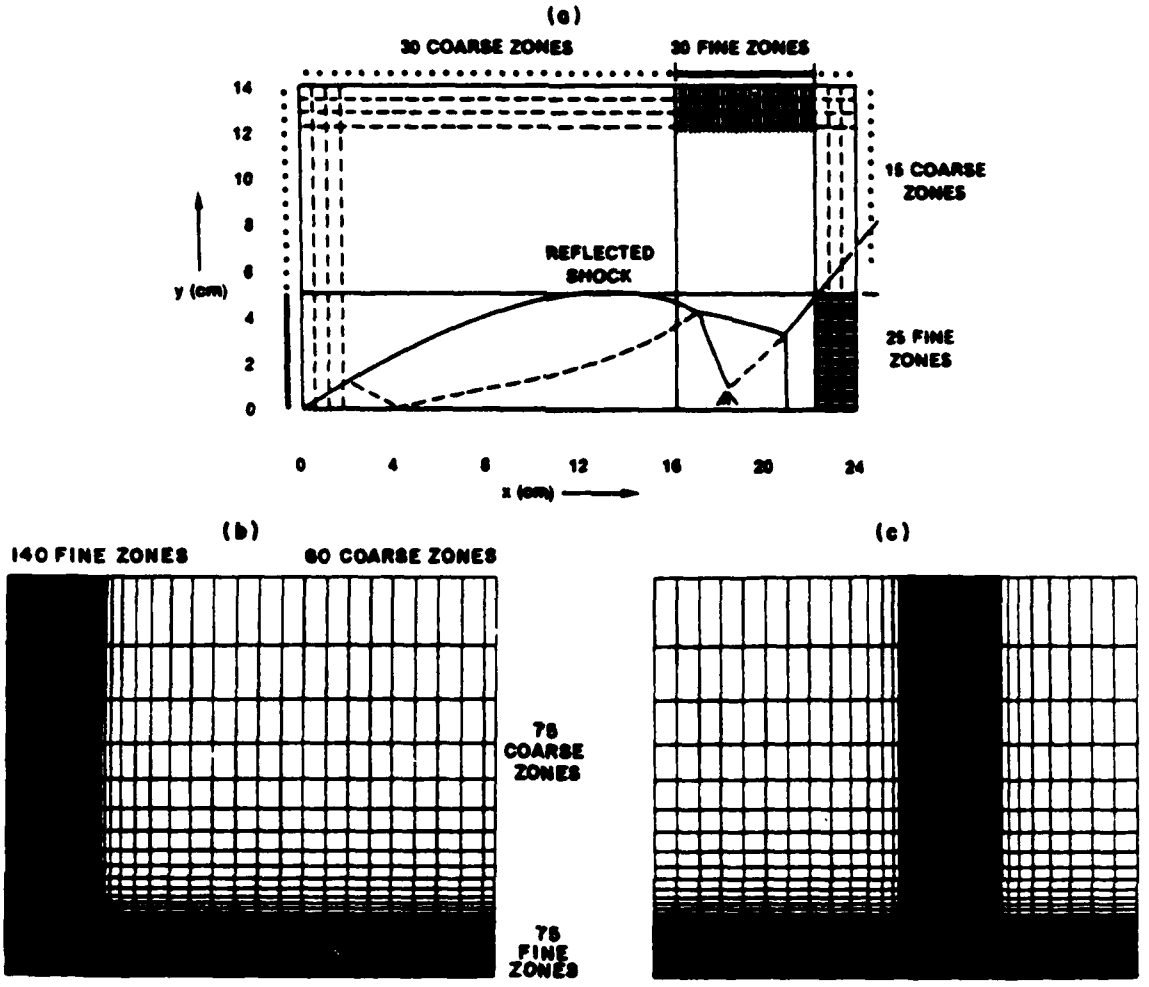

Fig. 1. Adaptive grids for a) planar shocks on wedge (double Mach shock features are indicated); b) and c) HOB problem initially and at transition point (grid lines in fine-zone region are indistinguishable).

SHOCK-ON-WEDGE CALCULATIONS

The JPBFCT algorithm was used in a 2-D Cartesian version of the FAST2D code to model the reflections of planar shocks from wedges of 20° to 60° and varying shock strengths. Four general classes which include regular, single, complex and double Mach reflection were calculated (referred to as cases a,b,c,d respectively). The bottom of the mesh, treated as a reflecting boundary, modeled the surface of the wedge. Quantities on the right hand boundary and on the top were set equal to the ambient values. The remaining boundaries were treated as permeable. In the single, complex, and double Mach reflection cases, the mesh was anchored on the left, essentially at the wedge tip where the incident shock first strikes, while the zones were stretched by a scaling factor proportional to t as soon as the reflection region filled a substantial portion of the grid. In case (d), the double Mach reflection case, the opening angle is so small that the incident shock has to traverse many zones before the mach stem has grown large enough to be well resolved. For this reason, the problem was solved on a uniform mesh in the frame of reference fixed

to the reflection point, with stretching being initiated after the first Mach stem reached $\sim$ 20 cells in length. The timestep was recalculated at every cycle with a Courant number of 0.5.

Figure 2 shows the pressure and density contours and the velocity field for cases a,b,c,d. The pertinent shock phenomena can be easily identified: incident shock, contact surface, first and second Mach stems. As shown in Fig. 1, the zoning is particularly sparse except for the region of interest. Adequate resolution of the key surfaces (contact and second Mach stem) is obtained with 5 zones in each direction. The accuracy can be evaluated by comparing the experimental density distributions along the wall (Fig. 3).

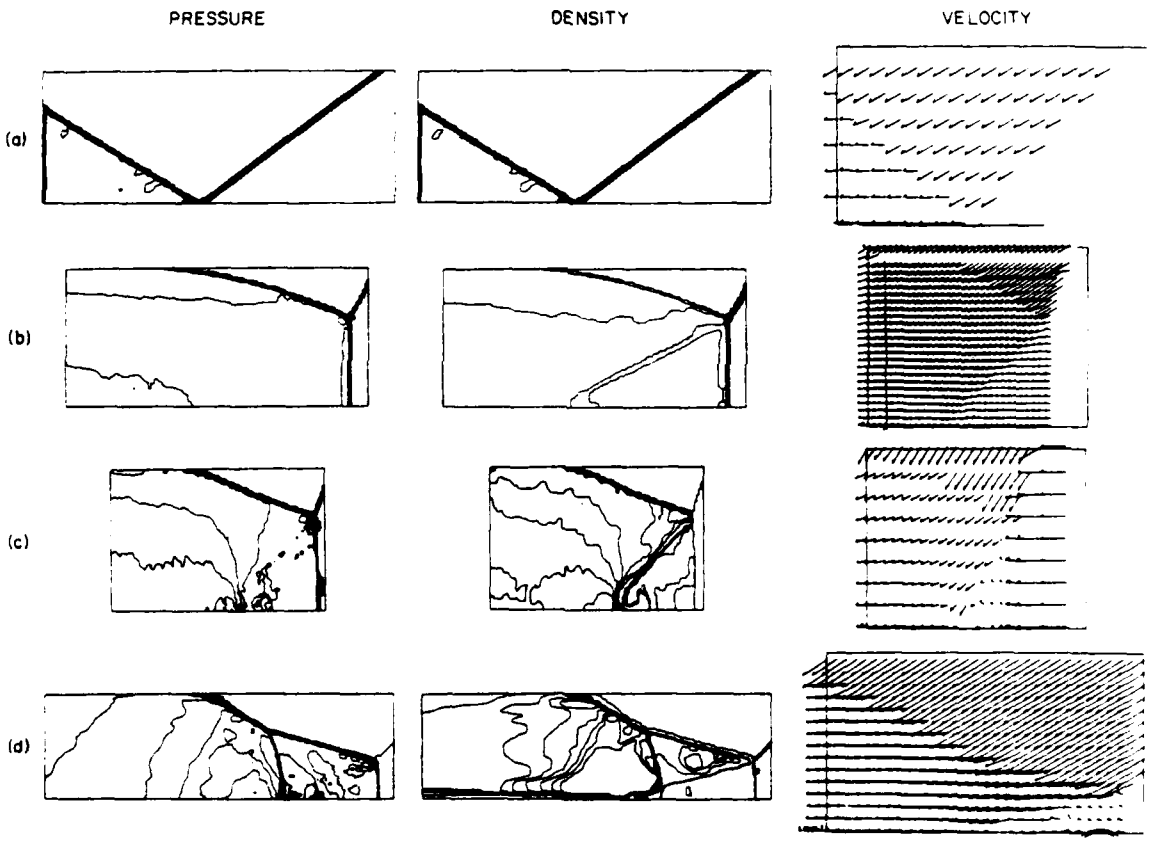

Fig. 2 - Pressure and density contours and flow velocity vectors (in frame of reflection point) for planar waves with Mach number M reflecting from wedges with angle θ for (a) M=2.03, θ=60°; (b) M=2.82, θ=20°; (c) M=5.29; θ=30°; (d) M=7.03; θ=50°

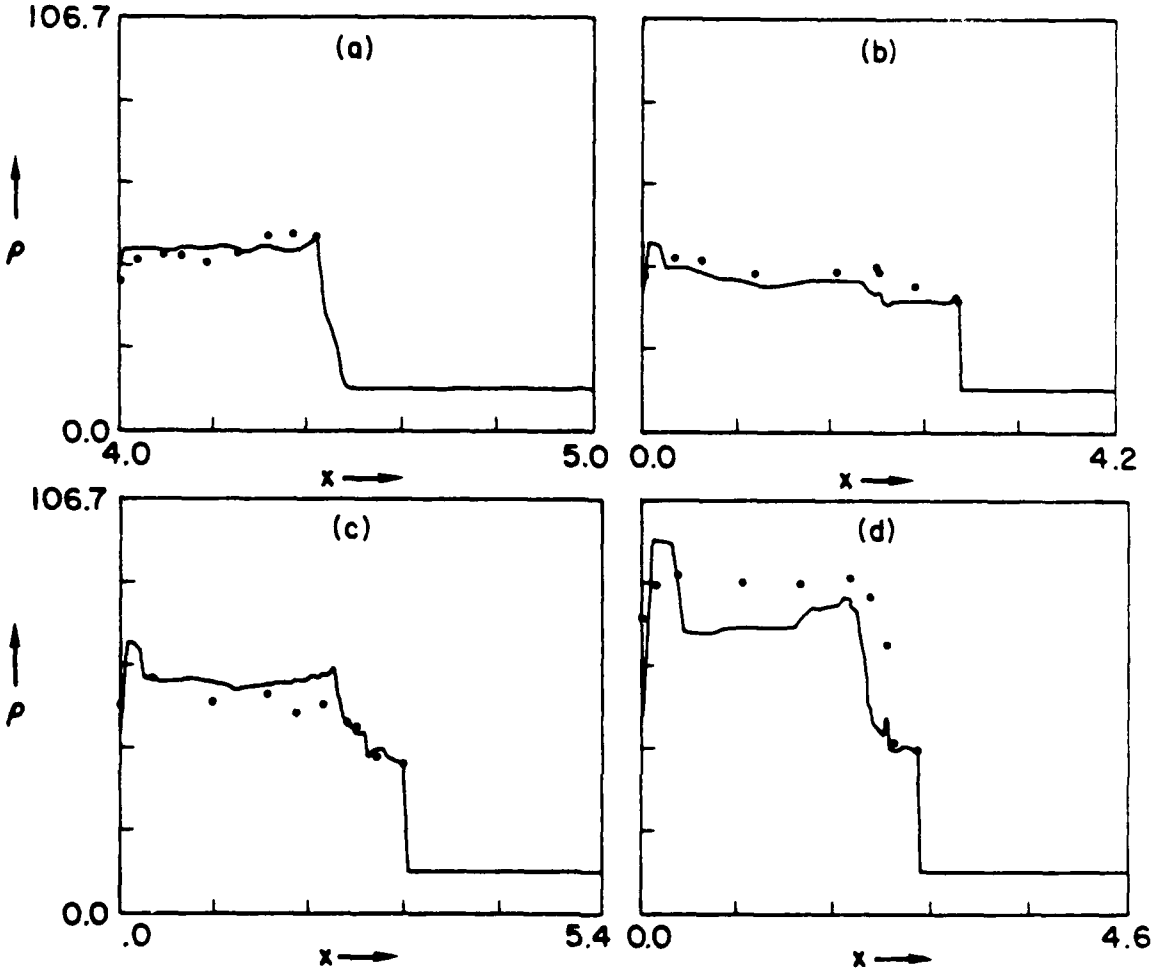

Fig. 3. Comparison of density (in units of ambient density ρ_o) for cases (a), (b), (c), (d) of Fig. 2 vs. distance from corner. Points are measured values reported in Ref. 13.

HEIGHT OF BURST CALCULATIONS

Next, we performed a numerical simulation of a 1KT nuclear detonation at 31.7 m HOB, a case which could be readily compared with high explosive data. A constant ambient atmosphere was used with a density of 1.22×10^{-3} g/cm^3 and pressure 1.01×10^6 dynes/cm^2. To relate the energy and density to the pressure, a real-air equation of state (EOS) was used. This table-lookup EOS was derived from theoretical calculations by Gilmore[14,15] for equilibrium properties of air and has been vectorized for the Advanced Scientific Computer[16]. The internal energy density used in the call to the EOS is found by subtracting kinetic from total energy; this can be negative due to truncation (phase) errors. When this occurred, the value of the pressure was reset to zero.

The transition from regular reflection to double Mach reflection occurs at a ground range approximately equal to the HOB. The size of the mesh should

therefore be roughly twice the HOB in both directions. The upper boundary should be far enough away from the blast front to be non-interfering. We chose boundaries of 55 m for the radial direction and 103.5 m for the axial direction. The fine grid in the radial direction contained 140 out of 200 total zones, each 5 cm in length. The rightmost zones were 80 cm in length, and a smoothing involving 40 zones was performed between the regions to guarantee that the zone sizes varied slowly. In the axial direction the fine grid contained 75 out of 150 total zones, each 5 cm in length. Beyond that region the zones were geometrically increased by a factor of 1.112.

Placement of the fine grid at the origin of the mesh (ground zero, the point at which reflection first occurs) was determined to be optimum for capturing peak pressure in the airblast wavefront. Thus, as the expanding wave moves along the ground surface, the fine grid is always locked to it and each point along the blast front encounters the same spatial gridding as it approaches the ground. By treating each point of the incident front in the same manner, we insure that the calculation is internally consistent and that the computed transition point is accurate to within the limits of the resolution.

The initialization provides a strong shock with approximate Mach number M=12. This speed and the need for restart capability led to the choice of 200 timesteps as an interval for the spatial display (snapshots). The dump interval that resulted was $\Delta t \sim 0.3$ milliseconds (ms). These dumps were stored on magnetic tape and post-processed.

A fit to the 1-D nuclear blast flow field (Ref. 17) was used to initialize the energy and mass density and velocity field at 3.76 ms. The corresponding peak overpressure was 113 bars. After the 1 KT flow field was laid down inside a radius of 31.6 m, the fine-zone grid was activated to follow the peak pressure as it moved along the ground surface, modelled as a perfectly reflecting boundary. This region comprised 140 zones, and a switch was set to keep 40 of these zones ahead of the reflection point. Permeable boundary conditions are used on the top and right edges of the mesh, i.e., density, pressure and velocity are set equal to ambient preshock conditions. Reflecting conditions were applied to the left and bottom. The total elapsed physical time in the 2-D calculation, 7.6 ms, required 5600 cycles. Times are referred to t=0 at the start of the calculation.

The numerical simulation begins just before the shock first reflects from the ground. Fig. 4a indicates the pressure and density contours and velocity vectors at time 3.18 ms. In Fig. 4b the reflected shock is shown moving upward, the outward flow begins to stagnate at the ground (transition). Fig. 4c, t=5.99 ms, shows an enlargement of the shockfront, and the development of the Mach stem, slip surface and second Mach stem. The angle of the shock front with respect to the ground is increasing with time, so that the effective wedge angle is decreasing. From Ben-Dor and Glass[18] one expects a transition to double Mach stem to occur at approximately 45°. The angle in Fig. 4b is about 45° and the shock front has entered the transition phase. Figure 4d shows the fully developed shock structure at 7.79 ms. Clearly visible is the second Mach stem and a vortex region behind the first Mach stem. Toeing out of the first Mach stem can be also seen in the contours of Fig. 4d and occurs as the fluid rolls forward where the slip line would otherwise intersect the ground. The velocity field in Fig. 4d also shows this detail.

One should also note the reflected shock properties. The reflected shock propagates rapidly through the high temperature fireball, due to the high local soundspeed. The shape of this reflected wave is a primary difference between the HOB case and the wedge case[19]. The other major difference, of course, is the spherically expanding blast wave which decreases in strength approximately proportional to r^{-2}.

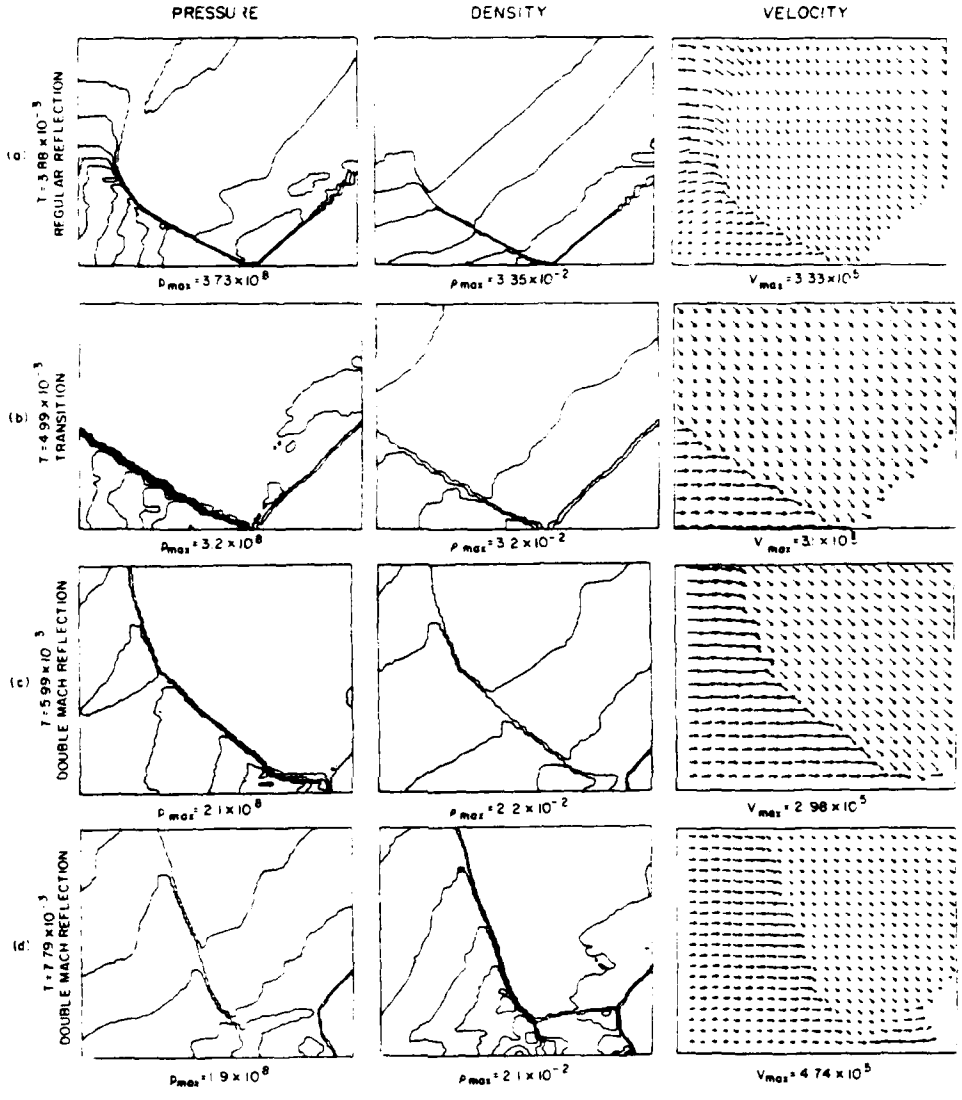

Fig. 4. Pressure, density, and velocity fields for HOB calculation (a) in regular reflection stage; (b) at transition to Mach reflection; (c) shortly afterward, when second peak has become larger than first; and (d) fully developed (note toe at base of first Mach stem).

Finally we consider the pressure/distance relation for the HOB case. In Fig. 5 we compare the results of the numerical simulation with the data of Carpenter and with empirical analysis. Carpenter's data are based upon careful HOB experiments with 8 lb PBX9404 spheres. The empirical analysis was based on a 1 KT nuclear free air curve and HOB construction factors. The calculated values in the regular reflection regime are 20% low and may be attributed to a combination of FCT clipping, the resolution of the grid, and inaccuracies in the initialization of the flow field. During and after Mach reflection, the peaks remain low until the Mach stem structure has grown large enough to be resolved on the mesh. By the time it occupies a region of 15 cells high and 35 cells wide, the peak pressures are in good agreement with the HE data and the empirical analysis.

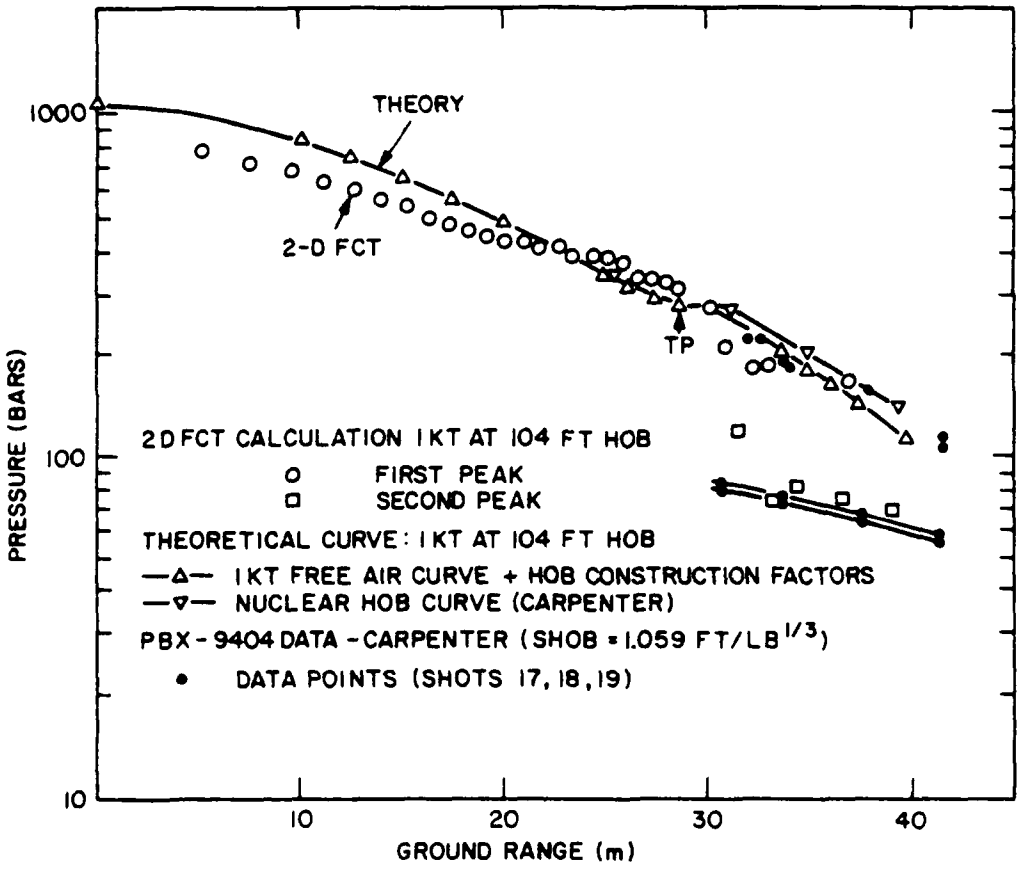

Fig. 5. Pressure-range curves for first and second (after transition - denoted by TP - to double Mach reflection) peaks.

SUMMARY AND CONCLUSION

The complex 2-D Mach reflection phenomena associated with shock diffraction on wedges and height-of-burst explosions have been modeled with the FAST2D computer code. Four wedge cases--regular, single, complex and double Mach reflection--have been calculated and the results compared to experiments. A nuclear detonation (1 KT at 31.7m HOB) was also simulated. The results give insight into the formation and subsequent evolution of the Mach stem, the triple point and the contact discontinuity. The transition from regular reflection to double Mach reflection is predicted. Excellent agreement with Ben-Dor's data is obtained. We suggest that the first signal for transition is the appearance of a second peak behind the shock front due to stagnation in the flow. Calculated first and second pressure peaks versus distance in the HOB case agree both with the HE data and analysis to within 20%.

The use of the adaptive regridding procedure, called "sliding rezone", along with the FCT algorithm allows one to accurately predict the nonsteady shock structures in two dimensions for diffractions on wedges and HOB cases. Comparison with data for both wedges and HOB yields the best results obtained to date.

ACKNOWLEDGEMENT

This work was supported by the Defense Nuclear Agency under Subtask Y99QAXSG, Work Unit 00001, and Work Unit Title "Flux-Corrected Transport."

REFERENCES

1. Von Neumann, J., "Oblique Reflection of Shocks", Explosive Research Report No. 12, Navy Department, Bureau of Ordinance, Re2c, Washington, D.C. (1943).
2. Taub, A. H., "Refraction of Plane Shock Waves", Rev. Mod. Phys., Vol. 21, p. 51 (1947).
3. Bleakney, W., and Taub, A. H., "Interaction of Shock Waves", Rev. Mod. Phys., Vol. 21, p. 584 (1949).
4. Lighthill, M. J., "On the Diffraction of Blast I", Proc. Roy. Soc., Vol. 198, p. 454 (1949), Vol. 200, p. 554 (1950).
5. Jones, D. M., Martin, P. M., and Thornhill, C. K., "A Note on the Pseudo-Stationary Flow Behind a Strong Shock Diffracted or Reflected at a Corner", Proc. Roy. Soc., Sec. A, Vol. 205, p. 238 (1951).
6. Shankar, V., Kutler, P., and Anderson, D., "Diffraction of a Shock Wave by a Compression Corner - Part II, Single Mach Reflection", AIAA Journal, Vol. 16, No. 1 (1977).
7. Ben-Dor, G., and Glass, I., "Nonstationary Oblique Shock Wave Diffractions in Nitrogen and Argon - Experimental Results", UTIAS Tech Note (1978).
8. Courant, R., and Friedrichs, K. O., "Supersonic Flow and Shock Waves", Interscience Publishers, New York (1948).
9. Booen, M., and Needham, C., "Two-Dimensional Hull Code Simulation of Complex and Double Mach Reflections", AFWL NTE TN 81-001 (1981).
10. Boris, J., and Book, D., "Flux-Corrected Transport: I SHASTA, A Fluid Transport Algorithm that Works", J. Comp. Phys., 11, 38 (1973).
11. Oran, E. S., Young, T. R., Jr., and Boris, J. P., "Applications of Time-Dependent Numerical Methods to the Description of Reactive Shock", Proc. 17th Symposium (International) on Combustion, The Combustion Institute, Pittsburgh (1979).
12. Boris, J. P., "Numerical Solution of Continuity Equations", NRL Memo Report 3327 (1976).
13. Ben-Dor G,and Glass, I.,"Domains and Boundaries of Non-Stationary Oblique Shock-Wave Reflections, II Monatomic Gas", J. Fluid Mech., 96, p. 735 (1980).
14. Gilmore, F. R.,"Equilibrium Composition and Thermodynamic Properties of Air to 24,000°K" RAND Corp, RM-1543 (24 August 1955).
15. Gilmore, F. R., "Equilibrium Thermodynamic Properties of High Temperature Air", Lockheed Missile and Space Co., DASA 1917-1 (April 1967).
16. Young, T. R., (Private Communication 1981).
17. Needham, C., et. al., Nuclear Blast Standard, AFWL 7R-73-55, Air Force Weapons Laboratory (April 1975).
18. Ben-Dor, G., Glass, I., "Domains and Boundaries of Non-Stationary Oblique Shock-Wave Reflections Diatomic Gas", J. Fluid Mech., Vol. 92, part 3, p. 459 (1979).
19. Book, D., et. al., "Two-Dimensional FCT Model of Low Altitude Nuclear Effects", NRL Memo Report 4362 (1980).
20. Carpenter, H. J., "Height of Burst at High Overpressures", 4th International Symposium on Military Applications of Blast Simulation (1974).

APPENDIX C

FCT Simulation of HOB Airblast Phenomena

NRL Memorandum Report 4613

FCT Simulation of HOB Airblast Phenomena

A. L. KUHL

R&D Associates
P.O. Box 9695
Marina del Rey, California 90291

M. A. FRY

Science Applications, Inc.
McLean, Virginia 22102

M. PICONE, D. L. BOOK, AND J. P. BORIS

Laboratory for Computational Physics

September 29, 1981

This work was supported by the Defense Nuclear Agency under Subtask XY99QAXSG, work unit 00001, and work unit title "Flux-Corrected Transport."

NAVAL RESEARCH LABORATORY
Washington, D.C.

SECURITY CLASSIFICATION OF THIS PAGE (When Data Entered)

REPORT DOCUMENTATION PAGE	READ INSTRUCTIONS BEFORE COMPLETING FORM
1 REPORT NUMBER: NRL Memorandum Report 4613	2 GOVT ACCESSION NO. / 3 RECIPIENT'S CATALOG NUMBER
4 TITLE (and Subtitle): FCT SIMULATION OF HOB AIRBLAST PHENOMENA	5 TYPE OF REPORT & PERIOD COVERED: Interim report on a continuing NRL problem. / 6 PERFORMING ORG. REPORT NUMBER
7 AUTHOR(s): A. L. Kuhl*, M. A. Fry**, M. Picone, D. L. Book and J. P. Boris	8 CONTRACT OR GRANT NUMBER(s)
9 PERFORMING ORGANIZATION NAME AND ADDRESS: Naval Research Laboratory, Washington, DC 20375	10 PROGRAM ELEMENT, PROJECT, TASK AREA & WORK UNIT NUMBERS: 62715H; 44-0578-0-1
11 CONTROLLING OFFICE NAME AND ADDRESS: Defense Nuclear Agency, Washington, DC 20305	12 REPORT DATE: September 29, 1981 / 13 NUMBER OF PAGES: 53
14 MONITORING AGENCY NAME & ADDRESS(if different from Controlling Office)	15 SECURITY CLASS. (of this report): UNCLASSIFIED / 15a DECLASSIFICATION/DOWNGRADING SCHEDULE

16 DISTRIBUTION STATEMENT (of this Report)

Approved for public release; distribution unlimited.

17 DISTRIBUTION STATEMENT (of the abstract entered in Block 20, if different from Report)

18 SUPPLEMENTARY NOTES

*Present address: R & D Associates, P.O. Box 9695, Marina del Rey, California 90291
**Present address: Science Applications, Inc., McLean, Virginia 22102

(Continues)

19 KEY WORDS (Continue on reverse side if necessary and identify by block number)

HOB (Height-of-burst)	Hemispherical	HE (High explosive)
Airblast	Environment	
Detonation(s)	Overpressure	

20 ABSTRACT (Continue on reverse side if necessary and identify by block number)

Height-of-burst (HOB) detonations can create airblast environments which are more severe than surface burst environments at high overpressures (>100 psi). A double Mach stem structure develops during shock reflection from the ground at a range approximately equal to the HOB. This creates double peak static pressure waveforms with enhanced early-time impulses. Blast diffraction on above ground structures also

(Continues)

DD FORM 1 JAN 73 1473 EDITION OF 1 NOV 65 IS OBSOLETE
S/N 0102-014-6601

SECURITY CLASSIFICATION OF THIS PAGE (When Data Entered)

18. Supplementary Notes (Continued)

This work was supported by the Defense Nuclear Agency under Subtask XY99QAXSG, work unit 00001, and work unit title "Flux-Corrected Transport."

This paper was presented at the Seventh International Symposium on Military Applications of Blast Simulation, July 13–17, 1981, Medicine Hat, Alberta, Canada, under the title "Simulation of High Overpressure HOB Airblast Environments on a Large Scale."

20. Abstract (Continued)

contains multiple peaks with enhanced loads and impulses. There is an ongoing interest in simulating these HOB environments for military applications. High explosives (HE) charges can be used to simulate the nuclear surface burst case below about 100 psi for reasonable yields (100T or more), but it appears that it is impractical to elevate large HE charges above grade to simulate the HOB case. In this paper we propose a new method for naturally simulating such HOB environments on a large scale. A hemispherical HE charge could be detonated near a natural slope which had been graded to form a large ramp. When the spherical blast wave reflects from this ramp a shock structure and environment is created which is similar to the HOB case. Validity of this concept is demonstrated by numerical simulations with a nonsteady 2-D FCT hydrocode. These calculations indicate that a 30° ramp located 200 ft from a 500T hemispherical HE charge will create 400 to 600 psi double peak static pressure waveforms at distances of 40 to 60 ft up the ramp; time between peaks is 1 ms. These waveforms correspond to a nuclear detonation at 100 to 120 ft/$KT^{1/3}$ and a ground range of 190 to 210 ft/$KT^{1/3}$.

CONTENTS

FCT SIMULATION OF HOB AIRBLAST PHENOMENA

I. INTRODUCTION

It is now recognized that height-of-burst (HOB) detonations can create more severe airblast environments than surface burst (SB) detonations, especially at high overpressures. In the HOB case, the spherical blast wave reflects from the ground, initially as a regular reflection. Then at a ground range approximately equal to the height-of-burst, the shock reflection makes a transition to a double Mach shock structure. This double shock structure creates secondary peaks in the static pressure at and near the ground and thus enhances the early-time HOB airblast impulses compared to the SB case. As shown experimentally by H. J. Carpenter at MABS-IV (Ref. 1), these secondary peaks of the HOB case can be much greater than the first peaks.

When a double Mach shock structure reflects from an above-ground structure, it can produce enhanced diffraction loads. HOB diffraction loads are compared with SB loads in Fig. 1 which was constructed by scaling data from the 1000-lb Pentolite sphere experiments on the recent MIGHTY MACH test series (Ref. 2). As is evident from this figure, the early-time HOB loading impulses are about twice the SB values. Similar effects are shown in Fig. 1 for the static pressure histories and impulses which apply to loads on flush mounted structures.

For military applications, there is a need to simulate these HOB blast environments on a large scale in order to test the response and survivability of large-scale or full-scale military systems. Explosive yields from kilotons to megatons are required. Suspension of such large high explosive (HE) charges is impractical and could lead to poor quality blast fields due to interference effects from the charge support structure.

In this paper we propose a novel approach for simulating HOB blast environments on a large scale. The concept is shown in Fig. 2. A hemispherical surface burst HE charge would be used to create a free-field blast wave. The charge would be situated near an up-slope which had been graded to form a large ramp. When the spherical blast reflects from the ramp, a double Mach shock structure can be created (within certain constraints on wedge angle, θ_W, and incident shock Mach number). This concept relies on the similarity between the HOB-produced environments on horizontal surfaces and the environments produced by shock reflections on wedges or ramps. In Fig. 3 we compare some recent

Manuscript submitted July 22, 1981.

calculations with the FAST2D code:* a nuclear detonation at HOB = 104 ft/$KT_N^{1/3}$ versus a Mach seven square wave shock reflection from a wedge. The pressure contours show that for similar shock strengths and angles, the shock structures in the wedge and HOB cases are qualitatively similar; density contours are also qualitatively similar with a slip line emanating from the primary triple point. There are, however, quantitative differences: the Mach stem structure in the nuclear HOB case is more complex, with a bulge at the foot of the Mach stem; also, in the nuclear case, the reflected shock races rapidly through the high temperature (10^4 to 10^5 ^oK) fireball, while in the wedge case, the reflected wave propagates slowly into the lower ($\sim 10^3$ ^oK) temperature constant field behind the incident square wave shock. We believe, however, that these differences are of secondary importance.

A remaining question is: how well does the blast wave from a hemispherical HE charge simulate the nuclear free-field environment? In Figure 4 we compare the static and dynamic pressure waveforms for the HE and nuclear cases from Brode's one-dimensional (1-D) free air burst calculations (Refs. 3,4) at shock overpressures of approximately 100, 200 and 400 psig. In the HE case a contact surface (CS) separates the air from the detonation products. This contact surface causes a sharp jump in dynamic pressure due to the high densities of the products. Also evident in the HE case is a secondary shock, S_2, which faces inward but is being swept outward by the rapid expansion of the charge. The HE-driven blast wave gives a rather poor simulation of the complete nuclear waveform at high overpressures, due principally to the HE contact surface and secondary shock. However, the HE blast wave outside the contact surface is a reasonably good simulation of the nuclear case. We propose to use precisely this part of the HE blast wave and reflect it from the ramp to simulate the early-time nuclear HOB cases.

The remainder of the paper is organized as follows: Section II gives a conceptual design of the ramp HOB simulator; Section III describes the 2-D finite difference scheme which we used to investigate numerically the flow fields on and near the ramp; Section IV presents the results of these calculations, while conclusions and recommendations are offered in Sections V and VI.

---

*This code uses the Flux Corrected Transport (FCT) algorithm, described in Section III, to maintain sharp discontinuities.

II. CONCEPTUAL DESIGN OF THE HOB SIMULATOR

The design objective for this simulator is to produce the high overpressure (say 100 to 1000 psi) double-peak flow fields which simulate nuclear HOB detonations in the Mach reflection regime with high fidelity. The simulator should be reasonably inexpensive and readily constructed. The design concept should be extendable to large yields.

The primary design parameters for the simulator are the location of the front edge of the ramp, GR_R, and the ramp angle, θ_W. The conceptual design process begins with an HE free-air pressure-range curve for 1 lb of Pentolite. A ramp was assumed to be located at a GR_R corresponding to free field shock overpressures of 500 psi or 150 psi. Assuming various ramp angles, we used reflection factors (Ref. 1) to determine the peak static pressure versus ramp ground range, RGR. Parametric results are presented in Fig. 5. Inserts give the results scaled to a 500T surface burst which are equivalent to about a one-kiloton nuclear surface burst case. Examination of the results in Fig. 5 indicates the following trends:

- A requirement for a high pressure (400 psi to 600 psi) simulator forces one to either move the ramp closer to the charge, or increase the ramp angle, or both.
- One would prefer to move the ramp away from the charge so that the HE free field is close to the nuclear case; however, this leads to large (and presumably impractical) ramp angles.
- Decreasing the ramp angle tends to make the Mach stem rise more rapidly thus increasing the separation between the first and second peaks; we speculate that this could lead to a yield amplification on the front-end of the waveform.
- Transition to Mach reflection occurs at the leading edge of the ramp for $\theta_W = 30^\circ$ and 40°; the transition point (TP) for the $\theta_W = 60^\circ$ occurs at about one-half the distance up the ramp.

The 30° ramp at the 500 psi station appears to be an interesting case—it is feasible to construct and the 600-psi shock overpressure will occur at about 50 ft up the ramp, thus allowing plenty of time for the Mach stem height to grow. Peak pressures will range from 1500 psi at the beginning of the ramp to about 300 psi at the far end.

III. COMPUTATIONAL TECHNIQUE

A numerical simulation of the shock diffraction for the ramp HOB simulator (a 30° ramp starting at 200 feet from a 500T hemispherical HE charge) was performed with a nonsteady two-dimensional (2-D) hydrocode, FAST2D. The objectives of the calculation were to validate the ramp HOB simulator design and to evaluate, in detail, the flow field in the vicinity of the ramp. The FAST2D code solves the balance laws of gasdynamics on a sliding grid in the general form:

$$\frac{\partial}{\partial t}\int_{\delta V(t)} \phi dV = -\oint_{\delta A(t)} \phi\,(\underline{u}-\underline{u}_g)\cdot d\underline{A} + \oint_{\delta A(t)} \tau dA \qquad (1)$$

where ϕ represents the mass, momentum, energy or species mass density (for multi-material calculations) in cell $\delta V(t)$, u and u_g represent the fluid and grid velocities, respectively, and τ represents the pressure/work terms. The finite-difference approximation to Eq. (1) uses a vectorized Flux-Corrected Transport (FCT) algorithm, ETBFCT (Ref. 5), which gives an accurate and well-resolved description of shock wave propagation without the necessity of an *a priori* knowledge of the number, location or character of the gasdynamic discontinuities in the problem. The linear portion of this algorithm is fourth-order-accurate spatially for constant-velocity advection problems, and has a nonlinear flux-corrected antidiffusion stage which automatically provides the local dissipation needed to accurately model discontinuities. The formulation of the algorithm allows the grid to slide with respect to the fluid without introducing additional numerical diffusion. This general adaptive regridding technique permits fine zones to be concentrated in the region of greatest physical interest, thus reducing computational costs with no serious loss in resolution.

Since the ETBFCT algorithm is one-dimensional, time-splitting must be employed to solve two-dimensional problems. Time-splitting makes the boundary condition on the ramp particularly easy to implement. The ramp is represented as a series of "stairsteps" (of varying height and depth) along the interface between the extremal interior zones and a corresponding set of guard cells. A guard cell is defined as the right-most cell in the r-direction during the r-sweep, and the bottom-most cell in the z-direction during the z-sweep. The stairstep boundary conditions are reflective, which requires pressure, density and energy to be continuous and the corresponding velocity normal to the stairstep to vanish.

The numerical simulation began with a 1-D FCT calculation of the blast wave driven by a one pound spherical charge of PBX-9404 in air. The initial conditions, which are shown in Fig. 6, were taken to be the self-similar flow field corresponding to a spherical Chapman-Jouguet detonation wave (Ref. 6), at the time the detonation wave reaches the charge radius, r_o = 3.89 cm/lb$^{1/3}$. A Jones-Wilkins-Lee (JWL) equation of state (EOS) was used for the detonation products and a real air equation of state was used outside the HE/air interface. These EOS specify the pressure as a function of density and internal energy. The HE/air interface was followed by solving a conservation law for the mass fraction ρf (where f=1 in the pure HE and f=0 in the pure air). The equations of state were blended in the mixed cells (0<f<1) according to Dalton's law. A fixed grid of 500 cells was used with a mesh spacing Δr = 0.1025 cm/lb$^{1/3}$, so that the initial flow field in the charge occupied about 38 computational cells. The flow field results at the end of the 1-D calculation (cycle 1281, t = 152 μs/lb$^{1/3}$) are shown in Fig. 6. The shock overpressure is 445 psig. The density distribution shows a jump at the HE/air interface; inside the interface is a secondary inward-facing shock which is being swept outward by the supersonic flow.

These results were scaled up to the 500 ton HE surface burst case by multiplying all times and ranges by the scale factor, SF = $(2\times10^6)^{1/3}$ = 125.992. The shock radius at this time of 19.15 ms/500T$^{1/3}$ was found to be 198 ft/500T$^{1/3}$ with an overpressure of 445 psig (note that this point checks with the HE free air curve in Fig. 5). These results were then inserted as initial conditions in the cylindrical r-z FAST2D code, with one approximation. Since the γ's ahead and behind the HE/air interface were quite close (γ_{HE} = 1.25 versus γ_{air} = 1.30), the HE products were modeled with the real air equation of state, and the 2-D interface was not followed specifically with a mass species conservation law. The 2-D mesh consisted of 150 x 150 cells with a moving fine mesh region (55 x 55 cells, Δr = 5 cm and Δz = 2.8868 cm with $\Delta z/\Delta r$ = tan 30°) which followed the Mach stem. The calculation was run 5601 cycles. Diagnostics for the 2-D calculation consisted of 46 environment time histories (at 40 stations on the ramp and 6 stations perpendicular to the ramp at a RGR = 60.5 ft) and contour plots of the flow field every 200 cycles. Times are denoted by the label $\Delta t=t-t_o$, which references everything to the incident shock arrival time at the foot of the ramp t_o=19.2 ms.

IV. CALCULATIONAL RESULTS

An overall picture of the spherical shock reflection from the ramp is displayed in Fig. 7 which gives the calculated pressure and density contours at various times ($\bar{t}$=3, 5.61, 9.27 and 13.4 ms/500$T^{1/3}$); Fig. 8 gives a magnified view of the flow field at $\bar{t}$=9.61 ms/500$T^{1/3}$. The shape of the shock structure for the simulator (i.e., the geometry of the incident wave, the Mach stem, and the kinked reflected wave) more closely resemble the shock structure for square wave reflections from a ramp (Ref. 7) than the nuclear HOB case (see Fig. 3). The density contours indicate that a contact surface (a slip line) emanates from the triple point (the confluence of the incident, Mach and reflected waves) and approaches the ramp at an angle of about 60°. Pressure contours indicate that a high pressure region is located in the vicinity of where the projection of the contact surface would strike the ramp.

Figure 9 gives an experimental shadowgraph of the shock wave structure formed by an 8 lb TNT driven blast wave (HOB = 1.04 ft/$lb^{1/3}$) diffracting on a 31° ramp. The incident shock pressure was about 120 psi at the foot of the ramp and about 75 psi at the time of the photograph (compliments of W. Dudziak, Ref. 8). The shock structure is qualitatively similar to that in Figs. 7 and 8. Fig. 9 shows that the reflected wave pushes the TNT products away from the ramp, thus maintaining a clean air flow (unpolluted by HE products) in the Mach stem region--a truly beneficial result! Note that this happens even in the low HOB case where the TNT products squish along the ground and push the TNT/air interface closer to the shock.

The calculated shock properties for the ramp HOB simulator are shown in Fig. 10 as a function of ramp ground range, RGR. The primary Mach stem pressure, p_1, ranged from about 600 psi to 400 psi. The second peak pressure, p_2, decayed from 1300 psi at the foot of the ramp to 400 psi at the 60 foot station. The peak pressures were determined from two methods: for RGR < 30 ft peaks were evaluated from pressure distributions at a fixed time, and these data are somewhat noisy due to the stairstep boundary condition modeling of the ramp; for RGR > 30 ft, peaks were evaluated by smoothing the pressure time histories two cells above the ramp, giving a smooth pressure-range curve.* Note that the second peaks are in reasonably good agreement with

*Unfortunately the pressure histories for RGR < 30 ft were not available for data analysis.

the prediction technique used to design the simulator. Also note that for RGR $\geq$ 40 ft the first and second peaks are equal.

The calculated shock arrival times for the first and second static pressure peaks are included in Fig. 10 The arrival time difference between peaks grows rapidly for the first 30 feet up the ramp, and then remains constant at about $1\,ms/500T^{1/3}$. In addition, Fig. 10 depicts the Mach stem growth versus ramp ground range. The top of the Mach stem traces a path at an average angle of about 9 degrees above the ramp surface, which is consistent with shock tube data for square wave shock reflections from wedges (Ref. 7). Note that the Mach stem growth for the equivalent nuclear case is more rapid than in the case of the simulator.

Calculated static pressure histories are presented in Fig. 11 for various stations on the ramp (34 ft $\leq$ RGR $\leq$ 60 ft). The second peak dominates for RGR $\leq$ 34 ft, and then gradually melts into backside of the waveform. For RGR > 60 ft, the second peak has essentially disappeared. Comparisons of static pressure histories at h = 0, 1 and 5.5 ft normal to the ramp for station 17 indicate that there is no vertical pressure gradient on the front end of the waveform.

Fig. 12 gives the calculated dynamic pressure histories on the ramp at stations corresponding to the static pressure histories of Fig. 11. At small ground ranges, the second peak dominates the first peak. The second peak decays in magnitude and duration as the Mach stem progresses up the ramp, and has essentially disappeared for RGR > 60 ft. Comparisons of dynamic pressure histories at h = 0, 1 and 5.5 ft normal to the ramp for station 17 indicate very little vertical gradient for times less than 0.8 ms after shock arrival. However, the h = 1 ft station shows a strong second peak at about 1 ms which is absent from the h = 0 and 5 ft records. We believe that this is caused by a high density slug of gas at this altitude. A slip line (with high density material above and lower density material below) emanates from the triple point. As the slip line approaches the ramp it curls forward forming a region of high density fluid near the ramp surface (h $\sim$ $1\,ft/500T^{1/3}$) while the Mach stem at this station is about 10 ft high. This effect is similar to the contact surface rollup observed in numerical simulations of nuclear HOB detonations and square wave shock reflections from wedges (Ref. 9). This increase in dynamic pressure near the ramp can be very important to airblast loads on above ground

structures--it increases both the peak loads and the impulses to approximately 2 ms/500$T^{1/3}$.

Let us now relate the simulator environment to an equivalent nuclear height-of-burst case. Fig. 13 gives the ideal, nuclear peak overpressure HOB curves as constructed by H. J. Carpenter (Ref. 10). Region A corresponds to the regular reflection regime, and region B corresponds to the Mach reflection regime where the static pressure waveforms on the ground contain two peaks. In regions B_1 and B_2, first and second peaks dominate, respectively. Along the dashed curve the first and second peaks are equal. Figure 9 indicates that for 30 ft $\leq$ RGR $\leq$ 60 ft, first and second peaks are equal and range from 600 psi down to 400 psi. Figure 13 then indicates that for this range in pressure, the nuclear HOB parameters are the following:

$$100 \text{ ft/KT}^{1/3} \leq \text{HOB} \leq 120 \text{ ft/KT}^{1/3}$$
$$190 \text{ ft/KT}^{1/3} \leq \text{GR} \leq 210 \text{ ft/KT}^{1/3}$$

Thus the simulator as analyzed in this report gives an airblast environment which is equivalent to a nuclear detonation at height-of-burst of about 110 ft/$KT^{1/3}$ and a ground range of about 200 ft/$KT^{1/3}$.

Finally, let us consider the effective yield of the simulator. A 500T high explosives surface burst produces a blast wave flow field which is equivalent to about a 1-KT nuclear surface burst (or a 2-KT nuclear free air burst). Nuclear static pressure waveforms in the 400 psi to 600 psi Mach reflection regime have double peaks with a time separation between peaks of about 2 ms/$KT_N^{1/3}$ (Ref. 10). The FAST2D calculation of the simulator flow field indicates a time separation between peaks of about 1 ms/$500_{HE}^{1/3}$/SB, i.e., the time separation for the simulator is too small by a factor of about two. We believe that the time separation between peaks can be increased by making the Mach stem climb more rapidly. This can be accomplished by simultaneously decreasing the ramp angle and moving the ramp toward the charge.

V. SUMMARY AND CONCLUSIONS

Height-of-burst detonations create airblast environments and diffraction loads which are more severe than the surface burst case in the high overpressure Mach reflection regime. There is an ongoing need to simulate these HOB environments on a large scale to validate the survivability of military systems to blast effects. We propose using an existing high explosives test bed, say a 500T hemispherical charge,

to create the free field blast environment. A large ramp would be located near the charge. Shock diffraction on the ramp generates, in a rather natural way, a flow field which simulates the HOB blast environment with high fidelity.

A parametric analysis of such HOB simulators indicates that a 30^{o} ramp situated about 200 feet from a 500T hemispherical charge would give useful environments. The flow field details near such a ramp were investigated with a 2-D hydrocode calculation. The calculation indicates that double peaked static and dynamic pressure waveforms were created near the ramp surface. In the 400 to 600 psi range, the calculated first and second static pressure peaks were equal. By use of the nuclear HOB curves, it was determined that the blast flow field corresponds to a nuclear detonation at a height-of-burst of 100 to 120 $ft/KT_N^{1/3}$ and a ground range of 190 to 210 $ft/KT_N^{1/3}$. Time separations between static pressure peaks were found to be about 1 $ms/500T_{HE}^{1/3}$; this value was too small by about a factor of two for the nuclear case.

VI. RECOMMENDATIONS

Additional analysis should be performed to refine the HOB simulator design. The 2-D hydrocode simulations are quite useful because they allow one to examine the entire flow field in a non-interfering way. An improvement is needed on the boundary condition modeling of the ramp--the stairstep model gave very noisy results on the ramp surface. Small charge (say 4-lb hemispherical PBX-9404 charges) tests can provide an experimental definition of the blast environment. Ramp angle, location and surface curvature could be varied parametrically in such tests. Pressure gauges on the ramps can measure static pressure histories with high fidelity, while shadowgraph photography can capture the shock structure on the ramp. These results could be used to design a simulator which, we suggest, should be fielded on the next 500T HE test.

ACKNOWLDEGMENTS

We would like to acknowledge the contributions of H. J. Carpenter in this work. In July of 1980, he and one of the authors (A. Kuhl) first postulated the idea that a large ramp, in conjunction with an HE charge, could be used to simulate HOB environments on a large scale. His careful critique of the manuscript and his stimulating discussions on this subject are greatly appreciated.

This work was sponsored by the Defense Nuclear Agency under Contract Number DNA001-81-C-0023. Dr. George Ullrich was project officer for this effort.

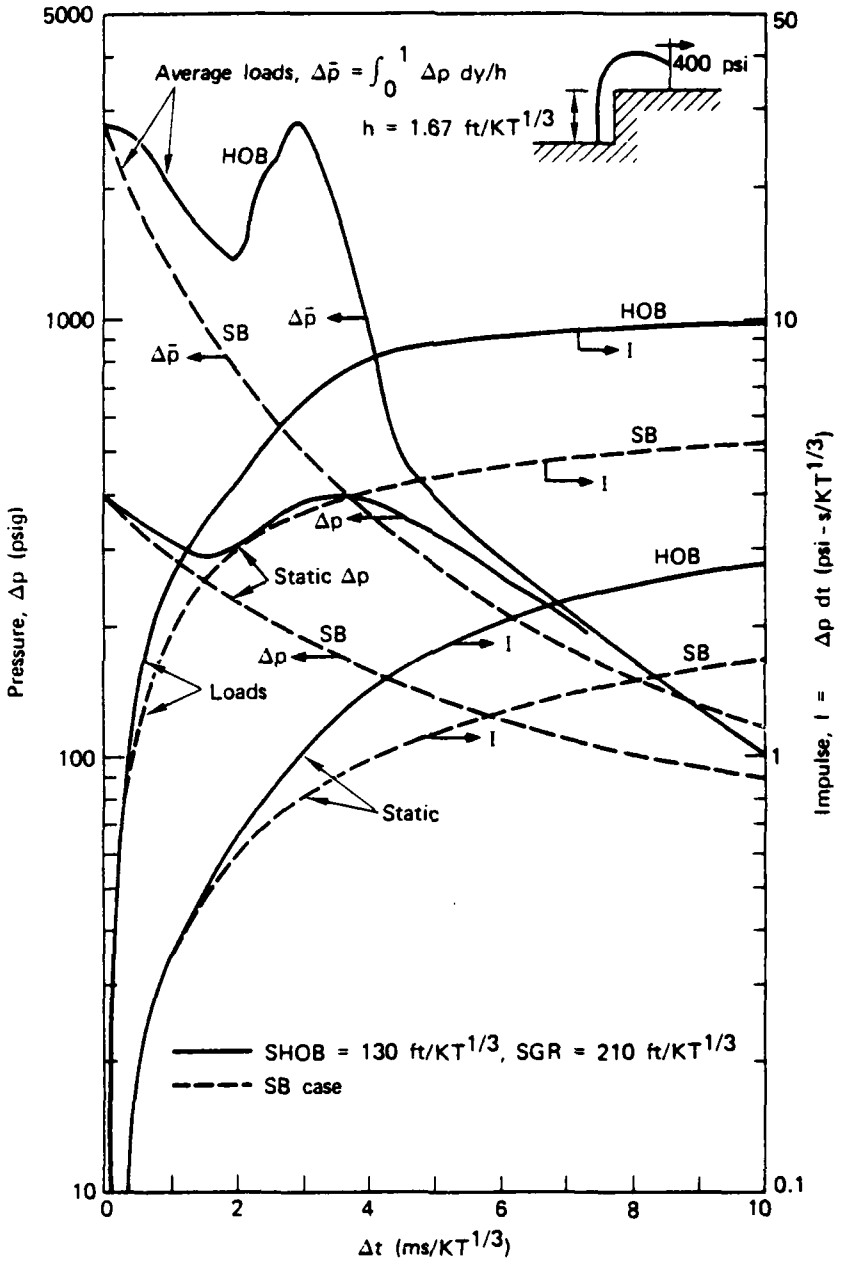

Fig. 1 — Comparison of nuclear surface burst and height-of-burst loads and impulses at the 400-psi station

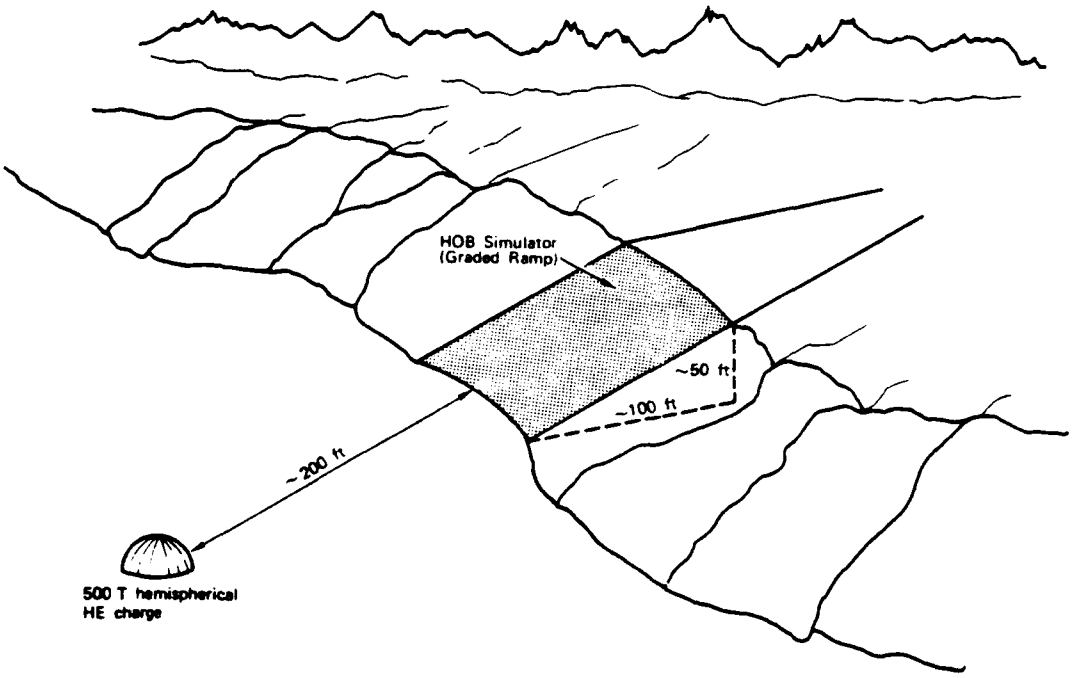

Fig. 2 — HOB simulator concept (graded ramp) on a large-scale HE test

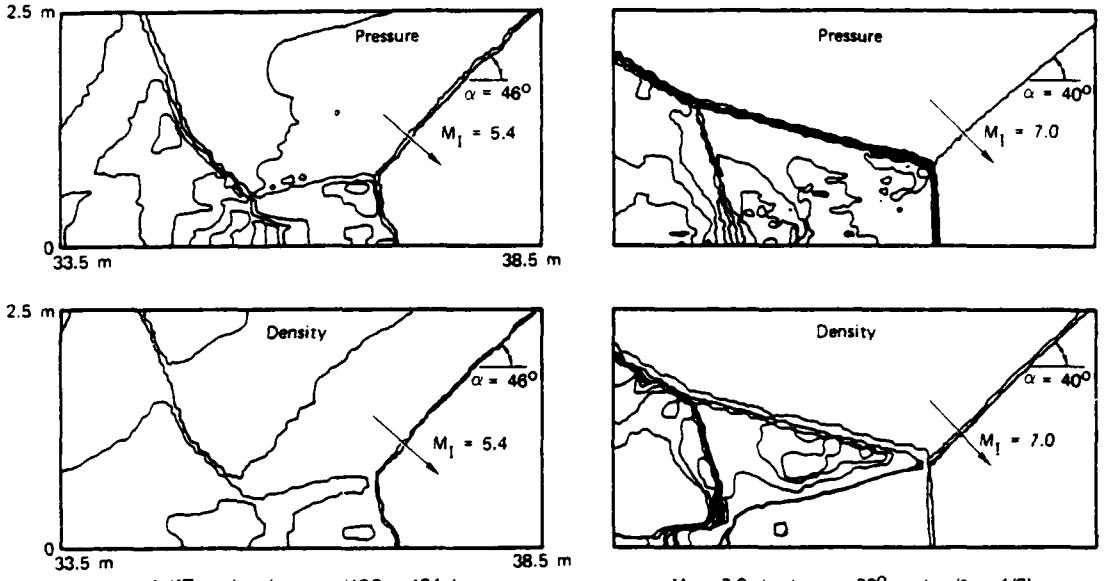

Fig. 3 — Comparison of calculated pressure and density contours for a nuclear HOB case and a square wave shock on a wedge

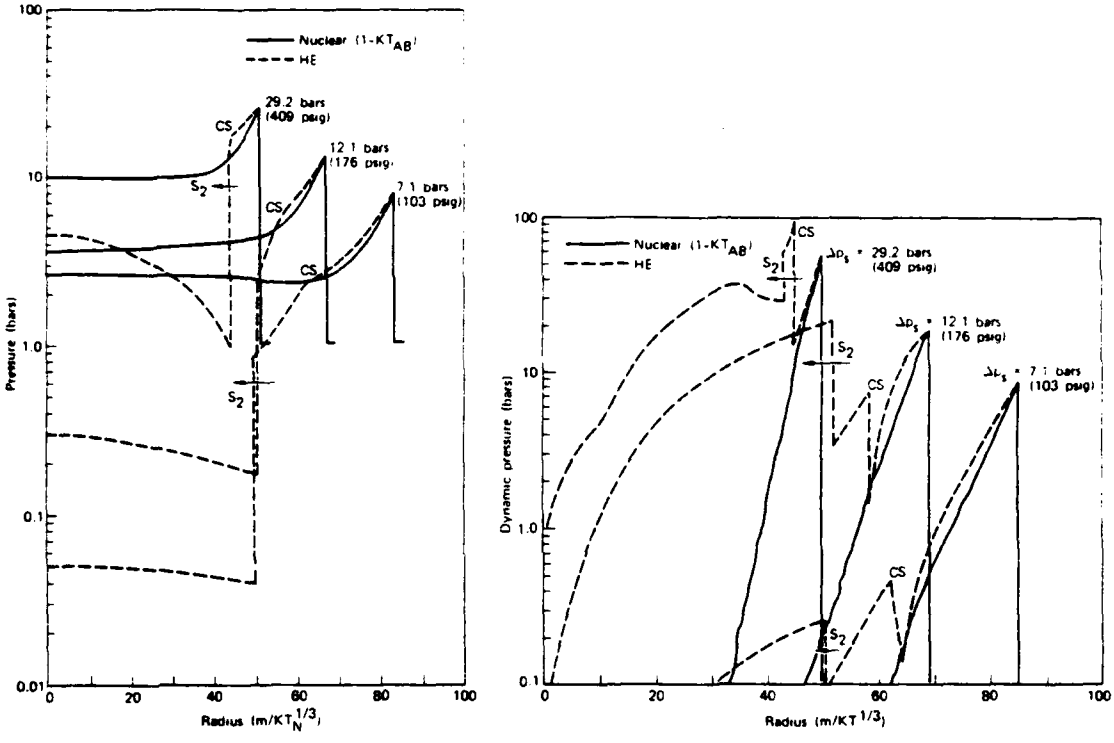

Fig. 4 — Comparison of HE and nuclear free-air burst static and dynamic pressure waveforms at shock overpressures ~ 100, 200, and 400 psi

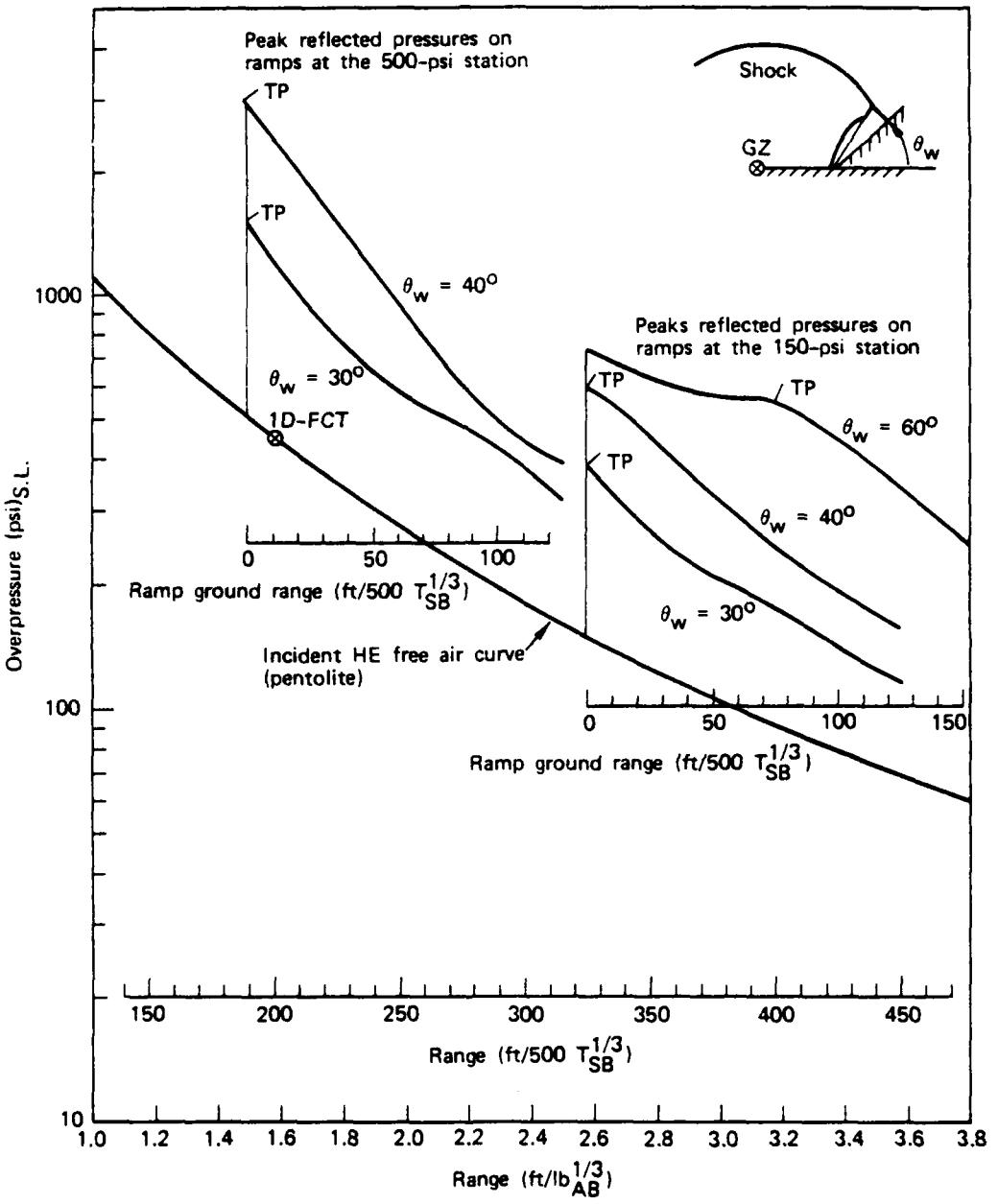

Fig. 5 — Parametric results of peak reflected pressures on the ramp HOB simulator

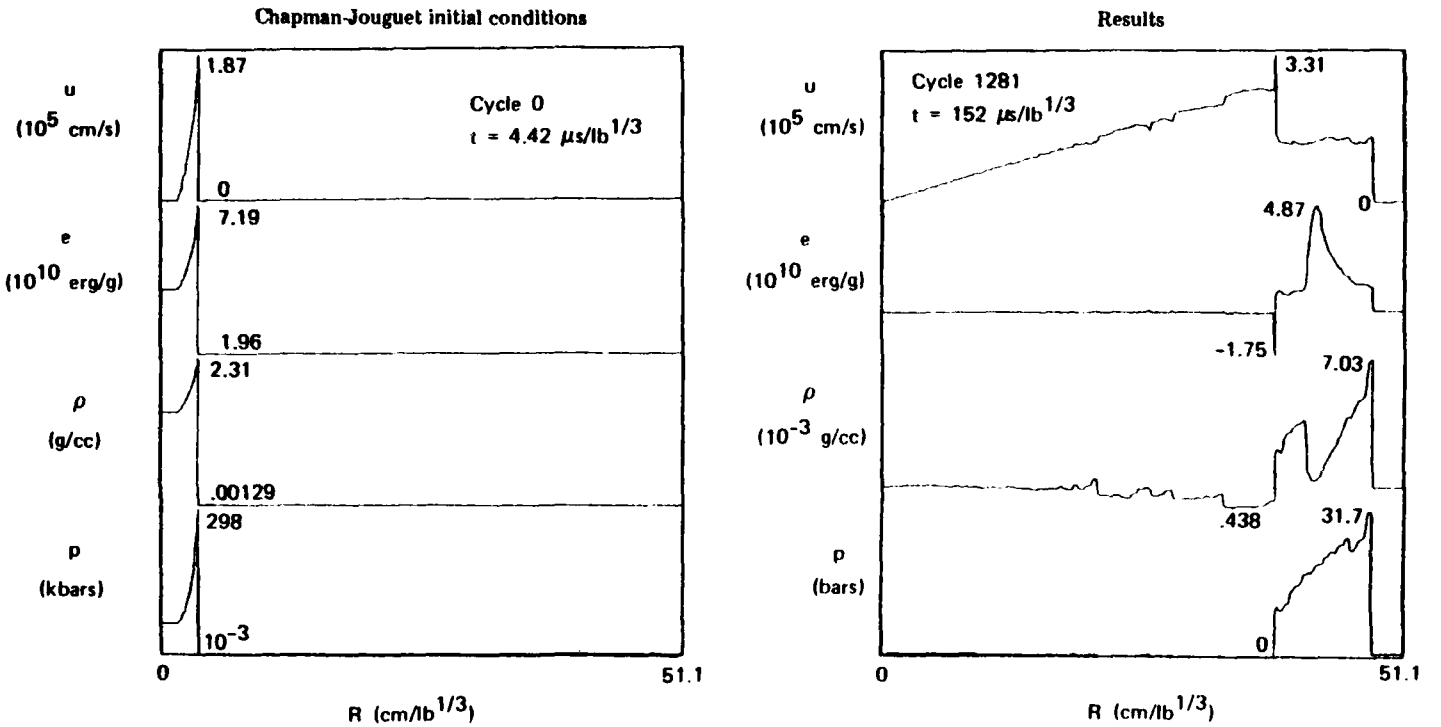

Fig. 6 — Calculated 1-D flow field distribution of a spherical 1-lb PBX-9404 charge
(Δr = 0.1025 cm, 500 cells, real air and JWL EOS)

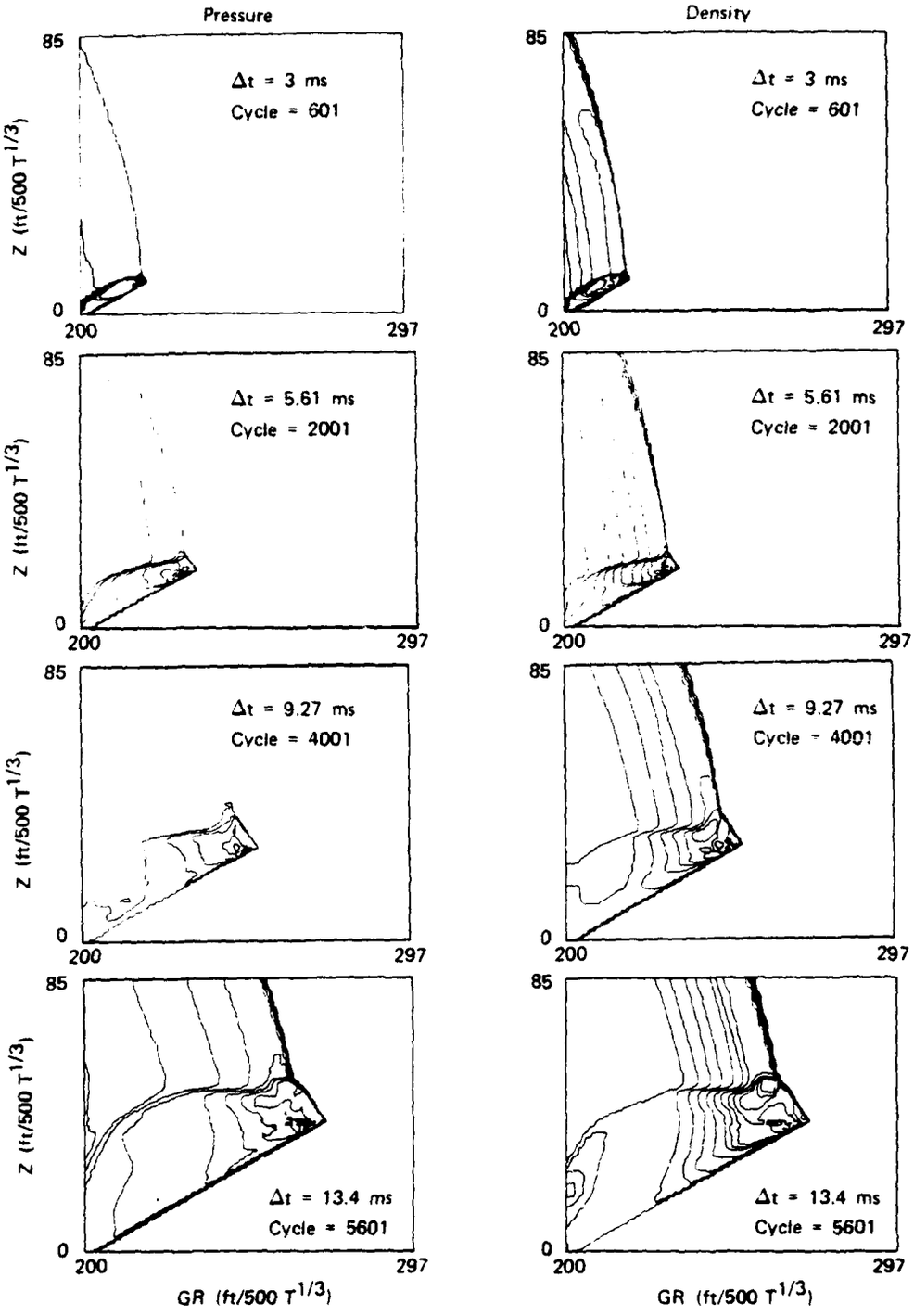

Fig. 7 — Calculated pressure and density contours at times Δt = 3.0, 5.61, 9.27, and 13.4 ms/500 $T^{1/3}$ (t_o = 19.2 ms/500 $T^{1/3}$)

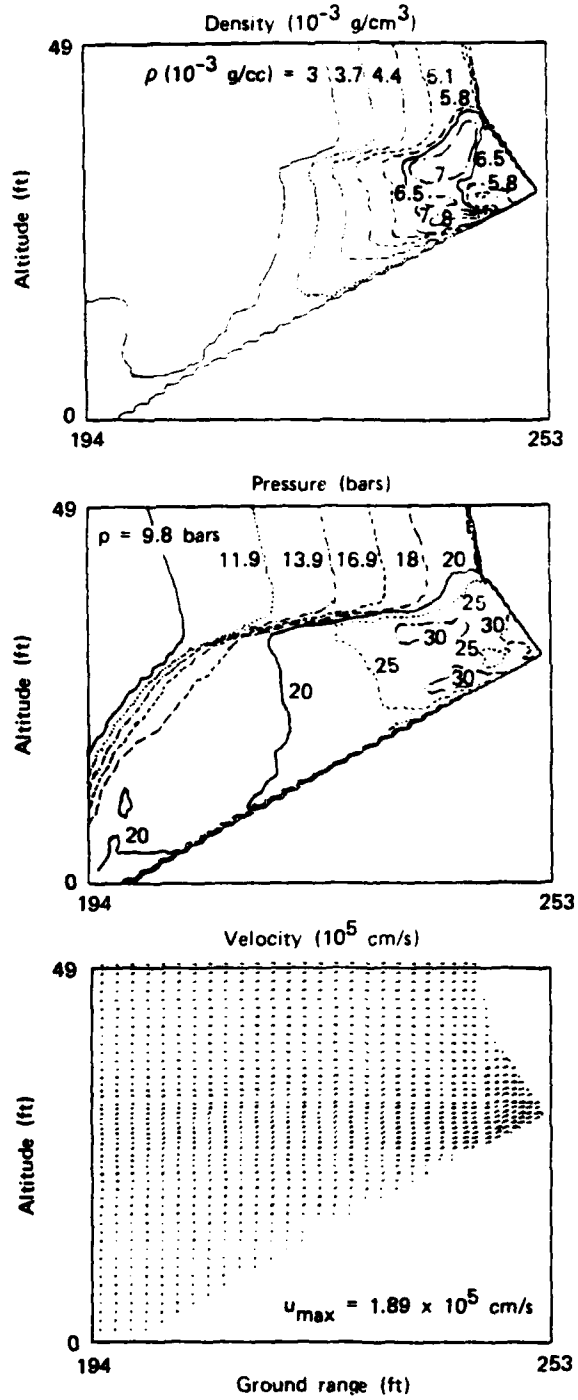

Fig. 8 — Calculated flow details at Δt = 9.61 ms/500 $T^{1/3}$

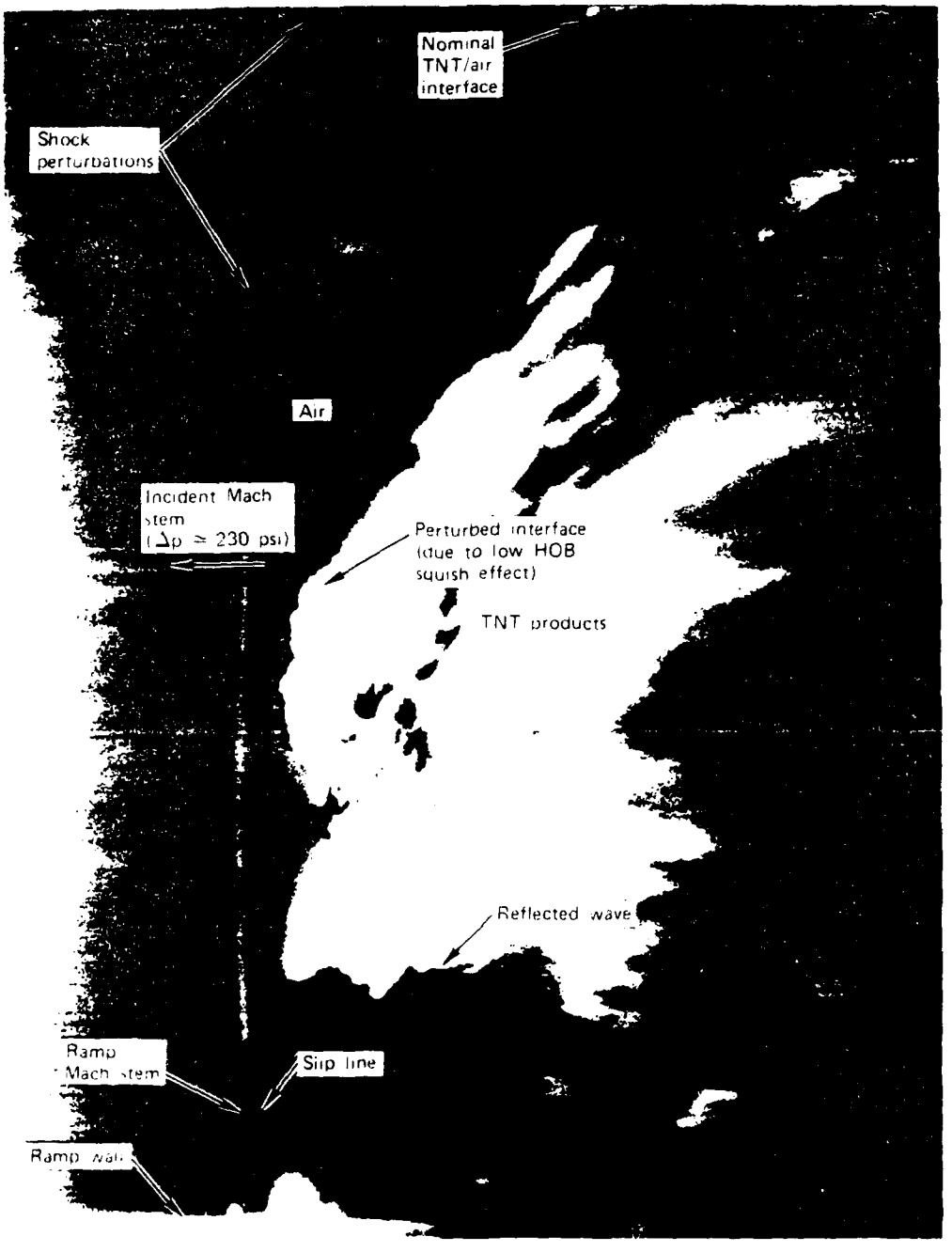

Fig. 9 — Shadowgraph of the shock wave structure formed by an 8-lb TNT-driven blast wave (HOB = 1.04 ft/lb$^{1/3}$) diffracting on a 31° ramp; incident pressure at the beginning of the ramp was about 120 psi. (Courtesy of W. F. Dudziak, Information Science, Inc.)

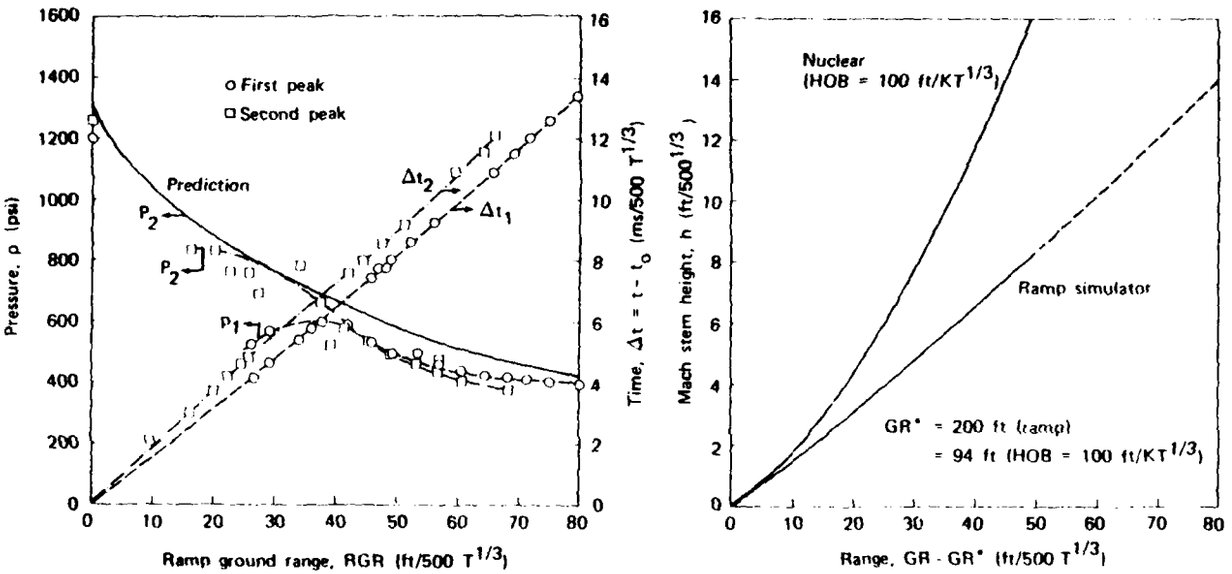

Fig. 10 — Calculated peak pressure, shock arrival time and Mach stem height vs ground range for the ramp HOB simulator (GR_{ramp} = 200 ft/500 $T^{1/3}$, t_o = 19.2 ms/500 $T^{1/3}$).

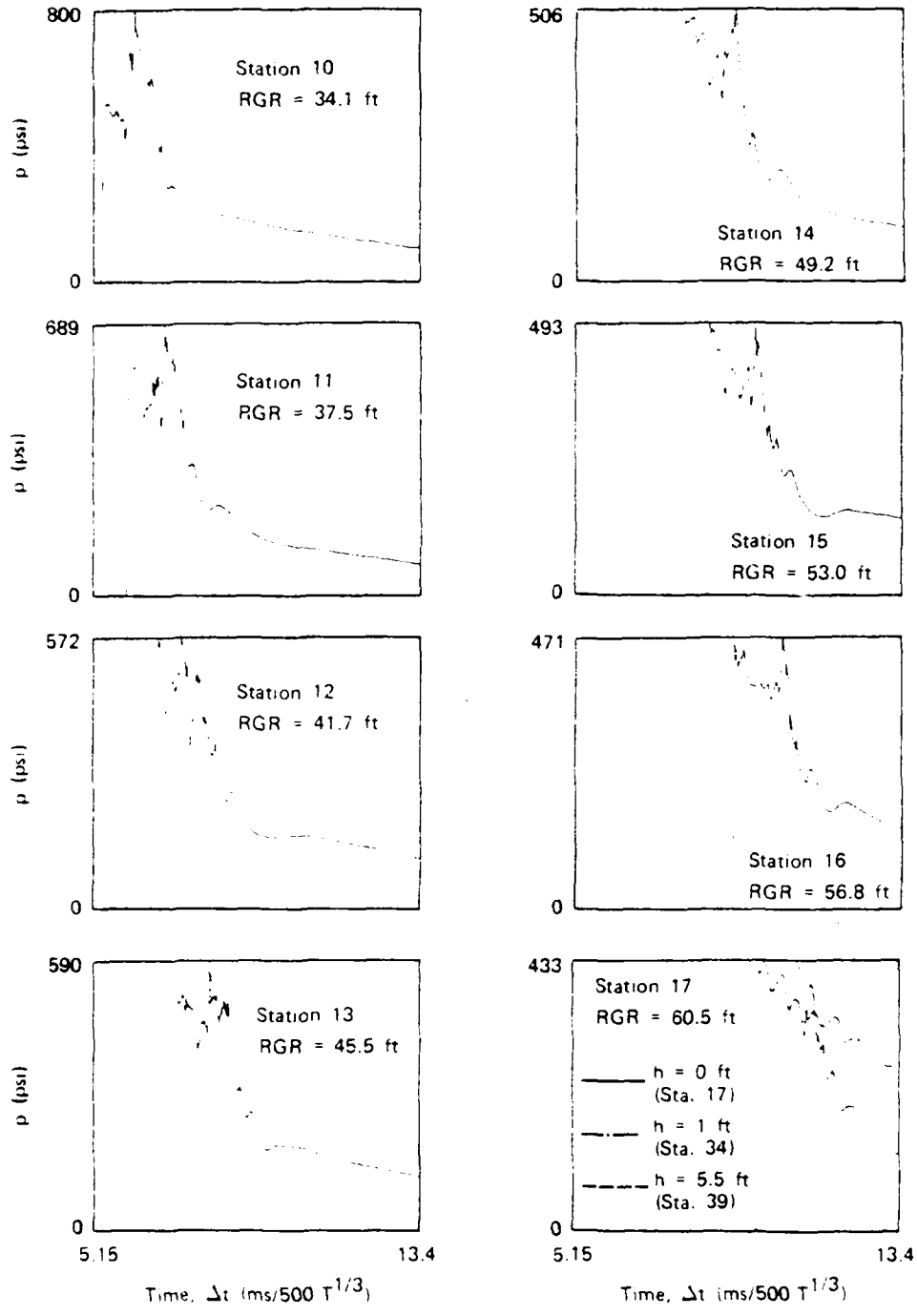

Fig. 11 — Calculated static pressure time histories at various stations on the ramp (t_o = 19.2 ms/500 $T^{1/3}$)

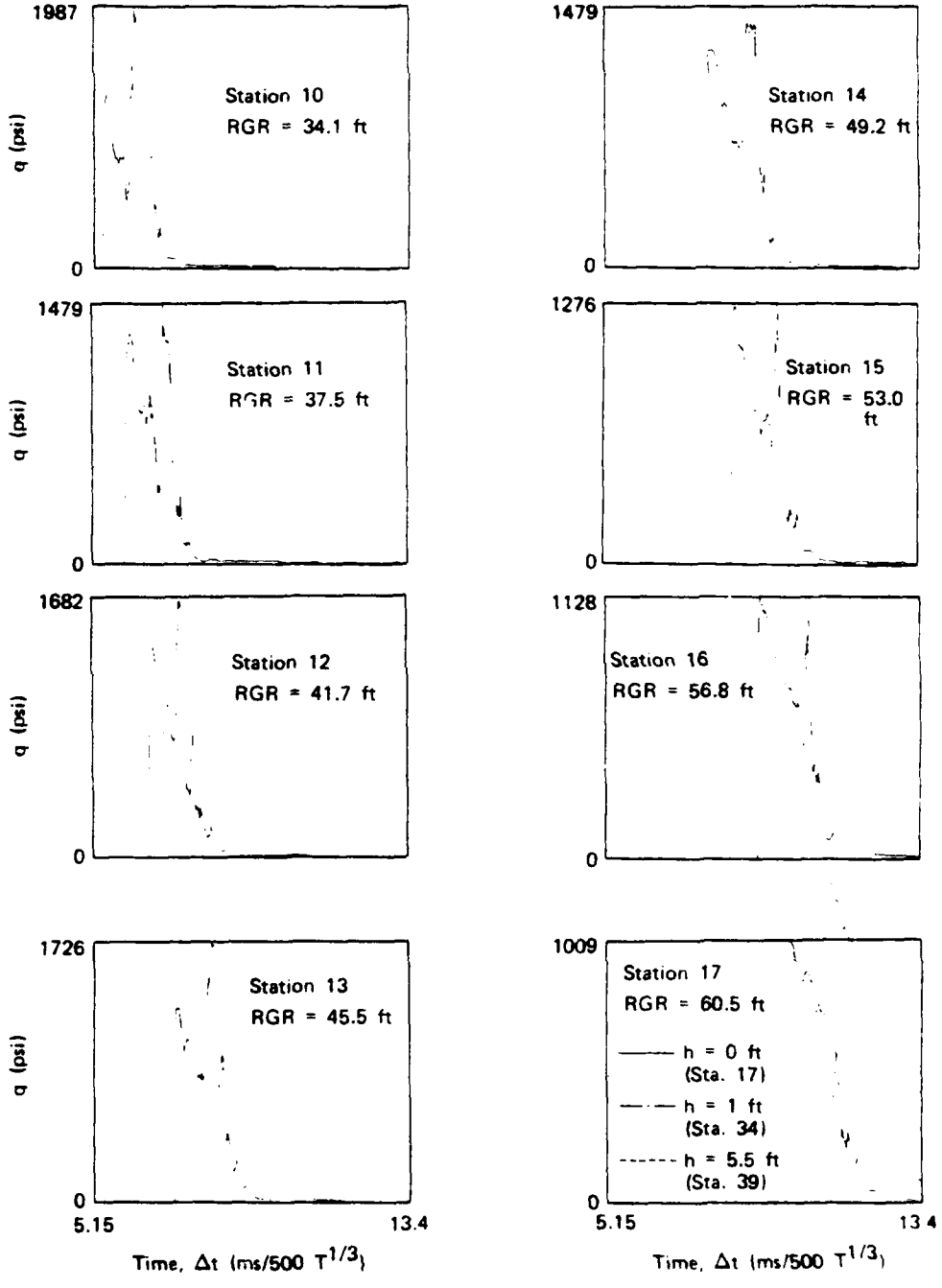

Fig. 12 — Calculated dynamic pressure time histories at various stations on the ramp (t_o = 19.2 ms/500 $T^{1/3}$)

AD-A117 436 SCIENCE APPLICATIONS INC MCLEAN VA F/G 19/4
NUCLEAR AIR BLAST EFFECTS.(U)
JUN 82 N FRY
UNCLASSIFIED SAI-83-836-WA N00014-81-C-2267
NL

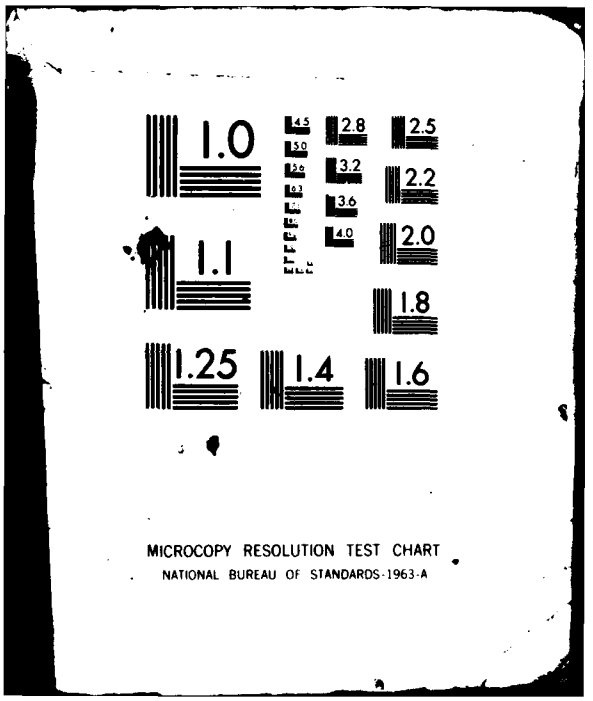
1.0
1.1
1.25
1.4
1.6
1.8
2.0
2.2
2.5
2.8
3.2
3.6
4.0
4.5
5.0
5.6
6.3
MICROCOPY RESOLUTION TEST CHART
NATIONAL BUREAU OF STANDARDS-1963-A

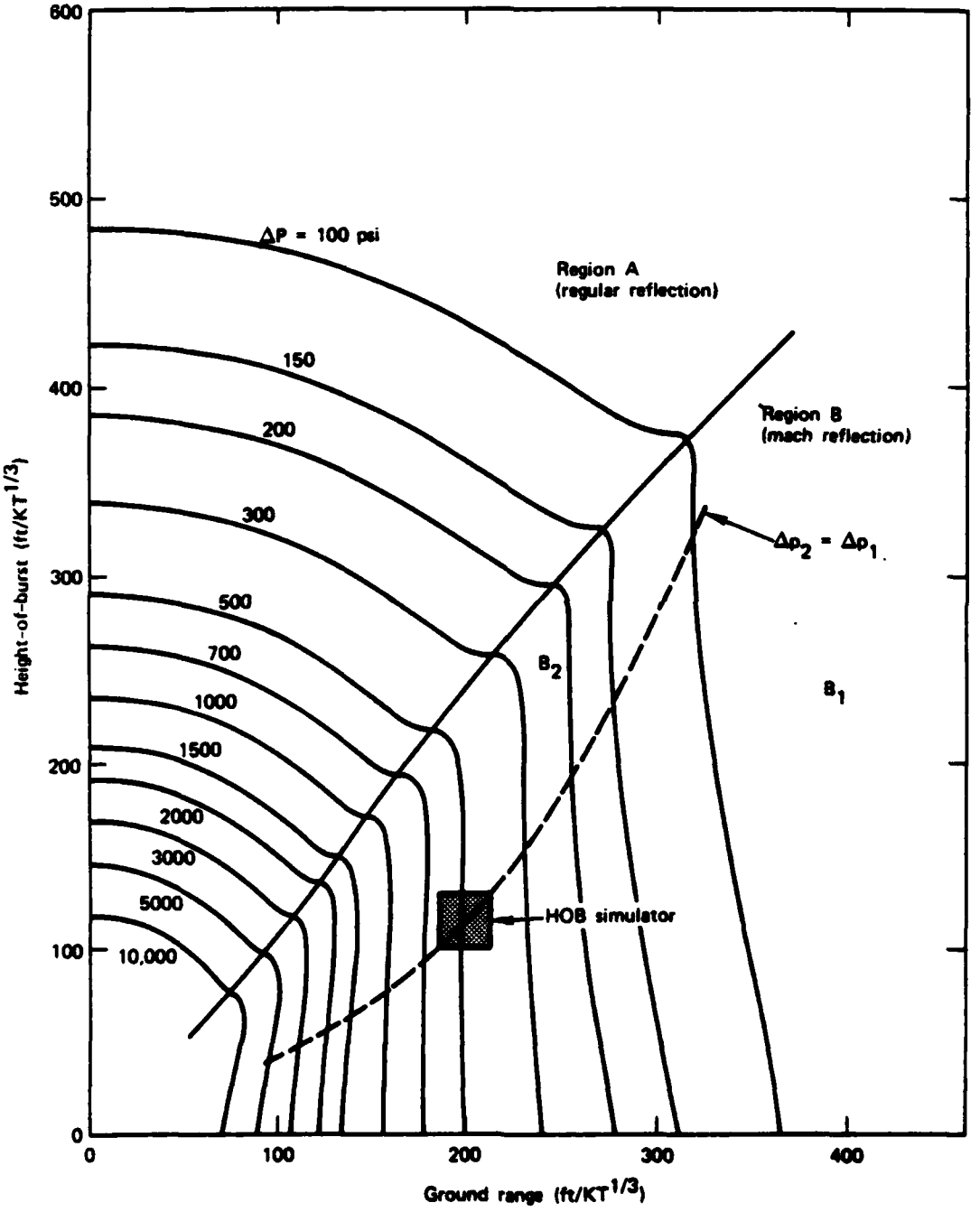

Fig. 13 — Ideal nuclear peak overpressure height-of-burst curves (Ref. 10)

REFERENCES

1. Carpenter, H. J., "Height-of-Burst Blast at High Overpressure," 4th Int. Symposium on Military Applications of Blast Simulation, (1974).

2. Keefer, J. and Reisler, R., U. S. Ballistic Research Laboratory, (private communication, 1979).

3. Brode, H. L., A Calculation of the Blast Wave from a Spherical Charge of TNT, Rand Report RM-1965 (1957).

4. Brode, H. L., Theoretical Description of the Blast and Fireball for a Sea-Level Kiloton Explosion (U), Rand Report RM-2246-PR (1966).

5. Boris, J. P., Flux-Corrected Transport Algorithms for Solving Generalized Continuity Equations, NRL Report 3237 (1976).

6. Kuhl, A. L., Seziew, M. R., Analysis of Ideal, Strong, Chapman-Jouguet Detonations, TRW Report 78.4735.9-13 (1978).

7. Ben-Dor, G., Glass, I. I., "Domains and Boundaries of Non-stationary Oblique Shock-Wave Reflections: 1. Diatomic Gas," J. Fluid Mechanics, Vol. 92, Pt. 3, pp. 459-496 (1979).

8. Dudziak, W. F., Information Science, Inc. (private communication, May 9, 1981).

9. Book, D., Boris, J., Kuhl, A., Oran, E., Picone, M., Zalesak, S., "Simulation of Complex Shock Reflections from Wedges in Inert and Reactive Gaseous Mixtures," Seventh Int. Conference on Numerical Methods in Fluid Dynamics, Springer-Verlag (1981).

10. Carpenter, H. J., RDA (private communication, 1979).

END

DATE
FILMED

10 · 82

DTIC